Università Campus Bio-Medico di Roma

Maria Chiara Simonelli

PhD thesis in Biomedical Engineering, XXVII cycle

ADVANCED MICROFLUIDIC DEVICES MIMICKING THE DYNAMIC AND 3D PHYSIOLOGICAL MICROENVIRONMENT FOR DIAGNOSTIC APPLICATIONS

PhD coordinator:
Prof. Giulio Iannello

PhD supervisors:
Prof. Marcella Trombetta
Dr. Alberto Rainer

Abstract

Despite a recognized value in nowadays research, conventional two-dimensional (2D) cell cultures still fail to provide accurate prediction of tissue functions and behavior *in vivo*. In fact, cells grown on flat tissue culture substrates can differ considerably in their morphology, cell-cell and cell-matrix interactions, and differentiation from those growing in more physiological 3D environments. On the other hand, animal models may not adequately reproduce several features of human tumors, drug therapeutic responses, and autoimmune diseases.

Recent advances in tissue engineering and biomedical technologies aim for the integration of biology with the spatial positioning capabilities allowed by microfabrication techniques. Physiological environments provided by extracellular matrices can be reproduced, besides the development of tissues, organs and tumors, paving the way to the so-called organ-on-chip technology.

Microfluidic devices are generally fabricated as polydimethylsiloxane (PDMS) replicas of a lithographically obtained master. They allow a precise control on cells and tissue microenvironment, thus enabling the exposure of cells to medium flow. These aspects led to advanced systems, faithfully reproducing physiologically relevant conditions. Furthermore, the additional ability of these models lays in the chance of manufacturing optically transparent platforms, which might be observed in real time under the microscope, allowing a high-throughput imaging analysis.

This thesis work aim was to highlight the power of these complex microengineered systems. In a first example, a "NAFLD-on-chip", exploiting a sinusoid-like geometry with a microchannel array to simulate the endothelial-like barrier, was used for high-density 3D hepatocyte culture, with the aim to recapitulate the onset of nonalcoholic fatty liver disease.

As a second example, a tumor-on-chip platform was developed to study the interaction between Cancer Stem Cell (CSCs) behavior with immune cells, in particular with Tumor-Associated Macrophages (TAMs).

These models would accelerate and facilitate translational research to perform the screening of new therapies. In this sense, *in vitro* 3D models provide a bridge on the gap between traditional cell culture and animal models.

Contents

SECTION I

Chapter 1

Microfluidic devices

Over the last years, miniaturized instrumentation and reactors research have started to develop more and more new interesting applications. It all began in 1979, when the first reported gas chromatograph air analyzer, constructed on a silicon wafer, could be traced back. Despite that, only several years later, when flow injection analysis was performed on a chip, microchips gained attention. After that, microfluidic devices expanded, incorporating sample preparation, fluid handling, microreactors, separation systems, cell handling and culturing. Nowadays these devices find an application in medical analysis, environmental monitoring, biochemical analysis and microchemistry. They can perform charged components separation based on capillary electrophoresis and magnetic microparticles, immunoassays, DNA analysis and even clinical diagnostics (Minteer and Moore, 2005).

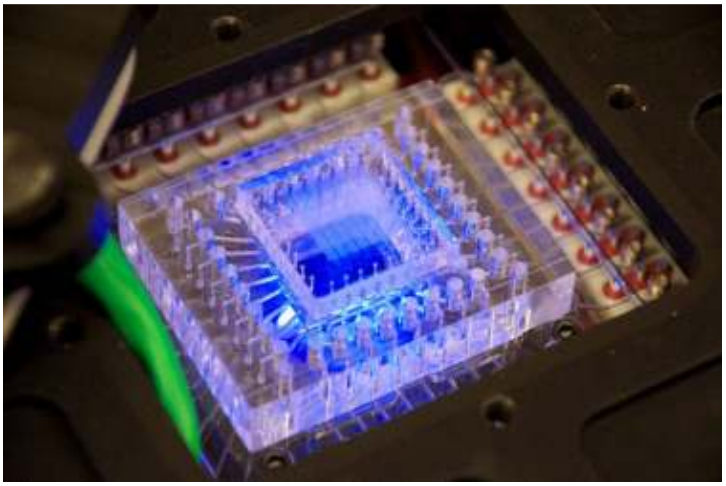

Figure 1.1: Microfluidic device.

Microfluidic is the science and technology concerning the manipulation of fluid systems. As the word itself says, at least one characteristic dimension has to be at the sub-millimeter scale (Tabeling, 2006). A microfluidic chip can be defined as a network of microchannels, which are molded or etched in a substrate and having dimensions between ten and one hundred microns. When it comes to dealing with microfluidics, it is extremely important to consider that physics may change as for **scaling** dimensions. This is the reason why **fluid dynamics** change and it is fundamental to understand how to **control flows** and how to manipulate it using **capillary forces**. **Dimensionless numbers** were introduced to more easily understand *ratios* between forces.

Microfluidic development has been carried out because of its use in important fields such as microelectronic, molecular and cellular biology and analysis. Before that, the conventional technologies used to be gas chromatography, low-pressure liquid chromatography and capillary electrophoresis.

The aim is to find systems able to detect chemicals and biological compounds added to a single-cell and molecular analysis with the high resolution and sensibility needed by genomics and regenerative medicine applications.

The main outcome of microfluidic sciences has been the development and the fabrication of **"labs-on-a-chip"**. The aim of a "lab-on-a-chip" is to integrate on a single chip most of the diagnostic operations actually carried out at hospitals and analysis laboratories. The final part of this chapter will be dedicated to **microfluidic cell cultures** in order to explain more in detail all the applications in the medical/biological field.

1.1 Physics of microfluidics

1.1.1 SCALING LAWS

Like in all the microsystems, the first thing that is clear when dimensions are scaled to very small levels, is that our normal intuition in analyzing and predicting the behavior of systems fails. That happens because quantum mechanics is needed to study physical systems due to the breakdown of Newtonian mechanics. Certainly the laws of physics do not change from the macroscale to the microscale, however the scale factor can give predominance to different forces. This effect is known as scaling effect and it is governed by the so-called **scaling laws** (Ghosh, 2011).

Volume and surface are the geometrical parameters related to mechanical/thermal inertia and pressure relatively. When these physical quantities are miniaturized, the possible consequences from the reduction on both need to be taken into account. In fact, as the size decreases, the *surface-to-volume ratio* increase and the surface properties become increasingly important. This can be expressed as

$$\frac{surface\ forces}{volume\ forces} \propto \frac{l^2}{l^3} = l^{-1} \underrightarrow{\quad} \underset{l \to 0}{\infty}$$

This relation explains why properties as diffusion, surface tension and viscosity become more significant when dimensions decrease. Furthermore, the inertia of a solid is related to its mass and acceleration, so to the dynamic of the system. If we consider a generic machine in which different forces are operating, and if we ideally scale down dimensions by a factor τ^s without altering the proportions among its parts, the ratios between two forces may change. In general, the intensity of each force will scale proportionally to τ, being s the *scaling exponent.* The latter

quantifies how the magnitude of forces changes during an ideal scaling process. Actually the intensity of forces shapes the morphology of the machine or body, which obviously exploits the predominant ones.

If we first consider the case of *isomorphic scaling*, the outcome is that all linear dimensions are scaled down by the same factor, while angles are kept unchanged. That can be modeled by a set of equations like

$$P_i = f_i(p_1, \ldots . p_n)$$

where Pi is the i^{th} property of the system we are analyzing and which depends, according to the f_i function, on the set of n parameters $p_1, \ldots, p_n$. These parameters can be physical constants, intensive quantities or extensive quantities (depending on volume or on mass, they should be written taking into account the typical linear dimension of the system). An ideal isomorphic scaling process consists in analyzing how P_i changes when the dimensions of the system are linearly scaled.

However, if we needed to compare two systems at different dimensional scales, we should model them in terms of non-dimensional groups, not depending on dimensions. Finding such non-dimensional groups involves analysis of the dimensions of parameters appearing in a given law. It is possible to do that by using the *Buckingham Theorem*. Two systems are said to be similar if the ratios of all relevant forces acting on them are identical (Berthier and Silberzan, 2010).

Moreover, the reduction of size makes the *frictional* forces gain influence compared to the *inertial* ones; this is the reason why **laminar flow** is easily formed in microfluidic channels.

Another point to be considered is molecules **diffusion**. When two soluble materials are put into contact, they mix through the action of molecular diffusion. Fick proposed the linear relation between the rate of species transport and the local concentration gradient, and it is simplified by the formula

$$J_A = -D_{AB}\nabla C_A$$

Where J_A is the *diffusive flux* (units of mass per unit area per unit time), C_A is the mass concentration, and D_{AB} is the *diffusion coefficient* of solute A in solvent B, also known as the intrinsic chemical diffusivity. The equation is known as *Fick's first law*.

In condensed phases, diffusion occurs by jumping and replacement of atoms mechanisms, so it is highly dependent from temperature. Diffusion coefficient often follows the Arrhenius-like relation, so it can be written as

$$D_{AB} = D_0 exp\frac{-E_D}{RT},$$

where E_D is the activation energy for diffusion, R is the gas constant (8.31 J/mol K), and T is the absolute temperature.

When viscous dissipation is negligible, the diffusion equation can be compared to the energy balance equation, and so the analogy with heat conduction can be made. Thus, the characteristic time for diffusion t_D is related to the characteristic length scale L by

$$t_D = \frac{L^2}{D_{AB}}.$$

So the time required for the diffusion of a molecule decreases as the square of the characteristic length. For this reason diffusive heat and mass transfer at the microscale enable fast media and environmental changes added to fast temperature control.

1.1.2 FLUID DYNAMIC GOVERNING EQUATIONS IN MICROFLUIDICS

Fluid dynamics concerns the description of how fluids move as an effect of applied forces. The way fluidic systems can rather quickly reach length scales, where the fundamental fluid physics changes dramatically, is noticeable. In fact, mass transport in micro fluidic devices is generally dominated by viscous dissipation, while inertial effects are generally negligible. Since inertia

provides the non-linearity that is responsible for numerous instabilities and for turbulence itself, the **Navier-Stokes equations** (derived from Newton's second law of motion) simplify the microdomain. Before introducing the fundamental equation governing the dynamics of fluids, some concepts need to be explained, such as the kinetic field concerning the velocity of a fluid, the **Continuity Equation** and the **Newton Equation** for viscous fluids (Berthier and Silberzan, 2010) .

In order to study the dynamics of fluids it can be useful to choose a specific element of fluids, called *fluid element* or *fluid particle*, and its velocity. What we should keep in mind is that a liquid has no definite shape, and each point can move quite independently from the others. This can be solved by defining a vector field, called *kinetic field*, v(x,y,z,t) having the following meaning: v(x,y,z,t) is the velocity of the fluid particle, which is at position (x,y,z) at instant t.

A velocity change (acceleration) can be expressed in differential terms as

$$dv = \frac{\partial v}{\partial t}dt + \frac{\partial v}{\partial x}dx + \frac{\partial v}{\partial y}dy + \frac{\partial v}{\partial z}dz.$$

If we introduce the operator (· grad), the same will become

$$\frac{d\vec{v}}{dt} = \frac{\partial \vec{v}}{\partial t} + (\vec{v} \cdot grad)\vec{v}.$$

On the left side, the velocity is written using the *Lagrangian* approach, which investigates the motion of a fluid by following the motion of a specific fluid element. Whereas on the right side the *Eulerian* (kinetic field) approach in used. As we said before, the kinetic field associates a velocity vector to every point of space and time, corresponding to the velocity of the liquid element in that point and at that time. In conclusion it is possible to evaluate the velocity of a specific fluid particle, once the kinetic field has been identified.

The *mass continuity equation* states that mass can enter or exit a volume only if the density of the fluid in that volume respectively increases or diminishes.

The mass flowing through a surface in the time unit is

$$\int_{\Gamma} \rho\, \vec{v} \cdot d\vec{\Gamma},$$

being Γ the surface, ν the velocity and ρ the fluid density. This can be written as follows, using the Divergence Theorem

$$\int_{\Gamma} \rho\, \vec{v} \cdot d\vec{\Gamma} = \int_{V} div(\rho\, \vec{v}) dV,$$

equaling that to the other way of writing the mass change, which is

$$-\frac{\partial}{\partial t}\int_{V} \rho\, dV.$$

If we use the hypothesis that V does not change in time, we can easily deduce as follows

$$\frac{\partial \rho}{\partial t} + div(\rho \vec{v}) = 0,$$

simplified with constant density it becomes

$$\mathrm{div}\vec{v} = 0.$$

Viscosity is the macroscopic effect of the energy dissipation, which is caused by internal friction during motion. It is responsible for the *no-slip condition* whenever a solid-liquid interface is created, in the sense that there is no relative velocity. Newton equation for viscous fluids says that the shear stress (i.e. tangential force per unit surface) applied by a fluid on a surface is proportional to the derivative of fluid velocity, if calculated in a direction orthogonal to the surface

$$\vec{\tau} = \eta \frac{\partial \vec{v}}{\partial n}.$$

The proportionality coefficient η, is called *dynamic viscosity*. Its units are: N· sec/m^2.

At this point, the Navier-Stokes equation can be introduced. Considering the force acting on V, the sum of forces exerted by the external environment through Γ (surface forces) and those

directly applied to V (volume or mass forces), the Second Law of Dynamics can be written as follows

$$-\int_{\Gamma} p\, d\vec{\Gamma} + \int_{\Gamma} \vec{\tau}\, d\Gamma + \int_{V} \rho\, \vec{f}\, dV = \int_{V} \rho\, \vec{a} dV,$$

where f represents mass forces (e.g. gravity, magnetic forces, etc.). The minus sign before the pressure surface integral comes from pressure, being conventionally taken as positive if pushing. Pressure and shear stresses are integrated over the surface (Γ), whereas body forces and inertial forces are integrated over the volume (V). This suggests that, as we shrink down the geometry of a given system, pressure and viscosity will be the dominant effects, which will mutually balance. Using the Green's formula and the Divergence Theorem, the last equation is equivalent to

$$\frac{\partial \vec{v}}{\partial t} + (\vec{v} \cdot grad)\vec{v} = -\frac{1}{\rho} grad\, p + \frac{\eta}{\rho} \nabla^2 \vec{v} + \vec{f}$$

In the field of micro fluidics, inertial forces can be considered negligible if two conditions apply simultaneously:

1. The flow regime is stationary: $\partial v / \partial t = 0$;

2. The flow is not position-dependent: $(v \cdot \text{grad})v = 0$.

If inertial forces are zero, as in the case of fully developed stationary or otherwise space invariant flow, or negligible compared to viscous body forces, the Navier-Stokes equation can be simplified as

$$\eta \nabla^2 \vec{v} + \vec{f} = grad\, p$$

Neglecting the viscous term, flow is governed by the Stokes equation that can be solved for various shapes of microchannels. In the case of cylindrical ones, a parabolic flow arises so that

the relation between pressure and flow rate is described by the **Hagen□Poiseuille equation** below

$$Q = \frac{\pi r^4 \Delta p}{8\eta l}$$

where Δp is the pressure drop between the two ends of the channel, l is the total length of the channel, Q is the volumetric flow rate, r is the radius of the channel and η the dynamic viscosity of the liquid. In the case of a planar channel with a very small height h compared to the width w (h<<w), the solution of the Poiseuille flow results as

$$Q = \frac{wh^3}{3\eta l}\Delta p$$

An electrical analogy can be made. The average flow rate of a liquid within a micro or nanofluidic channel is proportional to the pressure gradient imposed at both ends of the capillary. As a consequence, the Hagen□Poiseuille equation can be rewritten as a classical Ohm's law

$$\Delta p = R_{fluid} \cdot Q$$

Fluidic resistance will depend on the geometry of the cross section. Moreover it can be calculated for micro and nanofluidic networks by using the same method used for electrical circuits, for example using the classical Kirchhoff equations (Plecis and Houssin, 2015).

For complex micro□nanofluidics networks, or when viscous liquids are used, the *effective section* can be derived from the fluidic resistance calculation. The effective section is used to calculate the typical pressure drop as a function of the flow rate. The equation is as follows

$$S_{effect} \approx \sqrt{\frac{8\eta_0 L_0}{\pi R_{total}}}$$

with L_0=1 cm and η_0=8,90 $\cdot 10^{-4}$ Pa·s (Plecis and Houssin, 2015).

1.1.3 DIMENSIONLESS NUMBERS

To analyze the different physical phenomena it is useful to refer to some dimensionless numbers, those do not depend on the geometric size of the device, and express the relation between forces. The numbers used in microfluidics are reviewed elsewhere (Squires and Quake, 2005), here the most important are summarized.

- Reynolds number (Re)

Express the relation between the inertial forces to the viscous forces

$$Re = \frac{vD\rho}{\eta} ,$$

where v and D are a typical velocity and a linear dimension of the problem, whereas ρ and η are respectively the *density* and the *dynamic viscosity* of the fluid. Microflows have Re<2000, therefore they are intrinsically *laminar* because the dynamic forces acting on the fluid are not sufficient in order to initiate turbulence. The Figure 1.2 shows scaling exponents for forces of actual interest in the design of Microsystems.

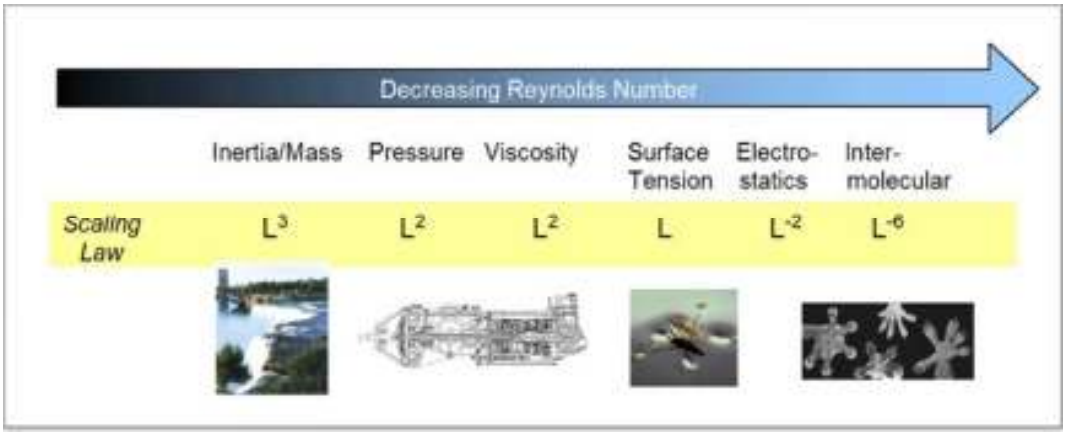

Figure1.2: Scaling exponents.

- Péclet number (Pe)

  Express the relative importance of convection to diffusion. Considering a T-junction (Figure 1.3) in which two different fluids are injected to flow alongside each other, imagine we want to calculate the distance where the fluid is completely mixed. Being D the diffusivity and ω the width of the channel, the time for the particles to diffuse is $\tau_D \sim \omega^2/D$. During this time, the fluid will have moved a distance $Z \sim v\omega^2/D$. So Pe number is defined as

$$Pe \equiv \frac{v\omega}{D} \sim \frac{Z}{\omega} \quad .$$

  This number can be used in sensing and separating techniques based on differences in solute diffusion rates (Squires and Quake, 2005).

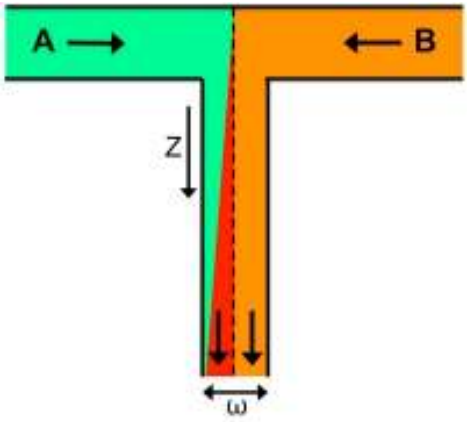

Figure 1.3: T-junction.

- Capillary number (Ca)

  When immiscible fluids enter in contact, there is a new force, named *surface tension (γ)* that affects the dynamics of the free surface. This is the reason why a thin central stream of water breaks into drops, causing the effect known as **Rayleigh-Plateau instability**. Following the same principle, microfluidic devices can be used to create controllable water–in-oil droplet emulsions within T-junctions. The two competing

forces are the capillary stresses (γ/R) and the viscous stresses (ηv/h). The characteristic droplet size is

$$R \sim \frac{\gamma}{\eta v} h = \frac{h}{Ca} \quad .$$

The capillary number (Ca) is the dimensionless parameter

$$Ca \equiv \frac{\eta v}{\gamma} \quad .$$

In microfluidic devices, due to the high surface-to-volume ratio, the surface tension effects become extremely important, especially talking about free surfaces deformations and liquid motion or confinement. To do so, it is possible to act on hydrophilicity/hydrophobicity of surfaces (Squires and Quake, 2005) (Figure 1.4).

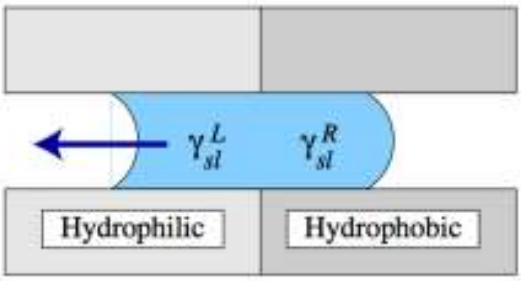

Figure 1.4: Water behavior at the hydrophilic/hydrophobic interface. Adapted from (Squires and Quake, 2005).

- Weber number (We)

It is used to predict the disruption of an interface. In fact it expresses the ratio between inertial forces and surface tension forces

$$We = \frac{\rho v^2}{\gamma / R} = \frac{\rho v^2 R}{\gamma},$$

where the numerator is a dynamic pressure and the denominator a capillary pressure. It can be used in droplet microfluidics to calculate the ratio between forces able to maintain a single droplet as a unique entity (Berthier and Silberzan, 2010).

- Weissenberg (Wi) and Deborah (De) numbers are instead related to the relative effects between fluid flow and polymers behavior. They are characteristic of non-Newtonian flows, where the viscosity of a fluid depend not only on temperature and concentration, but also on internal stress (like in polymers and body fluids) (Berthier and Silberzan, 2010). Hence, in more dense fluids, Reynolds and Péclet numbers needs to substituted by Grashof (Gr) and Rayleigh (Ra) numbers respectively (Squires and Quake, 2005).

1.2 Lab-on-a-chip technology

Many opportunities of microfabrication technology derive from the ability to fabricate a wide variety of systems ranging from microanalytical devices (Tian et al., 2015) and micro-volume reactors (Gemoets et al., 2015; Lin et al., 2009) to microelectromechanical systems (MEMS) (Puleo et al., 2007). In the past twenty years, a number of miniaturized total chemical analysis systems (μTAS) have been developed to integrate on the same platform different sample-handling steps. The major advantages of these devices are the small quantity of reagents, and the related short analysis time together with the automatization, parallelization and a better efficiency. Moreover it is possible to generate a large number of experiments with different individual conditions, so that a wide range of parameters can be explored.

These microdevices can be useful both as chemical and biological tools; for example high-speed DNA sequencing (Bashford et al., 2008; Liu and Mathies, 2009) and polymerase chain reaction PCR (White et al., 2011; Zhong et al., 2011) can be performed on chip as well as synthesis and characterization of libraries of peptides (de la Rica and Matsui, 2010; Kogot et al., 2011) and oligonucleotides (O-Charoen et al., 2007). Bontoux *et al.* developed a device,

which extracts total mRNA from a single human stem cell to perform gene expression profiling (Bontoux et al., 2008). A similar device was developed by Marcus *et al.* (Marcus et al., 2006). Compact platforms integrating simple readout can be used to detect environmental pollutants, hazardous pathogens (analytes) but also carbohydrates, proteins, disease markers, drugs or other small molecules. Therefore, fast and highly specific **biosensors** (able to detect biomolecules such as proteins, DNA and enzymes) with a low detection limit and an improved signal-to-noise ratio can be fabricated (Situma et al., 2006). Generally speaking, two principal recognition units, such as metal-ions and antibodies-binding peptides, can be distinguished. Furthermore, some peptides can act as target-specific transducers: the electrical signal can be measured as a function of the crystal growth catalyzed by the metal-binding peptide or metal ions can be detected by changes in the conductivity of the peptide-based substrate (de la Rica et al., 2011).

Microfluidics demonstrated to be powerful tools also in the chemical-pharmaceutical field. For example microfluidic chromatography can be exploited to investigate the best parameters, such as the adsorbent and buffer type, pH, and flow rate in the separation process. With this purpose, few years ago Shapiro built a column with polydispersed agarose beads to quantify protein-binding capacity (Shapiro et al., 2009). His group also used a modeling approach to further understand and describe biological species behavior (Gerontas et al., 2013). Moreover, electrophoresis (Abdul Keyon et al., 2014; Huang et al., 2008; Jubery et al., 2014; Mohanty et al., 2009; Saucedo-Espinosa et al., 2015) and genomics (Maercker, 2005) are some of the most important applications of microfluidics together with the possibility of running miniaturized assay so as to develop new diagnostic tools (Lei, 2012).

Therefore, the technology behind these bioplatforms integrating microengineered components, know as **Lab-on-a-chip** and Biological/Biomedical Micro Electro Mechanical Systems (**BioMEMS**), thanks to its high efficiency and reproducibility, is more and more present in

research laboratories and some of them already began to be commercialized. This is particularly true for the so-called point-of-care devices, useful for relatively simple diagnostic tests needed in everyday clinical practice (Lei, 2012; Tian et al., 2015).

Finally biological cells can be cultured on the so called cells-on-a-chip to study cell-cell and cell-matrix interactions. Different analysis can be performed to observe cell type autocrine (signaling factors affect the secreting cell itself) and paracrine (signaling factors affect other types of cells) signaling or to test drugs effects. Moreover, intracellular activities and analytes can be detected and analyzed. Next paragraph will focus on these microfluidic cell cultures, leaving to this one the role to explain all the elements that can be integrated on the platform depending on the specific application. A new generation of **valves, pumps, electrodes, channels and sensors**, exploiting different physical principles, is continuously fabricated and embedded on these devices (Weibel et al., 2005) , enabling an high resolution control of flows and chemical gradients (Hulme et al., 2009), and fast detection and manipulation techniques. Scholten *et al.* recently fabricated a microoptofluidic detector for volatile organic compounds (Scholten et al., 2014). Lee and coworkers (Lee et al., 2013a) fabricated instead an advanced combinational multiplexer able to address up to 19 fluidic channels, whose most immediate application is a series of dynamic pressure generators. Some of these elements can be also used to fabricate inegrated **mixers** when homogenization of flow is required; in fact, laminar flow produces relatively slow diffusive mixing.

It is possible to integrate them in microfluidic devices using soft-lithography (Hulme et al., 2009). PDMS can be used to fabricate integrated microvalves and other components (Ng et al., 2002) thanks to its low Young's Modulus (McDonald et al., 2000). Also hydrogels can be used to fabricate responsive elements, like valves with an improved time response (Beebe et al., 2000).

Electrode integration inside the device can generate localized electric fields using small voltages.

Nowadays challenge is finding effective fluid handling methods, to reduce reagent consumption, which often negatively balance microfluidics small volumes. Monitoring, actuating and controlling tools were created and are going to be developed in the next years, supported by a market, which is going to grow exponentially.

Soft-lithography has shown to be well suited to fabricate microstructures for biological applications as well, allowing to pattern and manipulate cells and molecules and to fabricate channels able to exploit microfluidic principles (Whitesides et al., 2001). The relatively large features used in biology make them rapid and inexpensive as well.

1.2.1 FLOW CONTROL AND MANIPULATION

There are different classes of systems able to control liquid motion in microfluidic and nanofluidic devices. Some of them like the hydrostatic or pressure generators, privilege controlling the flow rate through pressure difference, whereas syringe pumps directly impose a flow rate. Finally, liquid pumps and electro-osmotic pumps generate a liquid flow based on the fluidic resistance of the device.

Hydrostatic pressure is the simplest way to generate controlled flows in a micro fluidic system. In fact, the variation of altitude in the liquid relative to atmosphere interface causes a pressure difference. The major drawback of this technique is its limited resolution, in addition to a limited maximum pressure. For example, as for water-based liquids, where the difference of 1 cm corresponds to 1 mbar, the maximum resolution is 0,1 mbar and the maximum pressure is 100 mbar. Furthermore, the affinity between the liquid, the atmosphere and the reservoir shape has an effect on Laplace pressure, developed at the interface between air and liquid. This unpredictable overpressure represents an obstacle to predictions and a huge problem in

hydrophobic or hydrophilic reservoirs, thus showing a narrow cross□section. Finally, another limitation of this type of pressure control is the linear decrease of pressure drop with time, caused by liquid flow through the reservoir.

In pressure *generators* a compressor acts as pressure source. In the simplest pressure generator there are also a static membrane, pressure regulators and a manometer to monitor the pressure value. Good compatibility of all the components highly affects the robustness and precision of these systems. The major drawback is the response time that is limited by the mechanic deformation of the membranes. To quickly change the pressure (few μs), several pressure generators together with a computer-controlled multiplexer can be used. Another possibility is to control the pressure using a set of electrovalves, electronically regulated by a pressure sensor. The above-mentioned technology exploits the fast response allowed by micro valves. The major drawback is the fluctuating pressure, which is generated by an alternative opening of the positive pressure, so that the faster the system will be, the higher these fluctuations will go. This type of pressure regulator needs to be chosen every time sophisticated pressure patterns are required (e.g. gradient or sinusoidal pressure variation), despite being troublesome as compared to static pressure regulators in case of overpressure.

Syringe pumps were the first flow controller used in microfluidics. This idea was taken from perfusion systems and medical field. Since the pressure is automatically adapted in order to maintain a fixed flow rate, syringe pumps show the capability of controlling the flow rate across micro channels independently from the fluidic resistance, which is their main advantage. The major drawbacks of syringe pumps are the development of pulsatile flows at low flow rates, and the time required to stabilize the effective flow rates when compliance of the tubing is not negligible. For example, when a 10 cm-long tube having a diameter of 0,5 mm shows a 0,1% change in its internal diameter because of the pressure rise, 1 min is necessary to obtain 66% of the final flow rate (5 min to get 99% and 10 min to get 99,99%).

Liquid pumps cannot be modelled as perfect flow-rate generators, as backpressure lowers the flow rate. A wide range of technologies can be used. Peristaltic pumps show the main advantage of using interchangeable flexible tubes, limiting contamination problems and a large versatility; piezoelectric pumps, on the other hand, are the most compact pumps and can be used for intermediate flow rates (μL). Their control necessitates the constriction of the pump to a flow rate sensor, while fluctuations need to be observed for low flow rates. High-performance liquid chromatography pumps (HPLC) integrate all these components, while minimizing the fluctuations, but they are costly.

Electroosmotic pumps do not have fluctuation problems, as they are based on the electrical pumping of liquid through nonporous materials. Although they withstand larger backpressures, these systems need to be worked out with low conductivity liquids and are hardly reproducible (Wang et al., 2009).

In micromanipulation the adhesion force is undoubtedly greater if compared to the gravitational force. Thus, a stronger force is needed in order to control fluid motion. *Capillary force* can be defined as the forces between two solids, which are linked together by a liquid bridge (meniscus). It is possible to control them through different parameters, such as surface tension, contact angles, size and geometry of the solid surfaces, separation distance, volume of the liquid and tilt angle between surfaces. The force is directly proportional to the surface tension and it decreases as a function of the contact angle. Nevertheless, a non-linear effect should be observed: an increase of the surface tension will lead to a larger contact angle, and therefore to a smaller force. If volume of the liquid and angles are the same, the meniscus geometry will remain unchanged, provided that difference in pressure will proportionally change. Furthermore, a contact angle hysteresis can be observed. When the meniscus moves forward along a solid, the corresponding contact angle (advancing) is larger than the receding one observed when the meniscus moves backwards. Obviously, by increasing the separation gap,

capillary force exponentially decreases. On the other hand the geometry can be used to modulate this force, and tilt angle adds a degree-of-freedom. In some cases, the volume of liquid modifies the force. If that, evaporation can be exploited. Finally a capillary shear force acts, but it has been calculated that it is an order of magnitude smaller than the "main" one (Walker and Beebe, 2002). In addition, capillary forces can be used to manipulate and transport fluids with free surfaces. The balance between interfacial forces is kept balanced, but it can be actively destroyed if these energies are modified, thus causing fluid motion. Capillary manipulation of microfluids has been achieved either by modifying the solid-liquid surface tension, for example in electrowetting, surface gradients creation, with reactive flows, or by inducing a gradient in the liquid-gas surface tension. The latter includes thermocapillary, electrocapillary, and solutocapillary motion (Mohanty et al., 2009; Nikolov and Zhang, 2015; Songok et al., 2014).

1.2.2 MICROFLUIDIC APPLICATIONS

Microfluidics can be used for different purposes (Haeberle and Zengerle, 2007). Some examples are hereby shown:

- **Chemical synthesis.** Microchannel devices can be constructed to obtain microreactors. They are usually continuous flow reactors, through which chemical reactions can take place in confinement with dimensions below 1 mm. Together with other devices - such as microheat exchangers - they can be used for micro process engineering to host physical processes, with some advantages such as higher efficiency, speed, safety, reliability, scalability, on-site production and finer control (Larrea et al., 2015; Murzabaev et al., 2015; Yang et al., 2015).
- **Separation and analysis.** Reaction products often contain multiple chemical components. This is the reason why it may be interesting to be able to subsequently

separate and identify the individual species. Electrophoresis method is used with this aim. It consists in introducing detectable differences in the migration behavior between either charged or not charged components, through the application of an electric field. The technique needs relative simple hardware design and it is compatible to biological macromolecules such as DNA and proteins.

- **Biodetection**. The aim is the miniaturization and parallelization of classical immunologic and genomic detection assays. Biodetection can be used to precondition a sample where different reactions can take place, such as matrix change, cell lysis and purification. Moreover they can be used as biosensors in which the presence of the target analyte is transformed into an electrical or optical signal. The major detection technologies are based on real time PCR and enzyme or on classic ELISA immune-sensors (Bai et al., 2015; Brennan et al., 2014; Liu et al., 2011).
- **Single-cell biology**. Microfluidic devices enable parallel processing plus fast media and temperature changing. Due to the effects of laminar flow, precise and localized spatial control of liquid composition at subcellular resolution for single-cell handling and analysis is also possible (Chen et al., 2015; Huang et al., 2008).
- **Microdroplets.** In the so-called digital microfluidics, laminar flow can be exploited to facilitate the generation of monodisperse droplets for multiphase flows. The complex dynamics behind droplet formation and transport is well explained by Baroud *et al.* (Baroud et al., 2010). Emulsions can be used for nanoparticle synthesis, drug and active substances microencapsulation. Electrowetting can be used to manipulate independently fair controllable droplets (Chatterjee et al., 2006; Seemann et al., 2012; Song et al., 2006; Tan et al., 2004; Teh et al., 2008; Zeng and Korsmeyer, 2004).
- **Microfluidic rheology/rheometry.** Low Reynolds numbers enable to properly investigate viscous liquids and their non-linear viscous effects. Microfluidic rheometry

systems provide an alternative to conventional characterization methods. The study on fluids transport across micro□nanofluidic porous media is also of extreme interest. Finally the slip velocity at the solid-liquid interface can be investigated using microfluidic devices, together with particle velocimetry techniques (Aufderhorst-Roberts et al., 2014).

- **Optofluidics.** Optofluidics refers to manipulation of light through the use of fluids, or vice versa. Exploiting the microfluidic manipulation, optical properties of the fluids can be precisely and flexibly controlled in order to realize reconfigurable optical components, otherwise difficult or impossible to implement by solid□state technology (Mao et al., 2015; Scholten et al., 2014; Tung et al., 2012).

Microfluidics show some drawbacks explained hereby. First of all, it is not suitable for applications requiring fast homogenization of flow, unless integrated mixers are used. The reason is that laminar flows are used, and they only produce relatively slow diffusive mixing. In addition, a current lack of methods for fluid handling limits the small reagent consumption theoretically reachable. Moreover, changes in scaling can give difficulties in adaptation of biological protocols to fit experiments in microsystems. However, a careful comparison between data obtained in macroscopic experiments and data obtained in microsystems is required (Truskett and Watts, 2006).

1.3 Microfluidic cell cultures

Microfluidic represent an efficient method to fabricate devices suitable to recreate *on-a-chip* cellular microenvironment. This can be applied in the **tissue engineering** field, whose oldest issue was restoring, maintaining and enhancing tissue and organ functions, even though nowadays expanded to cells behavior studies *in vitro*. Tissue engineering research includes

different areas, from biomaterials design to functionalization with biomolecules, whose study is now possible at reduced dimensions, thanks to the *cell-on-a-chip* field.

Massive parallel processing, spatial control of liquid composition at subcellular resolution, fast *media* and temperature changes, and single cell handling and analysis are the major advantages that a microfluidic culture can offer (Velve-Casquillas et al., 2010); the parallelization of chambers (Chung et al., 2009; Khademhosseini et al., 2006) is just another example. Petri dishes or well plates can be coupled to a perfusion system, but this is only useful in case of adherent cells, and for those cells where secreted factors can be flushed away. Microfluidics may provide promising solutions to extend the application area. Dynamic infusion of media can be used for experiments lasting several days or even weeks (Tourovskaia et al., 2005) (Kobel et al., 2010). Diffusion between the feeding channel and the channel containing cells can be exploited. In fact, cells need to be maintained under perfusion in physiological condition (temperature, pH, CO_2). As said before, these advantages are opposed by some drawbacks regarding the difficulties in adapting biological protocols to microsystems. Anyway, once proved the efficiency of the device, microfluidics offer more advanced analysis methods better suitable to the intrinsic characteristic of the new system. This is further strengthened by the power of these platforms to recreate physiological microenvironments, in order to carry out high-throughput clinically relevant screenings (Lei, 2012). As a consequence, en early diagnosis of diseases can be achieved. Moreover, a new generation of biomaterials with finely controlled properties can be exploited (Barata et al., 2015).

Therefore, it comes out how the first and most important feature in single-cell analysis is **cellular microenvironment control**; in fact, depending on external biochemical and biomechanical signals, cells are extremely complex and dynamic entities, constituting a *heterogeneous* system. Understanding the complexity of their environment may help to better reproduce physiological *in vivo* conditions.

Cellular microenvironment is characterized by both **chemical and mechanical parameters**. First of all cells receive chemical stimuli from soluble molecules within the medium, secondly the extracellular matrix (ECM) composition and proportion provide different mechanical forces (stiffness, substrate topography, mechanical stress, shear stress). The molecular mechanism by which cells "sense mechanical forces and convert them into changes in intracellular biochemistry and gene expression" is called **mechnotransduction** (Ingber, 2008). Mechanochemical transduction mechanism proceed simultaneously, producing responses, and the reason should be found in the presence of isometric tension (prestress) within the interconnected networks constituting cells and their environment at all scales. Further analysis need to be done in understanding and modeling of tensionally integrated (**tensegrity**[1]) systems of mechanochemical control. Integrins [2], sometimes colocalized with ion-sensitive channels (ENaC family and Ca^{2+} channels), can be viewed as critical mechanoreceptors, while focal adhesions[3] as nanoscale mechanosensory organelles. Since cells use tensegrity to stabilize themselves, mechanical signals can be transmitted through discrete load-bearing cytoskeletal[4] elements; moreover wave propagation higher speed, compared to chemical diffusion, make them faster then chemical signals (Ingber, 2008). These discrete networks, composed by support elements, provide the transmission of mechanical forces along specific paths; hence stresses can be focused or concentrated on distant sites at different size scales. Furthermore, the necessary concentration to determine a biochemical change needs to be reached (Ingber, 2006). For example, cells elongation and polarization are processes controlled by

[1] TENSEGRITY: network composed of opposing tension and compression elements that balance each other and thereby create an internal prestress or resting tension that stabilizes the entire structure.

[2] INTEGRINS: specific cell surface receptors, which bind to collagens, glycoproteins, and proteoglycans of ECM.

[3] FOCAL ADHESIONS: macromolecular anchorage complexes on the inner surface of the cell membrane, where the integrins are mechanically coupled to the ends of the contractile acto-myosin filaments.

[4] CYTOSKELETON: internal molecular framework composed of actin microfilaments, microtubules and intermediate filaments that give shape to the cell.

mechanosensing; in particular they are a function of matrix rigidity and focal adhesions assembly (Prager-Khoutorsky et al., 2011). Balaban *et al.* (Balaban et al., 2001) used a PDMS micropatterned substrate combined with fluorescence imaging technique to measure forces applied by cells and understand molecular mechanisms of mechanosensory response. Lutolf and Blau (Gilbert et al., 2010) observed instead how muscle stem cell cultured on soft hydrogel substrates, thus mimicking the elasticity of muscle, contributed to tissue regeneration.

As said above, microfluidics allows both locally address parameters of the cell microenvironment and the ability of changing these parameters dynamically and automatically, due to the speed of the physicalprocesses at the microscale and the different automation possibilities. Engineered hydrogels are the extremely useful to mimic physiological ECM (Verhulsel et al., 2014) (Sant et al., 2010). It is also possible to integrate both hydrogel and PDMS into a hybrid technology mimicking 3D cellular environment, which is a fundamental step in the cellular behavior investigation (Velve-Casquillas et al., 2010). Lee *et al.* (Lee et al., 2006), for example, fabricated a matrix of aligned collagen fibers for endothelial cell culture and Lutolf *et al.* (Lutolf and Blau, 2009) used PDMS structures with proteins grafted through "microcontact printing" technique to recreate cellular *niches*[1] (Ranga et al., 2014). Derda *et al.* (Derda et al., 2011) studied cellular migration by creating alternate hydrophobic and hydrophylic areas on paper sheets while Karp *et al.* (Karp et al., 2007) made polyetilenglicole (PEG) platforms for stem cells analysis.

Concentration gradients can be generated within microfluidic channels with fine spatiotemporal resolution (Juncker et al., 2005), thereby mimicking natural microenvironment in cell differentiation, proliferation and migration processes. For example, molecular gradients can be exploited to study morphogenesis and chemotaxis within cellular microenvironments

[1] CELLULAR NICHE: 3D instructive cellular microenvironment that involves a dynamic interplay between biochemical and mechanical signals provided by the ECM, cell-cell interactions and soluble factors Lutolf, M. P., and H. M. Blau, 2009, Artificial stem cell niches: Adv Mater, v. 21, p. 3255-68.

(Kim et al., 2010; Moussavi-Harami et al., 2015). Microscale gradient generators (MGGs) have been used for cell growth and differentiation, chemotaxis, migration, cellular response to virus, and yeast gene expression under gradients of pheromone studies (Velve-Casquillas et al., 2010). These conventional methods were mostly based on hydrogels like fibrin, collagen or agarose. In microscale gradient generators (μGGs) (Figure 1.5), besides the laminar nature of flows, cells can be individually stimulated through growth factors (table 1), cytokines and chemokines (Borish and Steinke, 2003). Reynolds number within these systems is generally below 0.1 and laminar flow allows precise calculation of mass transport as a function of time. Moreover the flow profile, calculated from parameters such as channel geometry, fluid properties and pressure drop, is characterized by constant streamlines, so that mixing may occur primarily by diffusion (Breslauer et al., 2006). Microfluidics enables the creation of a large spectrum of gradients, from time invariant to subcellular resolution gradients, and from continuous or discrete gradients to fast response dynamic gradients. Most of the μGGs use simple technologies, like single PDMS layer, and have been applied to generate concentration gradient of diffusible molecules to study bacterial chemotaxis (Mao et al., 2003) and cell migration in response to chemokines (Barkefors et al., 2008). Surface gradient of adsorbed ECM molecules was used to study the dependence of axon growth of neurons on the surrounding ECM composition (Dertinger et al., 2002). Laminar flow□based μGGs use diffusive mixing between two or more parallel laminar streams of different composition. The shape of the gradient based on laminar flows depends on the flow rate and on the time the streams stay in contact. Gradients generated in these types of devices will maintain their shape at constant flow rate. The simplest μGGs of this type are the T-sensors composed by two microchannels (Kamholz and Yager, 2001). These gradient generators have a small time constant but are reagent□consuming. Furthermore, the useful region is limited to a short portion of the channel, which generates only sigmoidal□shaped gradients in a direction

perpendicular to the flow. To overcome this limitation, additional inlets can be added to generate more complex flow profiles. An upgraded version of the T□sensor, the so-called premixer μGG (Jeon et al., 2000), splits and recombines inlet fluids before mixing them in the culture channel, and thus it can generate more complex gradients, such as smooth and step ones. Another upgraded version of the T□sensor is the universal μGG, which includes a series of walls to split the streams (Irimia et al., 2006). This configuration can generate many profiles of concentrations and can reduce dead volume but it is more complicated to describe mathematically. A major drawback of all laminar flow μGGs is the requirement for precise control of the flow rate. Others μGGs are not based on the properties of laminar flow. The flow-resistive μGG uses flow-resistive elements in order to eliminate convection around the cells. This kind of device allows passive diffusion of biomolecules through a flow barrier to generate gradients. The flow barrier can be a hydrogel, a nanoporous membrane (Abhyankar et al., 2006) or a microchannel. The hydrogel completely eliminates convection, whereas microchannels (which are easier to integrate) only minimize convection. In both cases these devices can generate steady□state gradients, moreover they can eliminate shear stress generated by flow and preserve the autocrine and paracrine signals, which are secreted by cells. They are finally able to generate gradients in hydrogels for 3D-cell culture. A major drawbacks of this kind of μGGs is their inability to create complex profiles, their large time constant compared to laminar flow μGGs and a more difficult fabrication technique (Velve-Casquillas et al., 2015). Also **temperature gradient** devices can be fabricated to analyze temperature dependent processes and reactions (Mao et al., 2002).

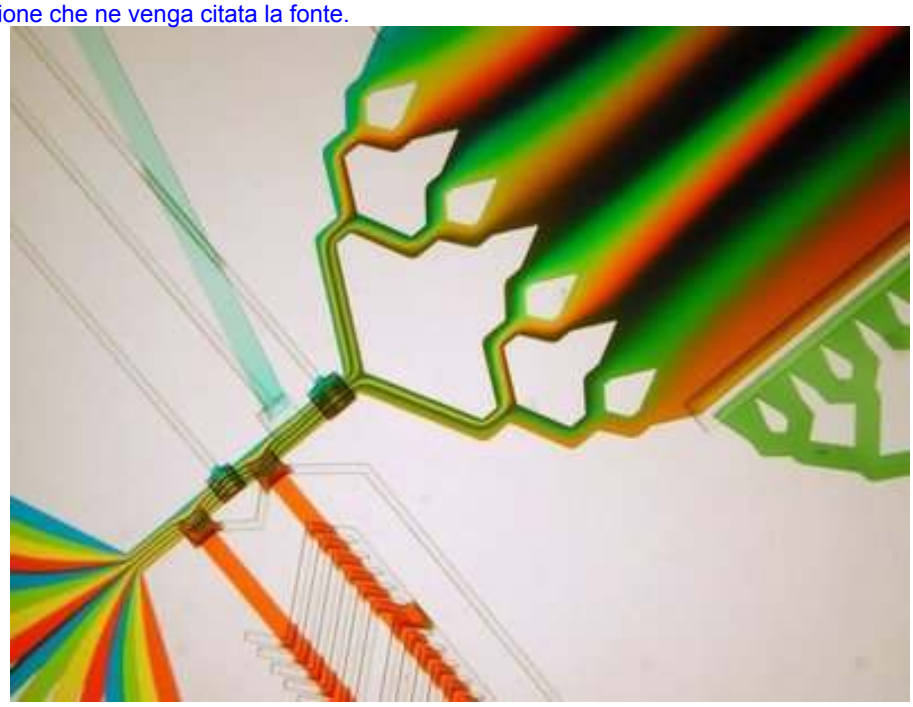

Figure 1.5: µGG from Albert Folch (University of Washington).

Table 1

GROWTH FACTORS: Growth factors are protein molecules which can activate cellular proliferation or differentiation binding to receptors on cell surface. They are produced by the body or by genetic engineering and can be versatile or specific to a cell-type. Their hormone-like function is stimulating or inhibiting growth, differentiation and chemotaxis as well by secreting diffusible factors in cells culture medium. Some examples are EGF, FGF, NGF, PDGF, VEGF, IGF, GMCSF, GCSF, TGF, Erythropoieitn, TPO, BMP, HGF, GDF, Neurotrophins, MSF, SGF and GDF. They act in autocrine, paracrine, juxtacrine or retrocrine manner. Hematopoietic ones are hormone-like substances that stimulate bone marrow to produce blood cells.

Depending on their sequence of aminoacids they can be classified into families, like insulin-like growth factor (IGF), multiplication-stimulating factor (MSF), sarcoma growth factor (SGF), transforming growth factors (TGFs), epidermal growth factor (EGF), nerve growth factor (NGF), fibroblast growth factor (FGF) and platelet-derived growth factor (PDGF). All of them are essential to normal cell cycle, mediate fetal development, play a role in maintenance and repair of tissues, stimulate production of blood cells but also participate in cancerous processes.

Single-cell analysis is a promising application based on the possibility to monitor the biological responses of sub-population of cells instead of usual bulk averages results. The opportunity offered by this strategy is a statistically significant analysis performed on individual cells, treated as single samples. On this purpose, cells micropatterning exploit different **entrapment techniques** to isolate and capture single cells, from chemical μCP cell immobilization, to microwells array (Lindström et al., 2009a; Rettig and Folch, 2005) and physical trapping. The latter is generally based on microfluidic pathways like hydrodynamic weirs and dams and is particularly used in case of non-adherent cells. Using this approach, Di Carlo *et al.* developed a device to automatically position single Hela cells on a glass substrate (Di Carlo et al., 2006); media can thus flow around the trapped cells. Single cell entrapment can be obtained also using trapping pockets, working thanks to drain channels connected to them (Noguchi and Yamaguchi, 2009). Burger *et al.* (Burger et al., 2011) designed an array of geometrical V-cup structures based on a magneto-hydrodynamic pumping entrapment principle. They were built on a centrifugal microfluidic platform and the mechanical actuator allowed the cell trapping at high rotational frequencies, while inducing hydrodynamic pumping recovery at low frequencies. Lee *et al.* (Lee et al., 2005) instead designed an array of traps to study cell□cell interaction between two different cell types to understand electrical transport mechanisms via gap junctions in soft membranes. Charvin *et al.* (Charvin et al., 2008) proposed a microfluidic device for bacteria cultures, using two layers of PDMS channel separated by a cellulose membrane. On the other side, chemical trapping can be obtained through proteins and antibodies surface-modified microchannels.

Droplet microfluidics find their application also in creating isolated subnanoliter volume cellular microenvinronment, allowing the compartmentalization of bulk samples (Niu and deMello, 2012). Droplet two-phase systems physically isolate cells in an aqueous microdroplet surrounded by immiscible oil (Figure 1.6); so that each droplet is an independent reaction

chamber with limited dilution of cellular contents and higher detection sensitivity. Therefore, power statistical analysis can be performed in parallel on a large number of samples relatively independent one from another. Schmitz *et al.* developed a microfluidic device, which was able to generate an array of thousands of droplets with embedded yeast cells (Schmitz et al., 2009), while Chabert *et al*. used droplet generator to isolate and encapsulate cancer lymphocyte cells from whole blood samples (Chabert and Viovy, 2008). This method can also be adapted for the encapsulation of single cells, and then measure the amount of molecules generated by the cell (Köster et al., 2008).

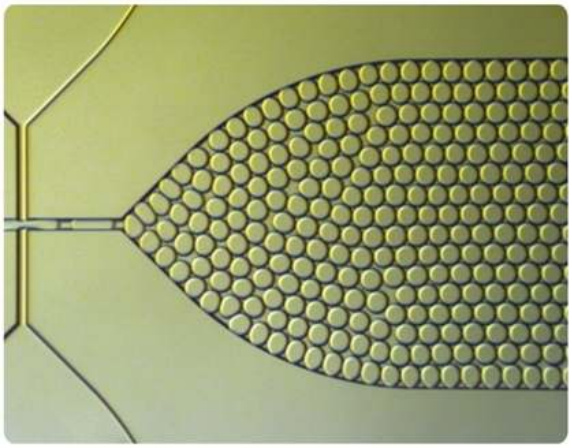

Figure 1.6: Oil-in-water droplets generated by Dolomite's Small Droplet Chip.

Positioning cells within the microdevices necessitates a strategy to move them without perturbing the analyte to be analyzed, so complex **manipulation techniques** can be exploited (Sims and Allbritton, 2007). Some examples are positive and negative dielecrophoresis (DEP), optical tweezers and capillary chromatography and electrophoresis (Huang et al., 2008). As a polarizable particle, when subjected to an inhomogeneous electric field, a cell is either attracted toward the higher field (pDEP) or pushed away from it (nDEP). Hence, dielectrophoretic tweezers can position a single cell in a threedimentionl space, while DEP electrodes can be used to create the desired biomimetic pattern (Müller et al., 2003). Some of them are based on

non-inertial forces, like the aforementioned DEP, but also magnetic, optical gradient, and acoustic primary radiation forces (Tsutsui and Ho, 2009); others, like gravitational and centrifugal techniques, exploit inertial ones (Burger et al., 2012; Strohmeier et al., 2015). More easily, sometimes non-invasive cell manipulation can be obtained by pressure control of the flow rate in separate channels. Finally, ultrasonic techniques are usually based on the creation of a pressure node, thanks to standing waves, that will attract/repel particles or cells (Mulvana et al., 2013). The operations that can be obtained are cell separation and sorting (Burger et al., 2012; Tsutsui and Ho, 2009), cell fusion (Chiu, 2001), purification, collection, counting and lysis (Burger et al., 2012; Tsutsui and Ho, 2009; Xu and Yin, 2011); furthermore particle ordering and separation, surface treatments at single-cell level and patch –clamp recording can be performed. The latter is a significant research tool for electrophysiology. It is performed by positioning the tip of a glass pipette against the membrane of a cell and applying negative pressure (Cheng et al., 2010; Ionescu-Zanetti et al., 2005).

Finally, **detection** methods are need for the analysis of interest. The most used are fluorescence-based; real-time dynamic monitoring, immunoassays and intensity measurements together with dequenching assays are examples of labeling fluorimetric methods. Chemiluminiscence is characterized by simple optical systems requiring no light sources. Amperometry instead is a really sensitive and selective electrochemical method based on the oxidation or reduction of electroactive compounds on the working electrode surface; the reaction can be directly correlated with analytes concentration (Huang et al., 2008). To measure forces, different principles need to be applied; for example, micromachined cantilevers or PDMS membrane patterned with arrays of elevated dots can be suitable to measure subcellular forces of single cells (Balaban et al., 2001).

Biological **analysis** includes prediction of efficacy and toxicity of drugs and their metabolism, chemotaxis, cell migration assays, individual responses analyzed in a statistically significant

fashion compared to the bulk averages, so that cellular heterogeneity can be observed in order to accurately predict system behavior. They include flow cytometry, electrophoretic analysis and quantification of cell contents, fluorescent-based analyses and single-cell PCR to name the principal tests carried out in research laboratories (Sims and Allbritton, 2007). Finally, these platforms can be observed under a microscope, enabling high resolution, long term, live-cell time lapse imaging and analysis (Frey et al., 2015) (Lee et al., 2011) (Skafte-Pedersen et al., 2012). Moreover, microfluidic components can be integrated within the devices to simplify the analysis of interest and avoid contamination (Lindström et al., 2009b) (Zhang et al., 2009a). In gene expression field, single-cell reverse transcriptase-polymerase chain reaction (SC-RT-PCR) has become an important tool for the determination of specific genes in heterogeneous tissues (Marcus et al., 2006). In the last years, digital PCR turned into the first method for nucleic acid quantification (Pavšič et al., 2015). Finally, traction force microscopy measure forces exerted by cells on their growth substrate; mechanosensors constructed on the dimensions of single cells makes it possible to perform direct measurements of the forces involved in single-cell adhesion and motility (Sims and Allbritton, 2007).

From single-cell on chip nowadays research is over and over moving to reproduce minimal functional modules called organs-on-a chip, which will be better discussed in the next chapters. Researchers are really interested in designing new microfluidic platforms and developing their cell-biology applications mostly because they show great promise for clinical diagnostics, high-throughput drug screening and cell migration studies.

Chapter 2

Microfabrication materials and techniques

Microfabrication is the process for the production of devices ranging from submicron to millimiter dimensions. Even though most of the research in microfabrication is focused in microelectronics, applications in different fields are rapidly emerging. In fact, in the last years, the types of devices and materials have widely increased. Most of them are fabricated using standard lithographic techniques from silicon bulk and surface micromachining (Zaouk et al., 2006).

The materials used to build these microsystems can be classified in rigid (silicon, glass, quartz, and some rigid organic polymers) and elastomeric materials (PDMS)(Qin et al., 1998).

The microfabrication technology comprises of different processes summarized below:

Wafer fabrication

Thermic oxidation

Lithographic process

Etching processes

Deposition processes

Bonding techniques

Microsystems packaging

Microtechnology develops and produces devices with different functions exploiting both "top down" and "bottom up" techniques (Figure 2.1).

A "top down" approach follows the breaking down of a system in gaining insight into its compositional sub-systems. After having first formulated an overview of the complete system, each sub-system is refined in greater detail, until reducing it to base elements. On the contrary, a "bottom up" approach is the piecing together of systems arising, layer by layer, to a bigger emergent system (Madou, 2011a). Top-down nanofabrication is principally based on lithography and traditional mechanical machining, and etching, whereas bottom-up nanochemistry is based on chemical synthesis and self-assembly. While top-down methods essentially impose a structure or pattern on a substrate, in self-assembly and self-organization thermodynamics makes molecular and atomic constituent organize in larger structures, therefore their potential is more based on the materials used. Chemical reactions are dominated by Gibbs free energy ($\Delta G=\Delta H-T\Delta S$) in creating and breaking bonds.

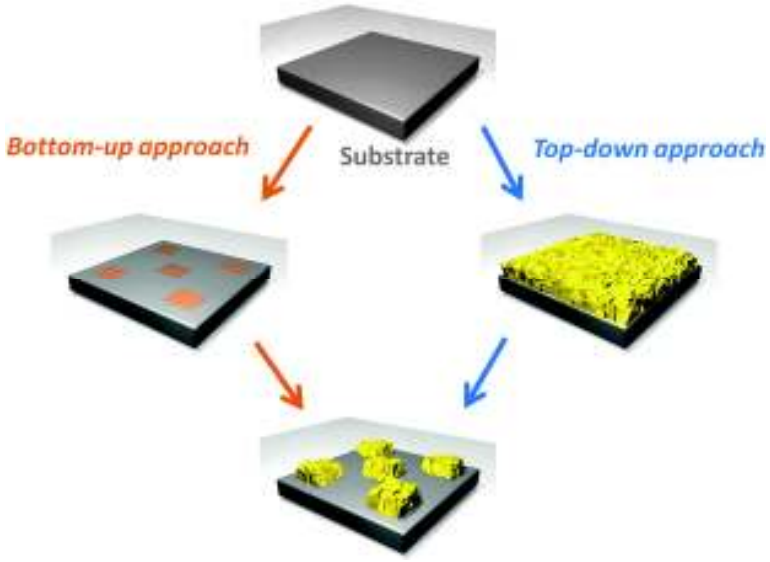

Figure 2.1: Bottom-up vs. top-down approach.

Starting from a silicon wafer, the silicon oxide is generally grown on its surface to be subsequently used during next processes. After the lithographic process, necessary to design geometric features on the external surface, further work is requested to transfer it to the underlying bulk. Addition techniques (deposition) or subtractive techniques (etching) can either be used. Subsequently bonding processes are generally needed to link different pieces or close opened cavities. Finally, after the packaging, the complete system will be ready to be used, except for sterilization or any other process required before its application.

2.1 Silicon

Silicon is a tetravalent metalloid, rarely present as a pure free element in nature. It is mostly distributed in oxides and silicates. In the semiconductor-device fabrication, Single Crystal Silicon (SCS) is needed. Here the atomic order is continuous and unbroken in the *crystal lattice*. This is the reason why SCS has anisotropic properties. That means that it is directionally dependent, so physical and mechanical properties are different when measured along different axes.

Crystallographic structure is a cubic lattice known as the diamond lattice structure (Figure 2.2 a) and the unit cell is made up of two interpenetrating FCC (face-centered cubic) lattices separated by 1/4 along each axis of the cell, following the direction given by Miller index (Zaouk et al., 2006). The lattice spacing at 300 K is 0.543 nm. Atoms are linked by covalent bonding, and the nearest neighbor distance at 300 K is 0.235 nm (Streetman, 1990).

To produce Single Crystal Silicon, first polycrystalline silicon (PS) has to be obtained from silicon materials. After that, PS is used for the epitaxial growth. Both Czochralski (CZ) and Float Zone (FZ) methods can be used, the former allowing cheaper technology and bigger

crystals production, the latter fewer impurities. In the end, pure cylinders of three or four inches of diameter are created. These cylinders are sliced into thin, high polished wafers (Figure 2.2 b) less then one-fortieth of an inch thick and usually silicon oxide is growth on their surface (Figure 2.2 c). The oxide layer is grown on the substrate by heating the silicon wafer between 900 and 1150 ºC in a dry or humidified oxygen stream of a tube furnace. This will be the substrate for microstructure production, where the elements are built in layers on the silicon wafer (Figure 2.2 d). Several chips can be etched onto each wafer. A primary and a secondary flat are given, thus indicating crystal orientation and doping (Bates, 2000).

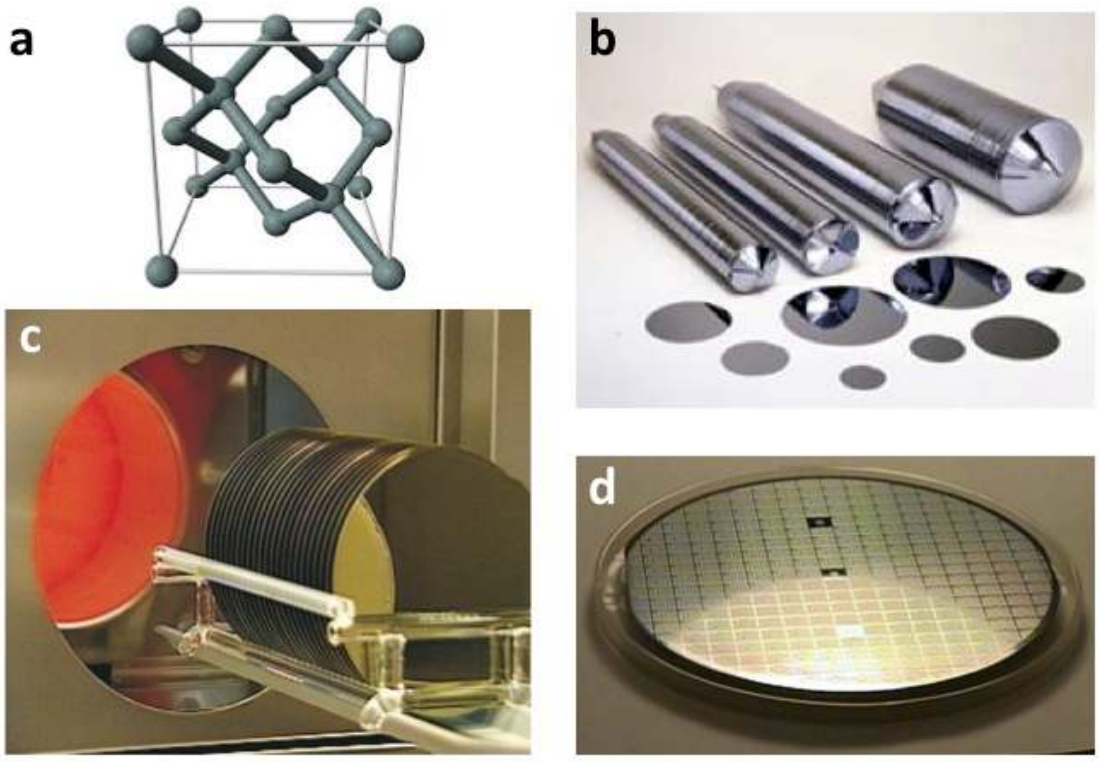

Figure 2.2:a) Silicon diamond lattice structure; b) mono-crystalline silicon ingots and wafers; c) oxidation of silicon wafers; d) multiple features patterned on a single silicon wafer.

Mechanical properties also change along with crystallographic directions. In addition, Young's modulus and stiffness are functions of doping and impurities. Young's modulus (E) is more influenced by crystallography than shear modulus (G). Silicon is a brittle material, so its deformation follows Hook's law up to the breaking point. The reason lies in the absence of grain boundaries, where the motion of dislocations usually takes place, therefore a plastic deformation is nearly inexistent. Other characteristics are high yield strength and low density, compared with stainless steels. The table 2.1 summarizes silicon and other materials' properties.

	Si (SCS)	**SiO_2**	**Si_3N_4**	**polySi**	**Stainless steel**
Yield strength [GPa]	2.6-6.8	8.4	14	1.8	0.5-1.5
Young's modulus [GPa]	186.5	73	323	161	206-235
Density [10^3 Kg/m^3]	2.32	2.5	3.1	-	7.9
Thermal conductivity [W/cmK]	1.56	0.014	0.19	-	0.329
Thermal expansion [10^{-6}/°C]	2.6	0.4-0.55	2.8	2.8	17.3

Table 2.1: Properties table.

2.2 Clean-room facility

Most of microfabrication processes need a particular working environment with specific properties, that is the *clean room (*Figure 2.1*).* It is an area in which concentration of airborne particles such as dust or pollen is controlled and kept under specified limits. These contaminants are generated by people, processes, facilities and equipment, and must be

continually removed from the air. The level at which these particles need to be cleaned away depends on the standards required. The most frequently used standard is the Federal Standard 209E. This is a document that establishes standard classes of air cleanliness for airborne particulate levels in clean rooms. A class-100 clean room is designed never to allow more than 100 particles (0.5 µm in diameter) per cubic foot of air. The following tables (Figure 2.3) show different classifications:

Class	maximum particles/ft³					ISO equivalent
	≥0.1 µm	≥0.2 µm	≥0.3 µm	≥0.5 µm	≥5 µm	
1	35	7	3	1		ISO 3
10	350	75	30	10		ISO 4
100		750	300	100		ISO 5
1,000				1,000	7	ISO 6
10,000				10,000	70	ISO 7
100,000				100,000	700	ISO 8

Class	maximum particles/m³						FED STD 209E equivalent
	≥0.1 µm	≥0.2 µm	≥0.3 µm	≥0.5 µm	≥1 µm	≥5 µm	
ISO 1	10	2					
ISO 2	100	24	10	4			
ISO 3	1,000	237	102	35	8		Class 1
ISO 4	10,000	2,370	1,020	352	83		Class 10
ISO 5	100,000	23,700	10,200	3,520	832	29	Class 100
ISO 6	1,000,000	237,000	102,000	35,200	8,320	293	Class 1000
ISO 7				352,000	83,200	2,930	Class 10,000
ISO 8				3,520,000	832,000	29,300	Class 100,000
ISO 9				35,200,000	8,320,000	293,000	Room air

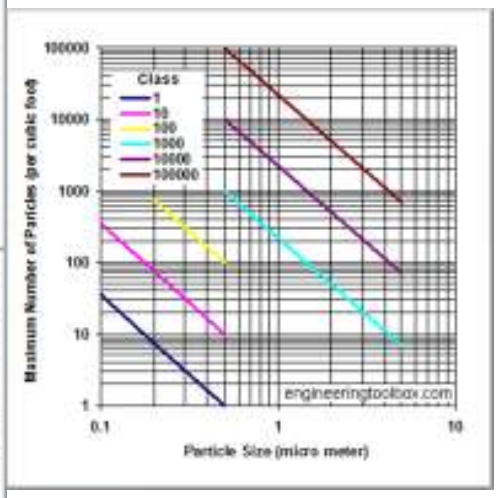

Figure 2.3: Clean room classifications.

Strict rules and protocols must be followed to prevent high-sensitive technology contamination and damage (Figure 2.4). Airflow rates and direction, pressurization, temperature, humidity and specialized filtration need to be highly controlled. People who work in this room must wear protective clothing called "bunny suits" that prevent human skin and hair particles from entering the room's atmosphere (McFadden).

CRITERIA	CLASS 10 M2.5 ISO 4	CLASS 100 M3.5 ISO 5	CLASS 1,000 M4.5 ISO 6	CLASS 10,000 M5.5 ISO 7	CLASS 100,000 M5.5 ISO 8
Air Changes Per Hr / Min	Per Hour/Per Minute 500-600/8-10	300 To 480 5 To 8	180/3	60/1	30/.5
Filter Coverage %	90 to 100	50 to 70	20 to 30	7 to 15	4 to 5
CFM Per Square Foot	85 to 90	36 to 65	18 to 32	9 to 10	4 to 8
Filter Efficiency	99.9997 (5-9s ULPAs)	99.997 (4-9s HEPAs)	99.997 (4-9s HEPAs)	99.997 (4-9s HEPAs)	99.97 (3-9s HEPAs)
Type of Ceiling	2" Aluminum Painted Grid	2" Aluminum Painted Grid	2" Aluminum Painted Grid	1 1/2" T-Bar Conventional	1 1/2" T-Bar Conventional
Light Fixture Type	Tear Drop or Flow Thru	Tear Drop or 2'x4' C/R Fixture	2' X 4' Cleanroom Fixture	2' X 4' Cleanroom Fixture	2' X 4' STD Fixture Field Sealed
Ceiling Panels	FRP or Epoxy Painted	FRP, Vinylrock or Mylar	Vinylrock or Mylar	Vinylrock or Mylar	Vinylrock or Mylar
Wall System	Modular	Modular	Modular	Modular or Drywall	Modular or Drywall
Floor Covering	Heat Weld Vinyl or Poured Epoxy	Heat Welded Sheet Vinyl	Solvent Welded Sheet Vinyl	Sheet Vinyl or VCT	Sheet Vinyl or VCT
Flooring Base	2" to 6" Cove	Cove or Aluminum Base Channel	Cove or Aluminum Base Channel	Cove or Aluminum Base Channel	Cove or Aluminum Base Channel
Air Returns	Raised Floor or Center Returns	Low Wall on Long Axis	Low Wall at Perimeter	Low Wall	Low Wall or Ceiling

Figure 2.4: Criteria to prevent high-sensitive technology contamination and damage.

2.3 Lithographic process

The main miniaturization method is lithography. This technique consists in the transfer of a pattern on a substrate with specific characteristics, thus belonging to the "top down" category. Nowadays various lithographic techniques, ranging from conventional methods to unconventional ones, are used to create small features.

The word *lithography* (Greek for the words *stone* [*lithos*] and *write* [*gràphein*]) refers to a process invented in 1796 by Aloys Senefelder. He found that stone, when properly inked and chemically treated, could transfer a carved image onto paper. Nowadays, due to the advent of the MicroElectroMechanical Systems (MEMS), the applicability of IC technology to the fabrication of commercial biomedical devices has increased interestingly (Zaouk et al., 2006). The current industrial standard ensures highly reliable processing with lithographic resolution of tens of nanometers within one square-inch area. In the recent years, using micro-nanofabrication techniques, trillions of basic electrical elements (transistors) and microchips

for various biological and clinical applications have been successfully produced. Implantable neural probes, microfluidic-based biological systems, physiological pressure sensors, and cochlear and retinal implants have been manufactured. Through the use of conventional clean-room fabrication technology it is possible to directly integrate the biochips with powerful electronic-processing units, thus eliminating extensive electrical wiring and further reducing overall system dimensions (Pan and Wang, 2011). Conventional lithographic techniques are based in silicon manufacturing. Silicon started being used for micromechanical elements in 1960, combining oxidation processes with substrate manufacturing. It was not until 1982 and Peterson's studies about its mechanical properties that it started to be massively used for micromechanical structures, and almost thirty years ago it has been possible to integrate sensors, actuators and other electronic elements. Silicon processing techniques can be divided into Bulk Micromachining and Surface Micromachining. With the first one it is possible to make physical and chemical etching, removing some of the semiconductor substrate, due to the high selectivity along one dimension. The thickness limit is given by the *wafer* itself (generally 500 μm). In the Surface Micromachining instead, a previous material deposition is expected. Then the conventional lithographic techniques are used to define the pattern. Finally the selective etch of the so-called sacrificial materials is made. Polysilicon, silicon nitride and oxide, polyimide and tungsten are generally used. Even if in the last few years other materials, like polymers, glasses, ceramics, shape memory alloys and piezoelectric materials, have been introduced, silicon has continued to be the most widespread material for master realization through conventional lithographic techniques (Accoto, 2010) (Madou, 2011b).

2.3.1 PHOTOLITHOGRAPHY

Photolithography is the most used lithographic technique (Zaouk et al., 2006). In this process, a pattern is transferred to a photosensitive polymer (*photoresist*) by exposure to a source of light, with a specific wavelength, through an optical mask. The photoresist can be positive or negative depending on its ability to polymerize or not when exposed to a specific radiation. The **mask** for the feature-definition on the wafer consists of opaque patterns (chrome or iron oxide) on a transparent support (quartz). Then the pattern is transferred to the underlying substrate using subtractive (etching) or additive (deposition) techniques. The photoresist task is to prevent the oxide underneath from being attacked. Once the exposed oxide is etched away, the remaining photoresist can be stripped off with either a strong acid (e.g. H_2SO_4), an acid-oxidant combination (e.g. Piranha, H_2SO_4 : H_2O_2 = 3:1), an organic solvent or alkaline strippers. This is the reason why the resistor is usually a sacrificial material. Multilayered structures can be made due to an alignment system and the use of markers. Moreover, microfluidic research promotes high-aspect-ratio plus resists feature development. Until now, the best photoresist in this field has been the negative SU-8, because of its really attractive characteristics. Madou research group has been pursuing research in C-MEMS derived from pyrolyzed photoresist. Patterned SU-8 is converted into carbon electrodes by subjecting the photoresist to high temperatures within an inert environment, in a process called pyrolysis. Complex three-dimensional structures can be obtained (Zaouk et al., 2006) (Madou).

The photolithographic process (Figure 2.5) involves a set of steps explained below:

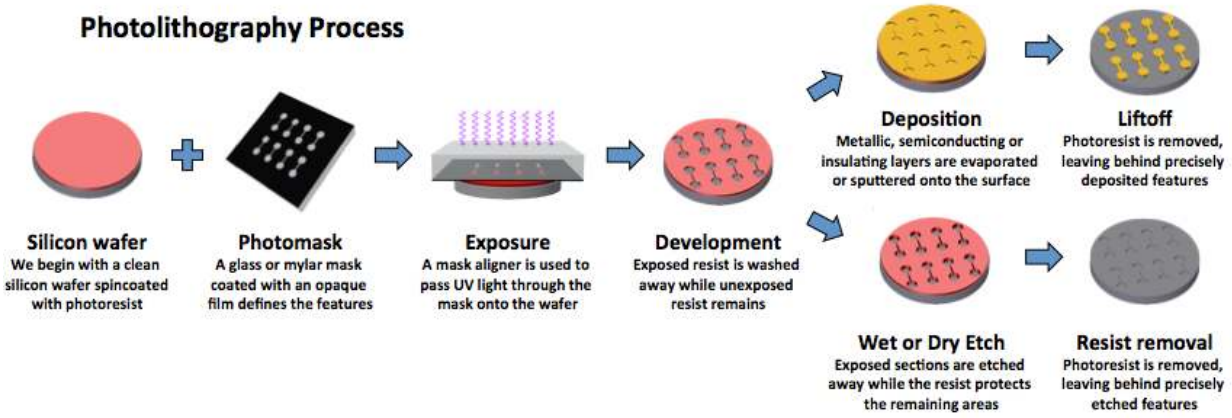

Figure 2.5: Photolithographic process.

Preparation of the wafer (cleaning and oxide growth)

Spin-coating

Soft bake

Exposure

Postexposure treatment

Development

Hardbaking

Pattern transfer

Stripping

First of all is necessary to clean the wafer from different kind of contaminants. Physical contaminants - such as dust particles - can hinder the process by preventing light from exposing the photoresists, or by disturbing surface uniformity. Chemical contaminants may react

creating unwanted effects. Different methods (HFdip, RCA1[1], RCA2[2], piranha) can be used for this purpose.

Once the wafer is ready, the liquid photoresists is dispensed onto it, held by a vacuum chuck in a resistance spinner. The thin layer of the organic polymer sensitive to ultraviolet radiation (UV) is then *spun* in one or more steps at precisely controlled speed (between 1500 and 8000 rpm) to form a uniform film. The resulting polymer thickness is a function of spin speed, solution concentration and molecular weight. The equation is as follows

$$t = \frac{ks^2}{\sqrt{\nu}} ,$$

where s is the polymer concentration, ν the angular speed and k a constant depending on the solution viscosity.

After spin coating, the resist contains up to 15% solvent and built-in stress. The wafer is therefore *soft backed* at 75-100 ºC to remove solvents and stress, and to promote adhesion of the resist layer to the wafer.

The next step is light *exposure* to UV radiation. The source used differentiates photolithography from similar techniques such as X-Ray, Focused Ion Beam, and Electron-Beam Lithography. Others methods, such as Electron or Laser Beam Writers, or the Dip Pen Lithography, which uses an AFM tip, even exclude the use of masks. UV wavelength is usually between 350 and 500 nm, but it can also be shorter in deep ultraviolet (DUV, 150-300 nm) and extreme ultraviolet (EUV, 10-14 nm). Depending on the mask-resist gap, there are three kind of exposure: contact, proximity and projection. Contact printing allows very high resolution, but resist can damage the mask. In a proximity exposure, a small gap of 10 to 25 μm is

[1] RCA1: Add 1 part of NH_3 (25% aqueous solution) to 5 parts of DI water, heat to boiling, and add 1 part of H_2O_2. Immerse the wafer for 10 minutes. This procedure removes organic dirt.
[2] RCA2: Add 1 part of HCl to 6 parts of DI water, heat to boiling, and add 1 part of H_2O_2. Immerse the wafer for 10 minutes. This procedure removes metal ions.

maintained. Projection printing uses a complex lens system to reproduce the image (Figure 2.6). Light intensity and exposure time determine exposure energy and dose, which measures the radiation on the basis of the ability to produce ionization. The action of lighting on a positive photoresists increases its solubility, while promotes polymerization in negative ones.

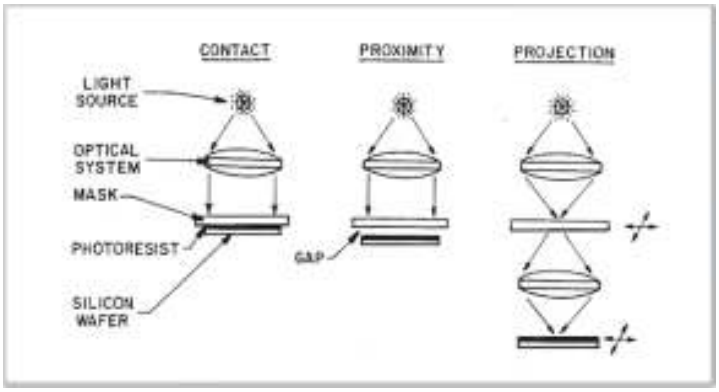

Figure 2.6: Light exposure in the photolithographic process.

The resolution of a photolithographic process with a self-aligned mask is measured by the specific minimal feature size that can be obtained, where the term critical dimension is typically used. The theoretical resolution is the minimum resolved dimension and is given by

$$R = b_{min} = k\sqrt{\lambda(s + \frac{z}{2})}$$

where s is the gap between the mask and the photoresist surface, λ the wavelength of the exposing radiation, z the photoresist thickness, and k a constant that theoretically is ~1.5.

In projection lithography the resolution is calculated with the Rayleigh criterion for far field as

$$R = 0.61\lambda/NA$$

where NA is the numerical aperture of the imaging lens system.

During exposure the principal drawback is diffraction, which causes diffusion of light just next to mask edges. Figure 2.7 shows the typical intensity distribution of light incident on a photoresist after passing through a mask containing an equal line and space grating.

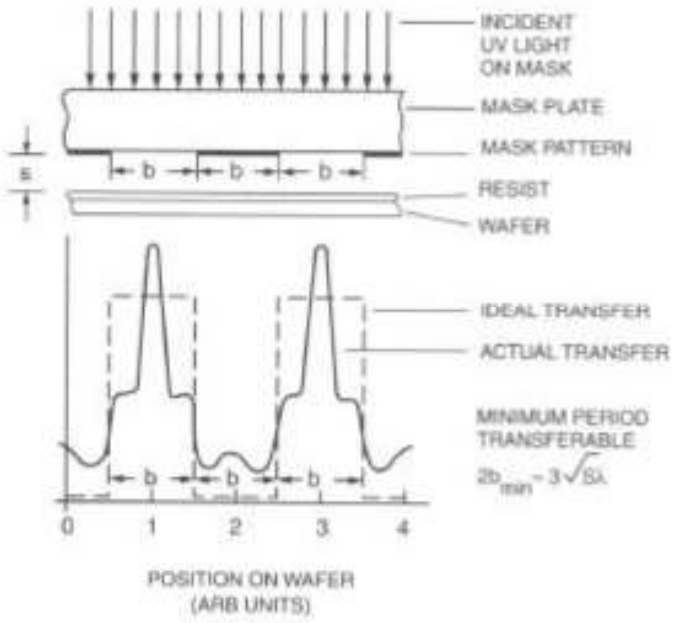

Figure 2.7: Light distribution profiles on a photoresist surface after light passing through a mask containing an equal line and space grating.

In contact and proximity exposure the pattern transferred is a consequence of near-field or Fresnel diffraction, while in projection exposure the limit is the far-field or Fraunhofer diffraction (Figure 2.8).

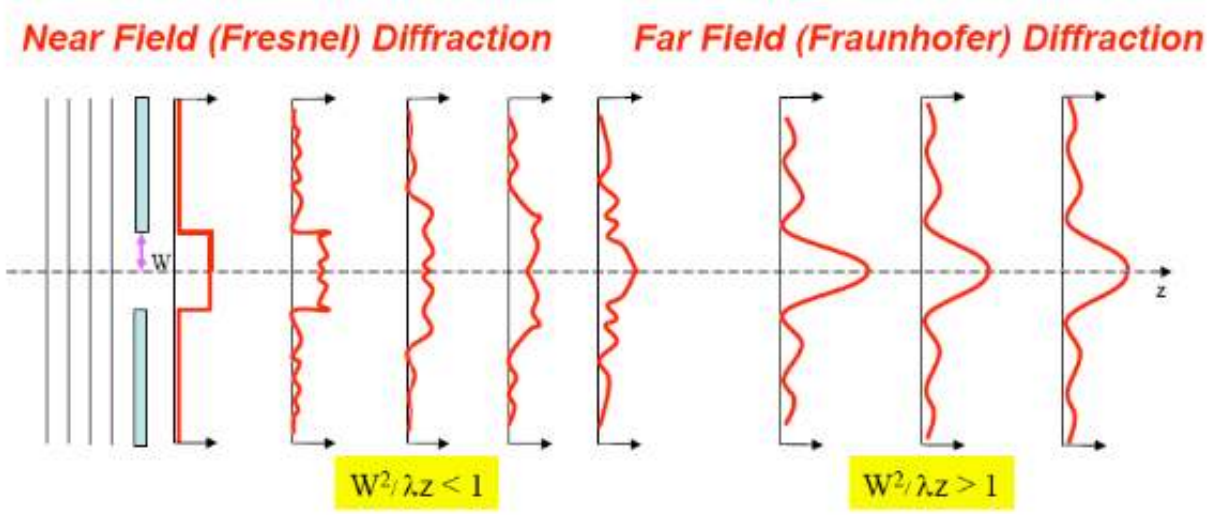

Figure 2.8: Fresnel (left) and Fraunhofer (right) diffraction.

Postexposure treatment is often desired because the reactions initiated during exposure might not have run to completion. It may include baking processes or treatments with reactive gas or vacuum.

During d*evelopment,* selective dissolution of the resist takes place. It can be done in wet or dry conditions; the *wet* development uses a liquid, typically alkaline for positive resists and organic for negatives, while the *dry* one uses gas or plasma. Furthermore, a mild plasma treatment can be made in order to remove some residual polymer. Highly energetic oxygen ions react and burn away the unwanted photoresist. Subsequent hardbaking removes residual solvents, promotes interface-adhesion and improves the hardness of the film. Finally *pattern transferring* to the oxide substrate and resist *stripping* are carried out (Accoto, 2010) (Madou, 2011b).

It is a relatively high-cost technology requiring also the adequate clean-room facility. Moreover planar substrates are needed and it is applicable to only a small set of materials. These limitations have motivated the development of alternative low-cost soft-lithographic techniques to complement and extend conventional fabrication methods. Some of these

methods include microcontact printing, molding of organic polymers and rapid prototyping (Qin et al., 1998)

2.3.2 PDMS-BASED SOFTLITHOGRAPHY

In the 80s and 90s, microfluidic devices were mainly fabricated on silicon substrates. Then, then introduction of soft-lithography allowed molding polymers and exploiting their physical properties with additional advantages, giving birth to a new class of cheaper microfluidic devices (Velve-Casquillas et al., 2010).

Elastomeric materials provide new advantages thanks to their tunable characteristics depending on the changes in the shape with mechanical compression or extension. In addition they can be deformed reversibly and repeatedly without permanent distortion and can be molded with the desired features. The most used elastomer is polydimethylsiloxane (PDMS) (Figure 2.9); the characteristic of being optically transparent, chemically inert, nonhygroscopic (does not swell with humidity), biocompatible, and gas permeable, make him a good choice for cell biological analysis.

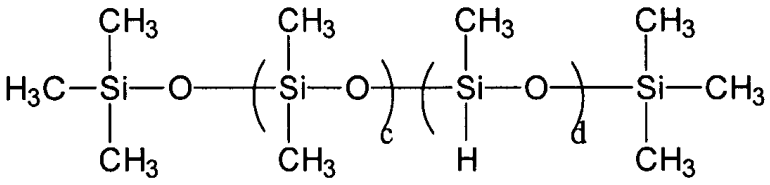

Figure 2.9: Polydimethylsiloxane (PDMS).

PDMS also has some drawbacks such as its affinity for small hydrophobic molecules; this could lead to biomolecules adsorption/absorption from the fluid inside the microchannels, thus biasing the experiment conditions (Paguirigan and Beebe, 2009). For experiments on cell signaling and on the determination of drug dosage response, the use of PDMS can strongly

skew the final result. To overcome this problem, a number of PDMS surface treatments have been developed.

Its permeability to gases can also change medium osmolarity due to water vapor evaporation and drying. It is generally possible to overcome this problem by using a hydration-channel network, a medium renewal system or a hygrometric controlled environment. Ideally, the PDMS device should be treated several hours before usage, thus to stabilize device hygrometry.

"Soft" fabrication techniques include molding, embossing, stamping, casting, thick film application, self-assembled monolayers, and array patterning using polymers and biological substances. A part from being a simple and cost effective method it can also expand the capabilities of these systems.

The most used PDMS softlithographic techniques are *replica molding*, also known as PDMS casting and *microcontact printing* (μCP). The first one is used to fabricate microfluidic devices, while the latter to pattern features on cell culture substrates.

Microfluidic devices are generally fabricated using PDMS molding methods. A silicon master mold, containing photoresist pattern representing the channel design, is built using photolithography. Once the master mold is constructed and if carefully used and properly treated with an adhesive, it can be used hundreds of times to mold PDMS replica of the channels.

In microcontact printing (μ-CP) (Figure 2.10), the PDMS rubber is coated with an in k of the molecules to print in selected patterns on solid substrates. The inking of the substrate consists of self-assembled monolayers (SAM) on the solid surface formed by covalent chemical reaction.

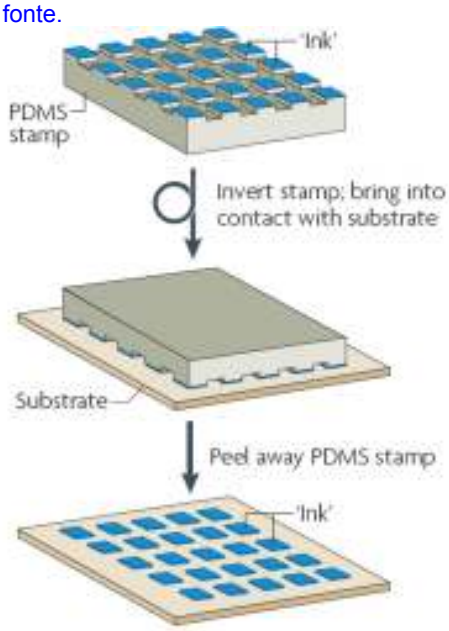

Figure 2.10: Microcontact printing.

Other techniques are microtransfer molding (μ-TM) and micromolding in capillaries (MIMIC) shown in picture 2.11.

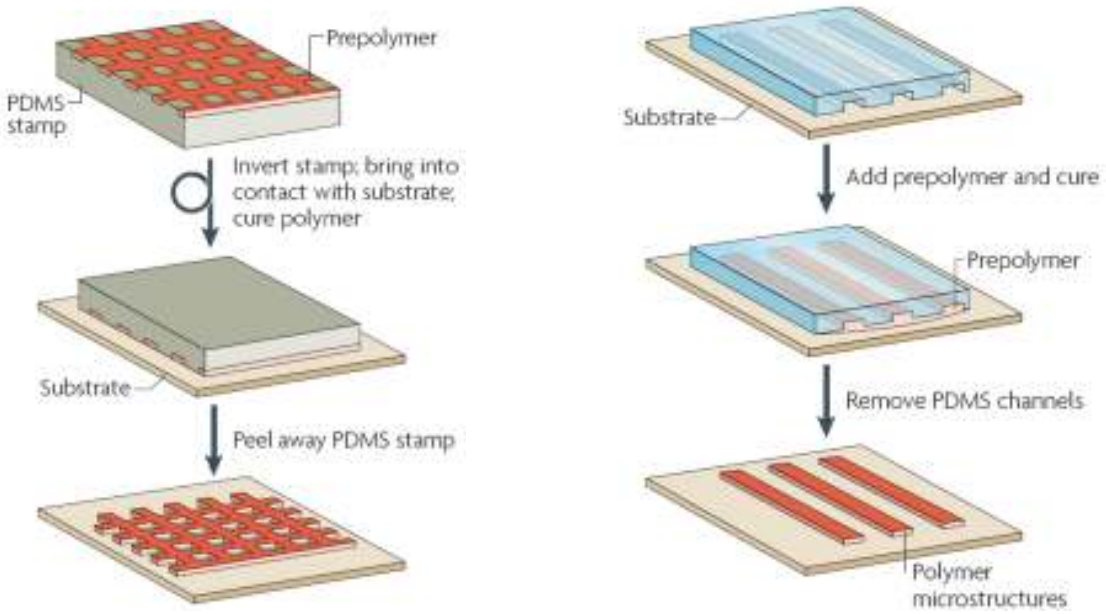

Figure 2.11: microtransfer molding (μ-TM) and micromolding in capillaries (MIMIC).

In μ-TM, a rubber mold is filled with a polymer precursor and pushed against a substrate; after curing, the polymer is transferred to the substrate, and the stamp is peeled off. In MIMIC, the rubber stamp is pushed against the substrate, and liquid is applied to access holes in the mold. The liquid wicks into the cavities formed by the rubber mold against the substrate, and once the polymer is cured, the stamp is removed (Truskett and Watts, 2006; Velve-Casquillas et al., 2010) (Madou, 2011a).

2.4 Subtractive and additive techniques

Lithography steps precede a series of subtractive and additive processes, where materials are either removed or added from the device in a selective manner, transferring the lithography patterns onto integrated circuits (ICs). Subtractive techniques are dry or wet chemical etching, while additive ones are physical and chemical vapor deposition. Thermal energy- based techniques can also be used (Figure 2.12).

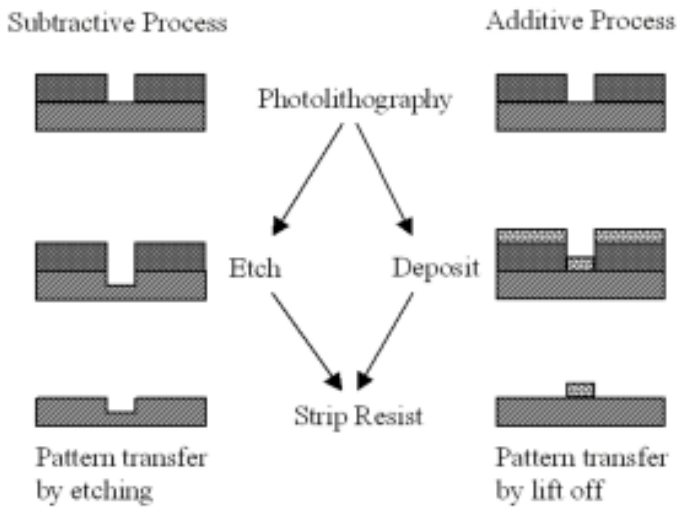

Figure 2.12: Subtractive vs. additive processes.

2.4.1 ETCHING PROCESSES

Etching is the principal subtractive technique, and can be a plasma-based dry process or a wet chemical removal.

In the first method, a solid surface is etched in the gas or vapor phase, physically by ion bombardment, chemically by a chemical reaction through a reactive species at the surface, or by combined physical and chemical reactive ion etching (RIE). Therefore, it is an anisotropic process and it involves the creation of plasma either by glow discharge (diode setup) or by ion-beam etching (triode). In physical sputter (momentum transfer), etching occurs as a consequence of physical effect of Ar^+ ions on the exposed substrate surface. On the other hand, in chemical etching, chlorine or fluorine atoms generated in the plasma, diffuse to the substrate, where they react to form volatile products with the layer to be removed. Thanks to high plasma densities operating at low a pressure, which increases ions directionality, deep reactive ion etching (DRIE) allows high-aspect-ratio features. In wet etching, material removing of preferentially exposed surfaced is purely chemical, photochemical, or electrochemical, hence it is isotropic.

In thermal removing processes, thermal energy, provided by a heat source, melts or vaporizes the material to be removed; while in mechanical subtractive machining, physical removal is achieved by mechanical energy applied at the work piece (Madou, 2011b).

2.4.2 DEPOSITION PROCESSES

Additive processes are often accompanied or followed by thermal processing to obtain desired material properties and substrate adhesion. To categorize these techniques, the name of the process that brings the depositing material to the substrate is used, even though the process that

generates the depositing materials might have a different source. They can be mechanical, chemical, and thermal. Mainly we can distinguish two types of deposition processes:

-Physical Vapor Deposition (PVD): evaporation (thermal evaporation, electron beam evaporation), sputtering, laser ablation deposition, ion plating, cluster deposition, molecular beam epitaxy (MBE), and aerosol deposition (AD).

-Chemical Vapor Deposition (CVD): plasma enhanced CVD (PECVD), high-density plasma CVD (HDPCVD), low-pressure CVD (LPCVD) melt dipping, and atomic layer deposition (ALD).

PVD constitutes a group of direct line-of-sight effect deposition techniques, while CVD represent a class of diffusive-convective mass transfer deposition techniques. The principal physical thin films deposition techniques are thermal evaporation and sputtering. Evaporation is based on the sublimating (solid source to vapor state) of a heated material and letting it condense on the substrate surface. During sputtering, the target (a disc of the material to be deposited, cathode), at a high negative potential, is bombarded with positive argon ions (other inert gases can be used) created in plasma. The target material is sputtered away mainly as neutral atoms, and ejected surface atoms are deposited onto the substrate placed on the anode. Once the patterns are defined by surface micromachining, they might need to be transferred underneath. In bulk micromachining, 3D features are etched into the bulk of crystalline and noncrystalline materials.

Sometimes integration of electrodes on a substrate is needed and it requires clean-room facilities. Metallic and dielectric layers are generally coated on glass substrates prior to plasma bonding onto PDMS devices. **Lift-off** process, for example, is frequently used for patterning catalytic metals, such as Pt, frequently used in chemical sensors. After the deposition process,

a solvent dissolves the positive photoresist underneath the deposited material, and lifts off the metal, which is kept in the areas unprotected by the photoresist itself (Madou, 2011b).

2.5 Bonding techniques and packaging

Different components can be integrated *bonding* materials to substrates. The most commonly used to bond layers in MEMS are:

- Anodic bonding uses electrostatic attraction to bring a glass wafer in contact with a silicon wafer and to form covalent bonds between them;
- Thermal bonding melt and bond together two glass wafers under controlled conditions;
- Silicon fusion bonding, where the two oxidized silicon wafers are joined at high temperatures.

In microfluidic devices, generally, the patterned channels are casted on PDMS, and they will need to be closed by bonding on a glass substrate or on another PDMS layer. Activating both the surfaces by oxygen plasma, they will convert to hydrophilic; and subsequently, putting them in contact, they will bond thanks to a condensation reaction (Figure 2.13).

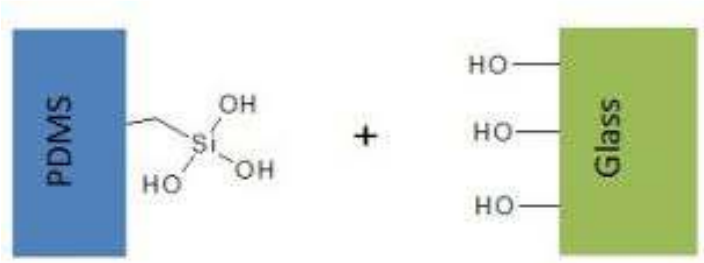

Figure 2.13: bonding PDMS-glass.

At the end of the process, miniature components need to be put together into housing structure in a microassembly step. This is called packaging and involves processes such as bonding and encapsulation in a protective body. It is the bridge between the components and their environment. In biological microfluidic devices the package must be biocompatible and need to be connected to a fluidic manifold able to guide liquids to different parts of the MEMS structure.

Finally, testing can be performed to prove device functionality before its implementation (Madou, 2011a).

Chapter 3

Objective

It was the objective of this thesis to develop specific in vitro models systems to reproduce human physiology. The huge difference between 2D and 3D architectures was previously demonstrated (Table 3.1) (Yamada and Cukierman, 2007).

Biological function	**2D versus 3D**	**Regulatory Mechanism**
Cell Shape	Loss of epithelial cell polarity and altered epithelial and fibroblast shape in 2D	Growth factor receptors and pathways; cell adhesion signals associated with cell survival and
Gene Expression	Cells in 2D versus 3D often have different patterns of gene expression	ECM, hormones, and adhesion molecules
Growth	3D matrix-dependent regulation of cell growth	Adhesion and growth factor-related pathways plus survival or apoptotic genes
Morphogenesis	3D matrix-induced vessel sprouting and gland branching	ECM, adhesion, growth factor-related pathways and apoptotic genes
Mobility	Altered single and collective cell motility patterns in 3D matrices	ECM and its regulators; adhesions and growth factor-related pathways; phospholipids
Differentiation	3D matrix-induced cell differentiation	ECM and growth factors; motor molecules

Table 3.1: 3D-dependent cell behavior and signaling

The goal of the work was to integrate the cells into functional tissue structures in order to establish the appropriate topological interactions and spatial organization of cells.

Two different cases are described. The first one is a liver-on-chip device, used to create a novel *in vitro* model of Non Alcoholic Fatty Liver Disease (NAFLD); and the second one is a microfluidic platform with the aim to describe the interface between cancer stem compartment and immunity.

In the first experimental work, based on the previous Lee work (Lee et al., 2007b), HepG2 cells were cultured in 3D under microfluidic perfusion, through a system of parallel micrometric channels that mimic the endothelial-parenchymal interface of a liver sinusoid, allowing for continuous diffusion of nutrients and removal of waste products.

The second one focuses on a co-culture platform able to observe and describe cells migration and interactions between MDA-MB-231 breast cancer cell line and M1/M2 polarized macrophages, in real-time with high precision detail and control of system parameters.

Each part starts with an introduction and background section to highlight the principal topics that will be discussed in the experimental part. The latter will be composed by the materials and methods section, followed by the results and discussion, which will include all the experiments. In the last part of the thesis, the conclusions are presented together with an outlook.

SECTION II

Chapter 4

Motivation and experimental approach

In the past years, several three-dimensional (3D) models were developed to increase spatial and chemical complexity, embedding cells within either natural extracellular matrix (ECM) molecules or synthetic polymers (Dutta and Dutta, 2009). On this purpose, hydrogels are often used to give tissues mechanical properties and to better recreate cell-cell interactions within their microenvironment (Tibbitt and Anseth, 2009; Verhulsel et al., 2014). In fact, 2D culture systems have shown to alter most of cells behaviors, being different the crucial features characterizing 3D scaffolds compared to 2D substrates (Hwang et al., 2006; Wirtz et al., 2011) Despite these 3D models are still fundamental in the regenerative medicine field, and although they are very useful to study signaling pathways and drug responsiveness in some disease states (Yip and Cho, 2013), enhanced architectural and cellular complexity can be achieved in simulating the physiological environment and functions, such as lung breath, peristaltic movements of gut, shear stress within blood vessels, and tension in the skin (Ghaemmaghami et al., 2012). Hence, more complex geometries can allow spatial and temporal control of cell growth, exploiting micron-sized patterned channels for fluids and soluble factors transport regulation. The challenge is to be able to carry out studies on chronic pathophysiological states, in clinically relevant time scales. In order to achieve this purpose, long term-survival of many cell types is necessary, besides *in situ* monitoring ability, to detect the quality of the

microenvironment (e.g. metabolites, pH and O_2 saturation) (Ghaemmaghami et al., 2012). Organs-on-chip arise from this necessity: the integration of biology and engineering on a single device exploiting microfluidic technology to improve disease monitoring and diagnosis (Beebe et al., 2013). Microfluidics is the study of systems that manipulate small volumes of fluids (Whitesides, 2006). In the last ten years it has been extensively used for biological analysis (Whitesides et al., 2001) (El-Ali et al., 2006) also thanks to the advances in the microfabrication filed (Borenstein and Vunjak-Novakovic, 2011) (Qin et al., 1998). This technology pave the way also to the point-of care devices applications, which started their successfully commercialization in the last years. Diagnostic platforms might also have a solid support from live cell microscopy and computational simulation models, which constitute powerful tools for cell analysis. Tourlomousis recently published a numerical investigation conducted on a dynamic microorgan platform for drug screening (Tourlomousis and Chang, 2015). Excellent reviews (Bhatia and Ingber, 2014) (Bhise et al., 2014) (Huh et al., 2011) (Huh et al., 2012) (van der Meer and van den Berg, 2012) underlie the importance of microfluidics integrated to 3D tissue engineering models as robust preclinical platforms. Nowadays research is aimed to reproduce living systems on a chip (Luni et al., 2014; Zhang et al., 2009b) without the presumption to totally replace animal testing, but certainly to reduce it and to provide new more reliable disease models (Benam et al., 2015).

Also in liver diseases study and analysis, many efforts have been made in the past decade to improve physiological mimicry and the diagnostic power of conventional bioartificial systems; from perfusion bioreactors (Chan et al., 2004) (Doré and Legallais, 1999) (Sharma et al., 2005), to porous membranes-based systems (Kasuya and Tanishita, 2012), to 3D organoids (Funatsu et al., 2001) (Soto-Gutierrez et al., 2010; Yip and Cho, 2013). Thanks to microengineering technologies (microfabrication and microelectronics), it is possible to go beyond these models by integrating microorganoids onto microfluidic platforms, giving birth to microfluidic

bioreactors as relatively simplified models of disease with a great diagnostic power. In the last years different liver-on-chip platforms were fabricated for drug metabolism screening analysis (Lee et al., 2007b; Schütte et al., 2011; Wagner et al., 2013; Zhang et al., 2008) (Lee et al., 2013b) (Esch et al., 2015), but there is still lack of *in vitro* modeling of chronic liver diseases. On the other side, cancer microenvironment and the factors influencing tumor cells growth, migration and metastasis keeps on raising the interest of scientists. Furthermore, the investigation of inflammation responses by adding cytokines or immune cells to the system could give crucial information about the evolution of the system itself. The great power of this approach lies in the chance to personalize the device by using patients' own cells.

The first part of this work will be concentrated in mimicking and investigating, within a microfluidic liver sinusoid under fluidic flow conditions, the pathogenesis of NAFLD using HepG2 cells, through the evaluation of liver steatosis in terms of intracellular triglyceride accumulation, cell viability/cytotoxicity, and analysis of the cellular levels of reactive oxygen species (ROS).

The second part of the thesis will deal with investigation of the interaction between cancer stem compartment and M1/M2 polarized macrophages. Micron-sized channels will be used for the migration analysis, and proliferation comparisons will be performed as well.

SECTION II (a): A NOVEL MODEL OF NAFLD IN A 3D LIVER-ON-CHIP DEVICE

Chapter 5

Introduction and background

5.1 Organs-on-a-chip

Nowadays translational research is evolving to a personalized and individualized medicine, thus allowing custom-tailored target therapies and disease prevention. To make this possible, new diagnostic tools are necessary to appropriately model systems by integrating cellularized constructs within microengineered platforms. This approach allows recreating *in vitro* physiological and pathological conditions of complex tissues and organs (Perestrelo et al., 2015).

The technology, better known as **organs-on-a-chip**, relies on modular and scalable devices, able to incorporate diseased or cancer cells to test their responsiveness toward new drug candidates (Bhise et al., 2014; Elliott and Yuan, 2011; Ghaemmaghami et al., 2012). These *in vitro* models have the potential to uncover key biological and physiological processes, besides the ability to identify determining factors involved in disease development. Therefore, they don't need to be an exact replica of the entire system, since they have to be able to mimic and understand the essential features of the disease, in order to study the biological and clinical questions (Hutmacher et al., 2015). Bhatia and Ingber define an organ-on-a-chip as " a microfluidic cell culture device created with microchip manufacturing methods that contains continuously perfused chambers inhabited by living cells arranged to simulate tissue- and organ-level physiology" (Bhatia and Ingber, 2014). In fact, the system can incorporate

mechanical cues such as fluid shear stress, cyclic strain and mechanical compression, thus reproducing organ development and function in health and disease (Mammoto and Ingber, 2010). Furthermore, they enable high-resolution, real-time imaging and *in vitro* analysis. Finally it is possible to integrate within these devices fluorescence microscopy, multiple electrode arrays and other analytical assays. They can be considered as the evolution of the traditional biosensors, conventionally used to monitor cell behavior and properties, which, thanks to microfluidics evolved to the LOC and BioMEMS. These models can reproduce different systems, ranging from the cardiovascular (blood-vessels and heart) to the respiratory (lung), and from the nervous (brain) to the musculoskeletal (muscle and bone), digestive (gut and liver), and endocrine (pancreas and kidney) systems (Figure 5.1). The general microfabrication protocol was previously described by Ingber group (Huh et al., 2013).

Organ	Incorporated cell types	Demonstrated organ-specific features
Liver	Hepatocytes Vascular endothelial cells Fibroblasts	Serum protein synthesis Bile canaliculi Liver sinusoid Liver zonation
Lung	Airway epithelial cells Alveolar epithelial cells Pulmonary microvascular endothelial cells	Airway closure and reopening Small airway protein (CC10) synthesis Alveolar–capillary interface Surfactant production Lung inflammation Extrapulmonary absorption
Kidney	Renal tubular epithelial cells	Molecular transport
Gut	Intestinal epithelial cells	Intestinal absorption
Bone	Osteoblasts Osteocytes	Lacuna–canalicular network
Breast	Mammary epithelial cells Mammary fibroblasts Vascular endothelial cells	Malignant tumor invasion Cancer metastasis
Eye	Corneal epithelial cells Vascular endothelial cells	Epithelial barrier function
Brain	Neurons Astrocytes Oligodendrocytes	Axon–glia interaction Tumor angiogenesis

Figure 5.1: Microengineered organ models (Huh et al., 2011).

The final goal is to exploit microfluidic principles and microfabrication techniques toward a complete **body-on-a-chip** (Figure 5.2), paving the way to more personalized treatments and strategies, being also potential alternatives to animal models. The body-on-a-chip approach aims to expand the system biology power and relies on the chance to build novel

pharmaceutical models able to study organ-organ interactions and physiological regulation (Huh et al., 2011; Huh et al., 2012; Wikswo et al., 2013; Zhang et al., 2009b).

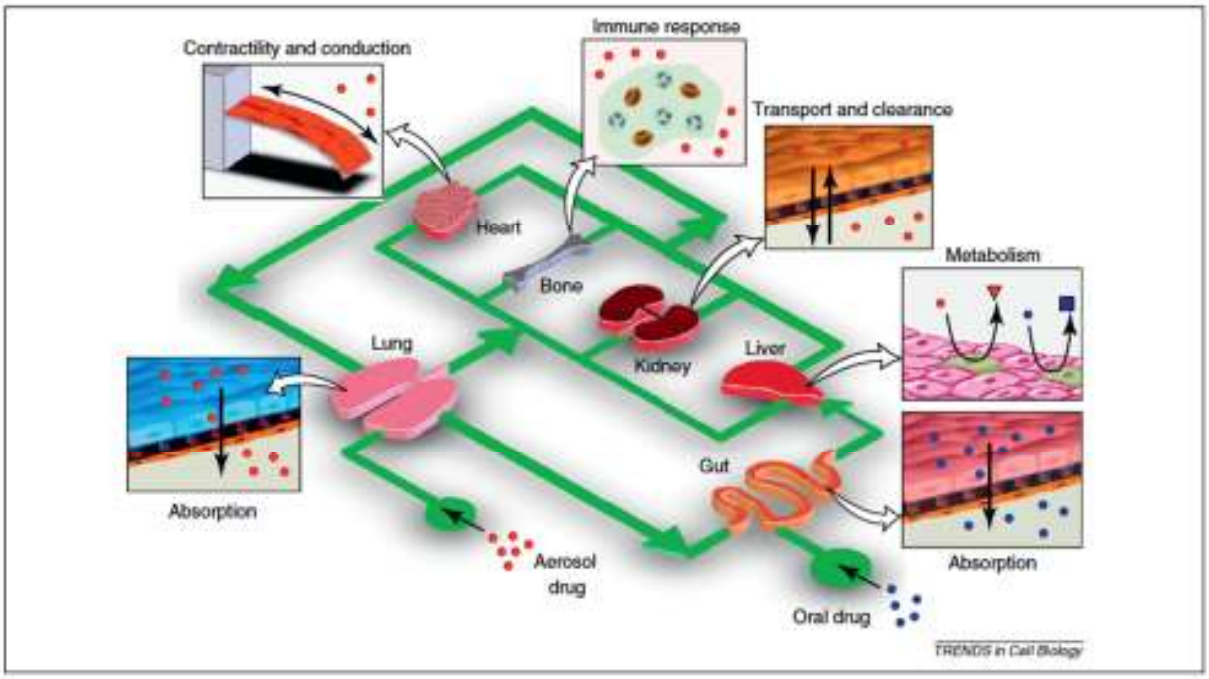

Figure 5.2: The body-on-a-chip concept (Huh et al., 2011).

Hereafter some organs-on-a-chip devices will be presented in detail.

5.1.1 LUNG

Respiratory diseases generally affect the airways, the lung tissue and blood circulation in the lungs. Huh et al. (Huh et al., 2010) developed a microdevice reproducing human alveolar-capillary interface, which is now the most famous lung-on-a-chip device (Figure 5.3). To accomplish that, they fabricated a microfluidic system containing two apposed channels separated by a thin microporous PDMS membrane, coated with fibronectin or collagen hydrogel. Subsequently, human pulmonary microvascular endothelial cells and human alveolar epithelial cells were seeded on opposite sides of the membrane. They created the air-liquid

interface by introducing air into the epithelial compartment, and cells medium in the opposite channel. The latter allowed fluid flow manipulation, as well as the delivery of nutrients to the cells.

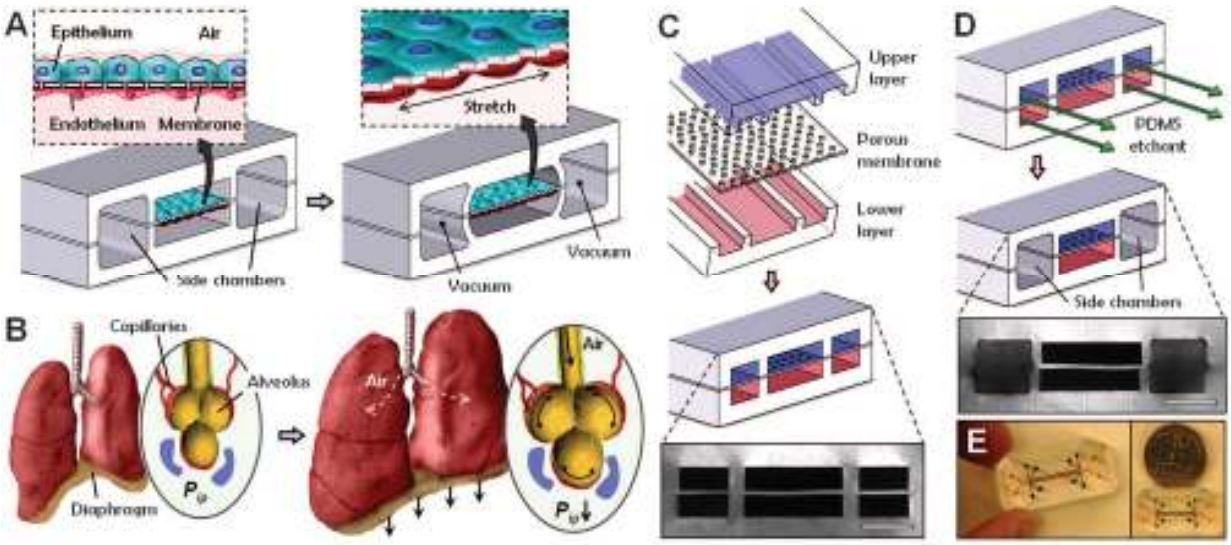

Figure 5.3: Lung-on-a-chip device (Huh et al., 2010).

This configuration reproduces normal inspiration, when intrapleural pressure decreases, determining alveolar expansion and the stretching of the epithelium and endothelium in the adjacent capillaries.

The scope of the work was to conduct toxicological studies in a more physiological configuration.

In a subsequent work (Huh et al., 2012), the same author created a model of drug toxicity-induced pulmonary edema, evidencing how the breathing motion played a crucial role in the development of the disease.

5.1.2 GUT

In a similar work, Kim et al. (Kim et al., 2012) fabricated an intestine model, mimicking the mechanical cyclic strain and intraluminal fluid flow. Two lateral channels, controlled by vacuum, were used to reproduce the peristaltic motions, which are critical for normal gut physiology. Human intestinal epithelial cells (Caco-2) were culture on the upper side of the PDMS membrane coated with ECM hydrogel, reconstituting intestinal villi shape, density, and size. Moreover a normal intestinal microbe (*Lactobacillus rhamnosus* GG) was successfully cultivated on the luminal surface. Thanks to the double layer configuration, microbial flora growth might be supported without compromising cells viability. The device allowed a perfused long-term cell culture with microbial symbionts, which enable the analysis of the human intestinal epithelial barrier functions *in vitro* (Figure 5.4).

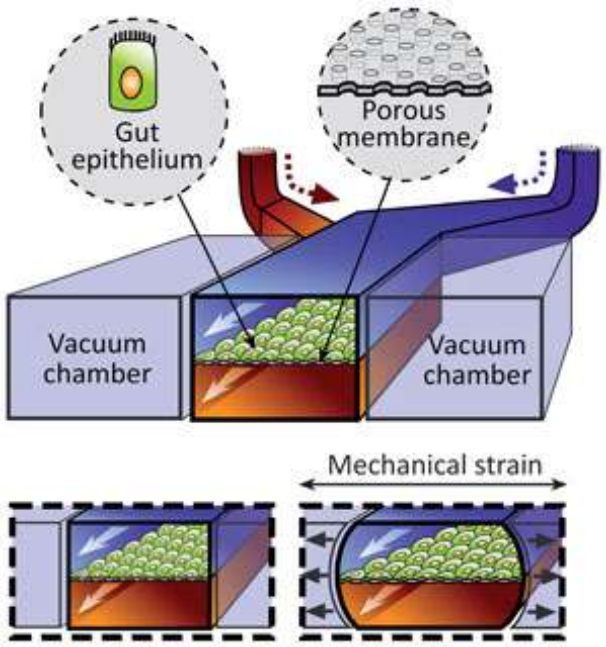

Figure 5.4: Gut-on-a-chip device (Kim et al., 2012).

The device is suitable for transport, absorption, and toxicity studies; furthermore it can constitute a valuable intestinal disease model for drug testing. Imura et al. (Imura et al., 2012) developed instead a system composed by microintestine connected to a microliver, and other target components to study the overall digestive properties of ingested anticancer agents.

5.1.3 KIDNEY, HEART AND BLOOD-VESSELS

Kidney toxicity is crucial when dealing with drug test, and we still lack reliable predictive models. Microfluidic complex platforms seem to be really suitable for this kind of task. Jang et al. (Jang et al., 2013; Jang and Suh, 2010) developed a human kidney proximal tubule-on-a-chip-device, which allows the analysis of active and passive epithelial transport (Figure 5.5). The platform consists as well of two channels separated by a porous membrane. The upper one is seeded with primary human proximal tubule epithelial cells where a low shear stress is applied, while the bottom channel works as a reservoir. They observed how the presence of physiological flow was critical for maintaining many functions of the cells.

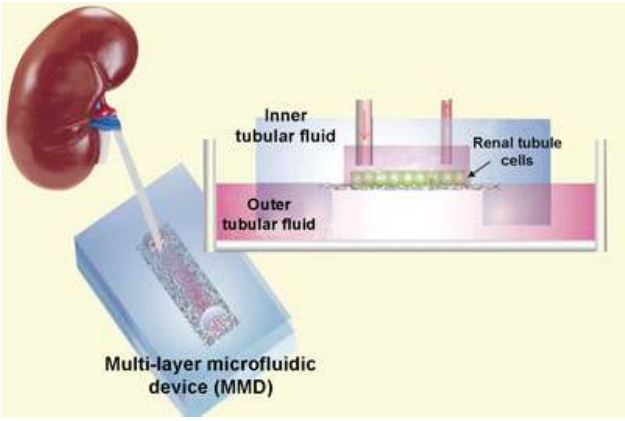

Figure 5.5: Kidney proximal tubule-on-a-chip device (Jang and Suh, 2010).

Microfluidic devices are also apt to model cardiovascular system, thanks to their ability to create channels with a high control of fluid flows, shear stress, and the possibility to reproduce pulsatile motions. By exploiting microchannels to mimic blood vessels, it is possible to perform studies of angiogenesis and cell migration within them (Chung et al., 2010). Kamm group was also able to build a functional, perfusable 3D microvascular network, co-culturing HUVECs and bone marrow-derived human mesenchymal stem cells (BM-hMSCs) by a vasculogenesis-like process (Jeon et al., 2014). They used a fibrin gel as the ECM (Figure 5.6). Very small volumes can be used to perform blood cells separation as well (Toner and Irimia, 2005).

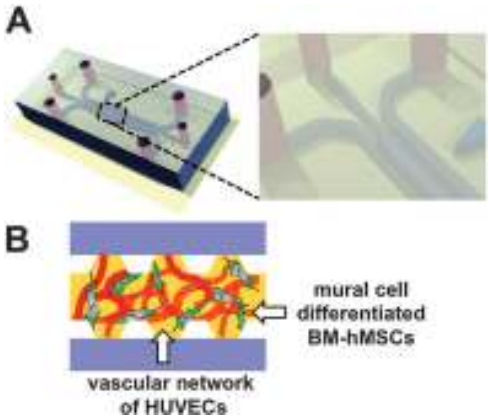

Figure 5.6: Microfluidic device (A) to reproduce angiogenesis within a fibrin gel (B) (Jeon et al., 2014).

In the cardiovascular biology field, tissue engineering most challenging aim is the formation of synchronously contracting engineered human cardiac tissue. Caspi et al. (Caspi et al., 2007) derived them from human embryonic stem cells. The 3D structure was composed by cardiomyocytes, endothelial cells (ECs), and embryonic fibroblasts in a porous scaffold composed by PLLA and PLGA, and contained an endothelial vessel network. The synchronous activity should be mediated by action potential through gap junctions, more precisely via transmembrane Ca^{2+} influx and intracellular Ca^{2+} release. By integrating these constructs onto

a microfabricated PDMS device, it is possible to characterize cells properties, besides the chance to make electrophysiological analysis (Serrao et al., 2012).

Next paragraphs will be dedicated more in detail to the liver and hepatic 3D cultures, which will be the argument of the first experimental section.

5.2 Hepatophysiology

5.2.1 LIVER AND HEPATOCYTES

The liver, weighing roughly 1.2-1.6 kg, performs many important life functions. It is located in the right side of the body under the lower ribs and is divided into four lobes of unequal size (Figure 5.7 a). Two large vessels carry blood to the liver. The hepatic artery comes from the heart and carries blood rich in oxygen. The portal vein brings the liver blood rich in nutrients absorbed from the small intestine. These vessels divide into smaller and smaller vessels, ending in capillaries. The blood then leaves the liver via the hepatic vein, returns to the heart, and is ready to be pumped to the rest of the body. Among the most important liver functions are:

- Removing and excreting body wastes and hormones as well as drugs and other foreign substances. These substances have entered the blood supply either through production by metabolism within the body or from the outside in the form of drugs or other foreign compounds. Enzymes in the liver alter some toxins so they can be more easily excreted in urine.

- **Synthesizing plasma proteins, including those necessary for blood clotting.** Most of the 12 clotting factors are plasma proteins produced by the liver. If the liver is damaged or diseased, it can take longer for the body to form clots. Other plasma proteins produced by the liver include albumin which binds many water-insoluble substances and contributes to osmotic pressure, fibrinogen which is key to the clotting process, and certain globulins which transport substances such as cholesterol and iron.

- **Producing immune factors and removing bacteria, helping the body fight infection.** The phagocytes in the liver produce acute-phase proteins in response to microbes. These proteins are associated with the inflammation process, tissue repair, and immune cell activities.

Other important but less immediate functions include:

- **Producing bile to aid in digestion.** Bile salts aid in fat digestion and absorption. Bile is continuously secreted by the liver and stored in the gallbladder until a meal, when bile enters the beginning of the small intestine. Bile production ranges from 250 mL to 1 L per day depending of amount of food eaten.

- **Excretion of bilirubin.** Bilirubin is one of the few waste products excreted in bile. Macrophages in the liver remove worn out red blood cells from the blood. Bilirubin then results from the breakdown of the hemoglobin in the red blood cells and is excreted into bile by hepatocytes. Jaundice results when bilirubin cannot be removed from the blood quickly enough due to gallstones, liver disease, or the excessive breakdown of red blood cells.

- **Storing certain vitamins, minerals, and sugars.** Liver stores enough glucose in the form of glycogen to provide about a day's worth of energy. It also stores fats, iron, copper, and many vitamins including vitamins A, D, K, and B12.

- **Processing nutrients absorbed from digestive tract.** Liver converts glucose into glycogen, its storage form. This glycogen can then be transformed back into glucose if the body needs energy.

The fatty acids produced by the digestion of lipids are used to synthesize cholesterol and other substances. The liver also has the ability to convert certain aminoacids into others. Despite the wide variety of functions performed by the liver, there is very little specialization among hepatocytes. Aside from the liver macrophages, called Kupffer cells, hepatocytes seem to be able to perform the same wide variety of tasks. One of the liver's most interesting abilities is self-repair and the regeneration of damaged tissues. In clearing the body of toxins, the liver is damaged by exposure to harmful substances, demonstrating why this capability is so important (Tzanakakis et al., 2000).

The Hepatic circulation (Figure 5.7 b) is unique among vascular beds. The most obvious unique features include the dual vascular supply; the mechanism of intrinsic regulation of the hepatic artery (the hepatic arterial buffer response); the fact that portal blood flow, supplying two thirds of liver blood flow, is not controlled directly by the liver; the fact that 20% of the cardiac output rushes through the most vascularized organ in the body, driven by a pressure gradient of only a few millimeters of mercury; the extremely distensible capacitance and venous resistance sites; the unidirectional blood flow that regulates parenchymal cell metabolic specialization; and the high concentration of macrophagic (Kupffer) cells filtering the blood. The liver is the only organ reported to have regional blood flow monitored by the autonomic nervous system. This mechanism, when dysfunctional, accounts for the hepatorenal syndrome and offers a mechanistic therapeutic target to treat this syndrome. The trigger for liver regeneration is dependent on hepatic hemodynamics so that chronic liver blood flow regulates liver cell mass. In severe liver disease, the whole body circulation is reorganized, by forming portacaval shunts,

to accommodate the increased intrahepatic venous resistance. These shunts protect the venous drainage of the splanchnic organs but lead to loss of major regulatory roles of the liver (Lautt, 2009).

The liver is covered with a connective tissue capsule that branches and extends throughout the substance of the liver as septae. This connective tissue tree provides a scaffolding of support and the highway along which afferent blood vessels, lymphatic vessels, and bile ducts traverse the liver. Additionally, the sheets of connective tissue divide the parenchyma of the liver into very small units called **lobules** (Figure 5.7 c). The hepatic lobule is the structural unit of the liver. It consists of a roughly hexagonal arrangement of plates of hepatocytes radiating outward from a central vein in the center. At the vertices of the lobule are regularly distributed portal triads, containing a bile duct and a terminal branch of the hepatic artery and portal vein. **Hepatocytes** are the principal functional cells of the liver and perform an astonishing number of metabolic, endocrine, and secretory functions. Roughly 80% of the mass of the liver is contributed by hepatocytes.

In three dimensions, hepatocytes are arranged in plates that anastomose with one another. The cells are polygonal in shape and their sides can be in contact either with **sinusoids** (sinusoidal face) or neighboring hepatocytes (lateral faces). A portion of the lateral faces of hepatocytes is modified to form bile canaliculi. Microvilli are present abundantly on the sinusoidal face.

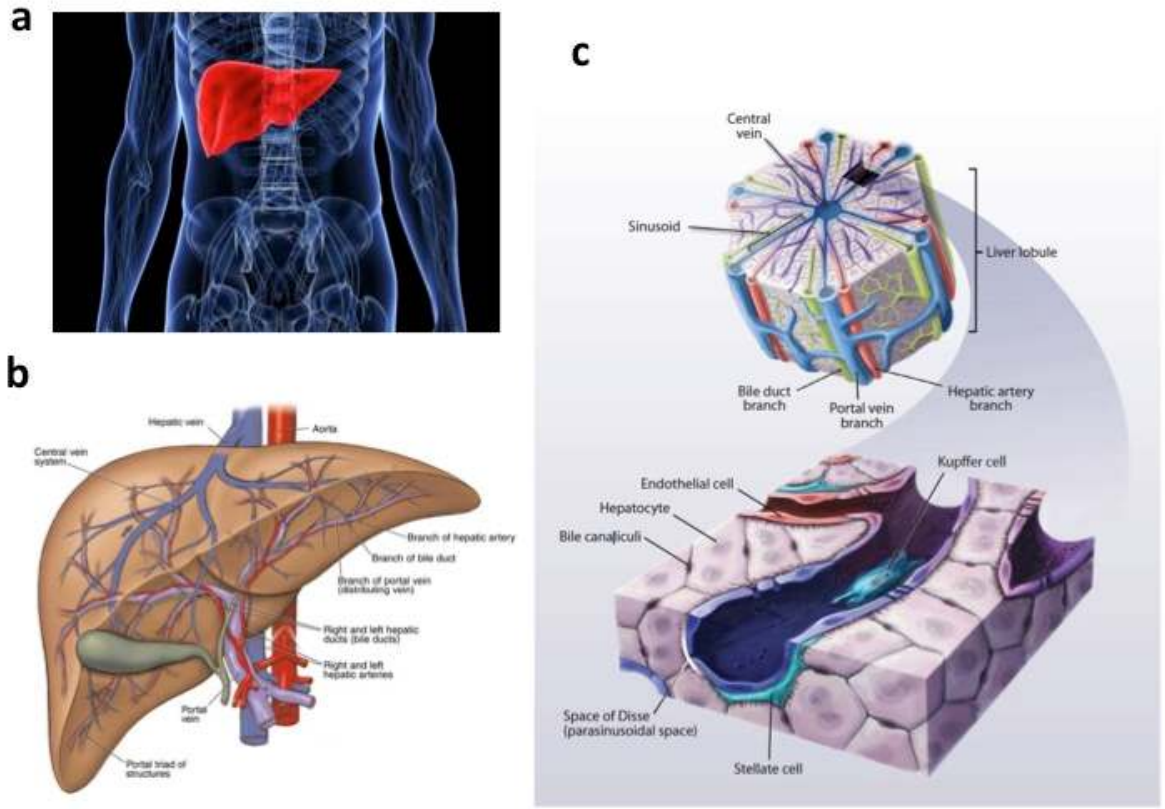

Figure 5.7: a) Liver; b) hepatic circulation; c) functional tissue unit (liver lobule) (top) and detail of liver cells (down).

5.2.2 NON ALCOHOLIC FATTY LIVER DISEASE (NAFLD)

Nonalcoholic fatty liver disease (NAFLD) is a chronic liver condition that has become the most common form of chronic liver disease worldwide, with particular incidence in developed countries (Starley et al., 2010) (Veteläinen et al., 2007). NAFLD is considered the hepatic manifestation of the metabolic syndrome, and a risk factor for type 2 diabetes mellitus, dyslipidemia, and hypertension (Adams et al., 2009; Marchesini et al., 2003). Being associated with increased cardiovascular- and liver-related mortality, it is now widely recognized as a public health issue (Lazo and Clark, 2008).

NAFLD encompasses a broad spectrum of liver pathologies ranging from simple steatosis to nonalcoholic steatohepatitis (NASH), advanced fibrosis and cirrhosis with its related complications, leading eventually to the development of hepatocellular carcinoma (HCC)

(Figure 5.8). HCC ranks as the third highest cause of cancer-related death globally, requiring an early diagnosis of NAFLD as a potential risk factor (Angulo, 2002; Starley et al., 2010). Steatosis is characterized by enhanced fatty infiltration within the liver in the absence of alcohol consumption, which may promote the progression to the more severe NASH, which is featured by mixed inflammatory-cell infiltration, hepatocyte ballooning and necrosis, portal hypertension and fibrosis (Angulo, 2002; Marra et al., 2008). However, the exact molecular mechanisms underlying NAFLD pathogenesis and progression are far from clear, and need to be further elucidated. At present, it is not yet possible to diagnose NAFLD, and to predict disease outcome based solely on routine blood tests and tissue biomarkers, such as the detection of elevated liver enzymes, or by performing an ultrasound. Thus, an invasive, potentially dangerous, and expensive liver biopsy still represents the gold standard for the diagnosis and staging of NAFLD, requiring the need of alternative non-invasive biomarkers, such as microRNAs as recently suggested (Gori et al., 2014a; Yan et al., 2007). HepG2 cells, a human hepatoblastoma cell line that retains many characteristics of normal differentiated and quiescent hepatocytes, including liver-specific metabolic functions, have been frequently used as a human-derived *in vitro* model system for investigating basic hepatic metabolism, drug hepatotoxicity as well as liver steatosis (Feldstein et al., 2003; García-Cañaveras et al., 2015; Javitt, 1990; Ricchi et al., 2009; Zhang et al., 2008). So far, despite the use of such reliable hepatic cell models, many *in vitro* studies on NAFLD have been hampered by the intrinsic limitations of 2D culture systems, in which cells rapidly lose tissue-specific functions. Although, as mentioned above, several works have exploited the technical advantages provided by a 3D microfluidic environment with cultures of hepatocytes and hepatic cell lines mostly for *in vitro* liver metabolism and toxicological studies (Baudoin et al., 2014b; Lee et al., 2007b; Zhang et al., 2008), none of them have so far used these platforms for developing novel models of NAFLD.

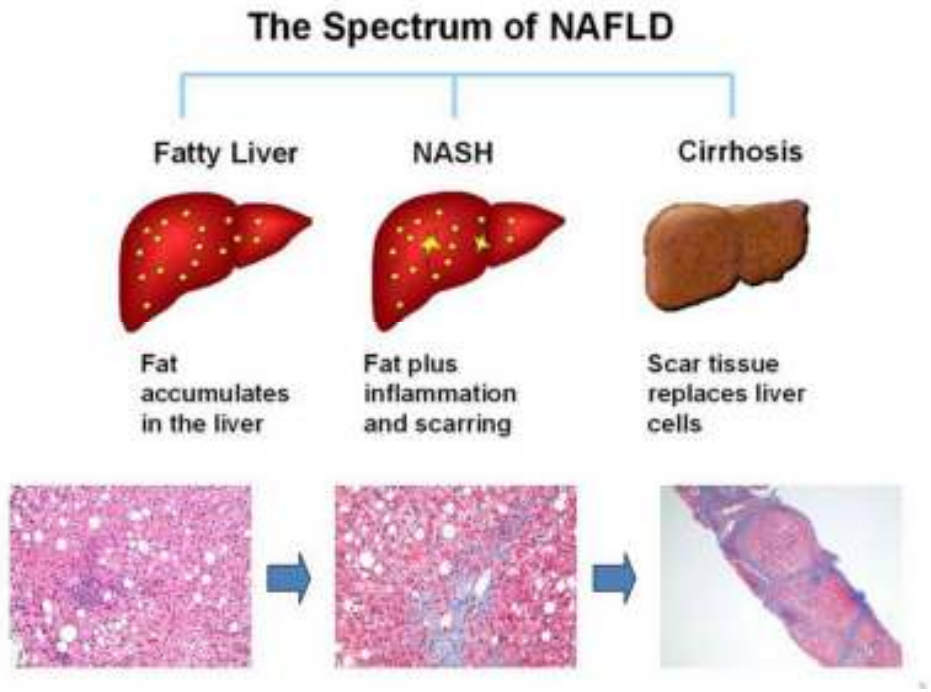

Figure 5.8: The spectrum of NAFLD.

5.3 Hepatic cells culture devices

The first clinical treatment for liver failure is transplantation, which nowadays is the only therapy able to affect mortality. Nevertheless, these procedures cannot meet the increasing demand of emerging liver diseases, from NAFLD to steatohepatitis and hepatocarcinoma. Moreover, extracorporeal support devices, with exchange and filtering functions, actually seem to exhibit an insufficient level of efficiency (Bhatia et al., 2014).

The principal reason is that liver cells grown in cell culture suffer from a rapid loss of their liver specific functions; therefore it is very difficult to perform analysis on liver toxicity or, more generally, on diseases affecting this organ. Most of all, it is very challenging to reproduce model systems for the study of liver function in healthy and diseased states, especially the chronic ones. This is due to the complex microenvironment of hepatocytes, which are subjected

to different signals from soluble factors to ECM components and heterotypic cell-cell interactions. Also the "biomarkers" indicating the clinical response are limited and very different in case of acute versus chronic disease, more than patient related. Thus, animal models are often scarcely predictive as diagnostic tools and must be carefully chosen. Extracorporeal liver devices are principally aimed at providing temporary support until a liver become available for transplantation (Figure 5.9). Extracorporeal bioartificial liver (BAL) devices incorporate liver cells with the scope to provide several liver functions, such as detoxification and metabolism by processing the blood outside the body.

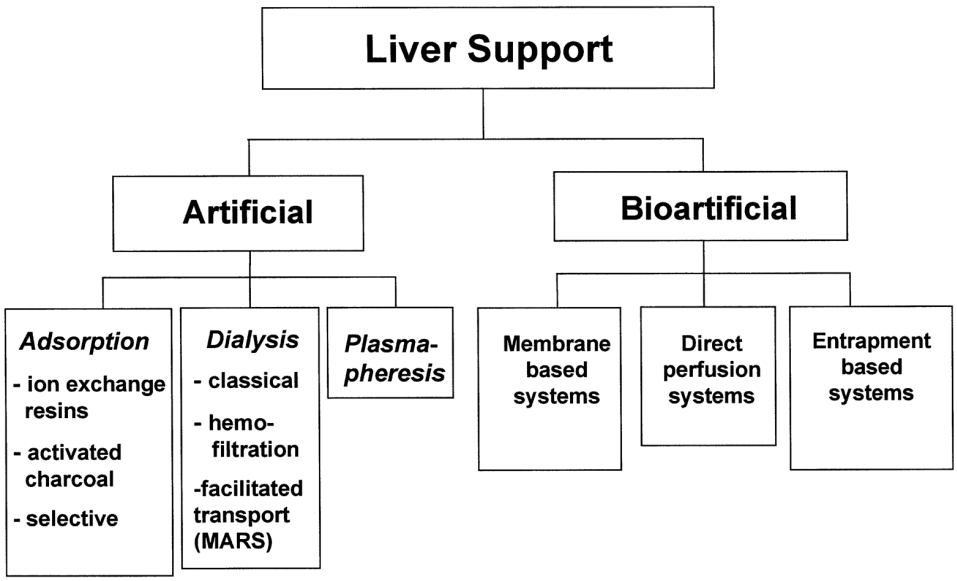

Figure 5.9: Classification of the different systems for temporary liver support (Legallais et al., 2001).

BALs are effectively bioreactors with the scope to offer an adequate environment to liver cells, whose mandatory requirements include the maintenance of cells viability and functions,

Principal drawbacks of BAL systems are the inefficient mass transport for synthesis and detoxification functions, the above-mentioned problems in culturing hepatocytes, transport and cryoconservation issues and the possible immunogenicity.

Tissue engineering approach concentrated on seeding hepatocytes within adequate scaffolds, able to preserve their phenotype and physiology. The field evolved from a top-down approach,

where cells are seeded into macroscopic polymeric scaffolds, to a more sophisticated bottom-up approach, were complex biomaterial constructs, made by hydrogels actively participate in tissue regeneration (Ananthanarayanan et al., 2011).

Great effort was done in identifying and reproducing specific culture architectures and molecular stimuli derived from the culture medium, the ECM and cell-cell interactions (Li et al., 2014). It was previously demonstrated how liver functions are better reproduced in a 3D spheroidal configuration (Landry et al., 1985). In this sense, numerous technologies were developed including arrays, rotational cultures and encapsulation methods.

These progresses in liver tissue engineering paved the way to several therapeutic models to study pharmacokinetics, metabolism and potential toxicity of new drugs. They can be classified in perfused hepatic cultures in bioreactors (Domansky et al., 2005; Hwa et al., 2007) and static monolayer cultures in 2D or aggregates in 3D spheroids (Lee et al., 2013b), eventually adding non-parenchymal cells, which showed to enhance hepatic cell functions when co-cultured with hepatocytes. The liver-on-chip idea could be considered the mixture of these two approaches, by combining the perfused bioreactor within a microfluidic platform enabling a threedimensional culture with a custom-made complex geometry. Furthermore, thanks to the advances in microfabrication techniques, it is possible to manufacture optically transparent platforms, suitable to be observed in real-time under a microscope. The above-mentioned quality paved the way to a new generation of diagnostic devices.

5.3.1 LIVER-ON-CHIP

Several microfluidic bioreactors were developed in the past years for *in vitro* liver model systems with the aim to recreate liver specific functions.

The first advantage is the possibility to integrate perfused systems (Leclerc et al., 2004) inside complex geometries with co-cultures of several cell types and the possibility to add electrodes and other microfabricated tools reproducing biomechanical stimuli (Baudoin et al., 2007).

Based on this idea, Lee et al. (Lee et al., 2007b) developed his artificial liver sinusoid. The device is composed by a central channel for hepatocyte culture in the cell-cell contact configuration, typical of liver sinusoid. An external channel, for continuous feeding of nutrients and waste removal, is separated from the latter by pillars mimicking the endothelial barrier function (Figure 5.10) and reproducing physiological mass transport properties.

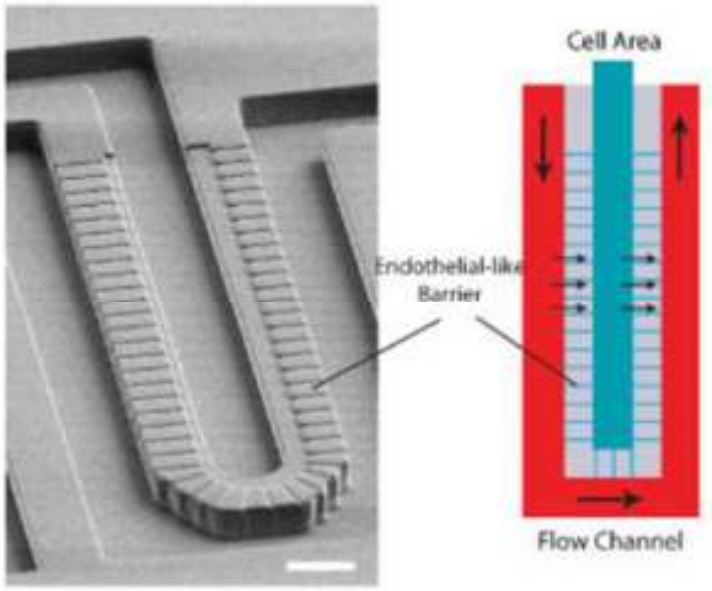

Figure 5.10: Photograph (left) and schematic view (right) of the device which resembles a liver sinusoid, including the endothelial barrier layer, developed by Lee et al. Cells were cultured in the Cell Area. Medium flowed around the outside of the endothelial-like barrier, with a portion crossing the endothelial barrier to the cells (Lee et al., 2007b).

The same group presented a similar device enabling the culture of high-density cells (<2,000 cells/mm^2) (Zhang et al., 2008). They used a microporous sieve-like barrier to allow the continuous flow of medium, and HepG2/C3A cells could grow within the platform for one week without loose viability (Figure 5.11).

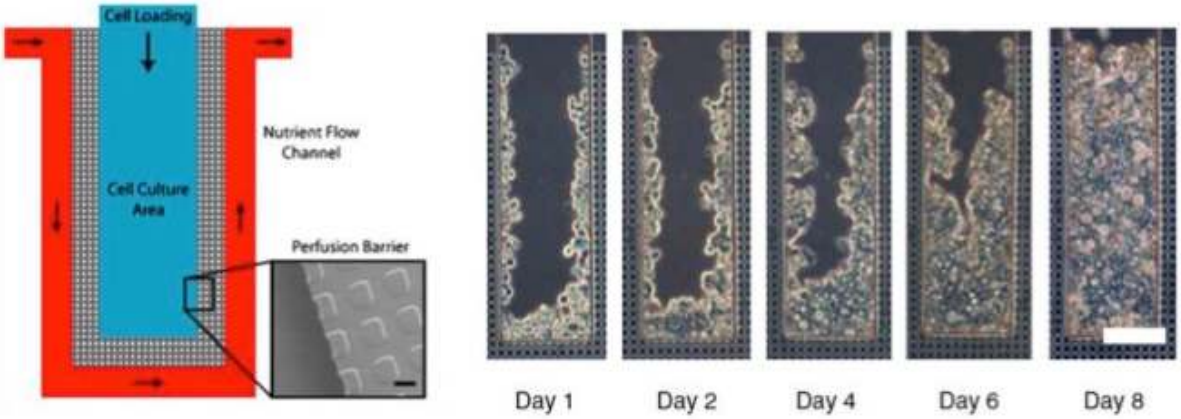

Figure 5.11: Schematic view (left) of the device with the microporous microfluidic barrier and photographs (right) of cell growth for one week within the device (Zhang et al., 2008).

Different chamber designs can be optimized with regard to hydrodynamic flow profile and call trapping rate, also thanks to the help of numeric simulations. These platforms have the great advantage to allow the study specific culture parameters effects. For example Baudoin et al. (Baudoin et al., 2011) designed a microfluidic bioreactor to investigate the behavior of HepG2/C3A liver cells with respect to variations of cell density and flow rate (Figure 5.12).

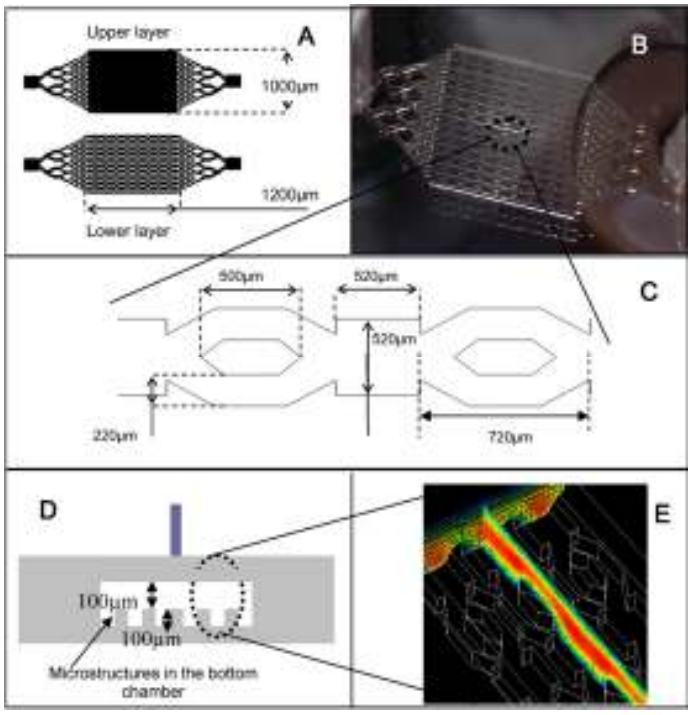

Figure 5.12: Microfluidic bioreactor developed by Baudoin et al. (Baudoin et al., 2011).

In a subsequent work, Baudoin et al. used the microfluidic platform, to study the effects of cell densities and perfusion flow rates parameters on primary rat hepatocyte expression and activity (Baudoin et al., 2014a). Illa et al. (Illa et al., 2014) developed a modular bioreactor enabling the co-culture of endothelial cells (EC) and hepatic stellate hepatocytes separated by a home-modified porous membrane under a dynamically perfused system, thus preserving the paracrine factor varied out on the hepatic cells by the EC.

On the other side, by using the dielectrophoresis as the driving force for cell manipulation, the morphology of liver lobule tissue can be achieved (Ho et al., 2013; Schütte et al., 2011). Lee et al. (Lee et al., 2013b) instead incorporated a liver microsome into a 3D PEG-hydrogel embedded inside a microfluidic channel to simulate physiological transport phenomena and reaction kinetics. They exploited a combination of mathematical analytical tool and the experimental one to simulate the convection-diffusion-reaction characteristics. Shear stress is another factor that influences metabolic activity; most importantly it should be low and independent from the direction. Esch et al. (Esch et al., 2015) developed a rocking platform that tilts the cell culture in order to periodically change the hydrostatic pressure drop between reservoirs. Microfluidic devices principal employment in the hepatology field is for drug metabolism and toxicity assays, which can be enriched by the chance to finely control cellular microenvironment and to expose cells to continuous medium flow (Esch et al., 2011) (van Midwoud et al., 2011). In fact, they were used for several metabolic characterizations (Chang et al., 2010; Choucha Snouber et al., 2013; Leclerc et al., 2015; Legendre et al., 2013; Legendre et al., 2014). In addition, hepatochips can also be used for diagnostic applications, eventually coupled with biosensors (Matharu et al., 2014).

Finally 3D liver platform can be combined with other tissues cultures, leading to multi-organ-chip, which might be useful for systemic substance testing (Baudoin et al., 2007; Wagner et

al., 2013) and metabolic profiling (Shintu et al., 2012). In their work, Guzzardi et al. (Guzzardi et al., 2009) demonstrated how hepatocytes and endothelial cell cultured in a dynamic multicompartmental microfluidic bioreactor, show a higher rate of metabolite synthesis and secretion, compared to the traditional static co-culture. In a different work Bricks et al. (Bricks et al., 2014) developed a platform integrating intestinal and liver cells. They showed to be able to maintain intestinal barrier integrity and functionality, while preserving liver cells viability and metabolism. A complex body-on-a-chip system was manufactured by Esch group (Esch et al., 2014), combining in vitro models of the human intestinal epithelium and liver cells (Figure 5.13). Moreover, other chambers represented all other organs, and they were able to use it to simulate the oral uptake of nanoparticles.

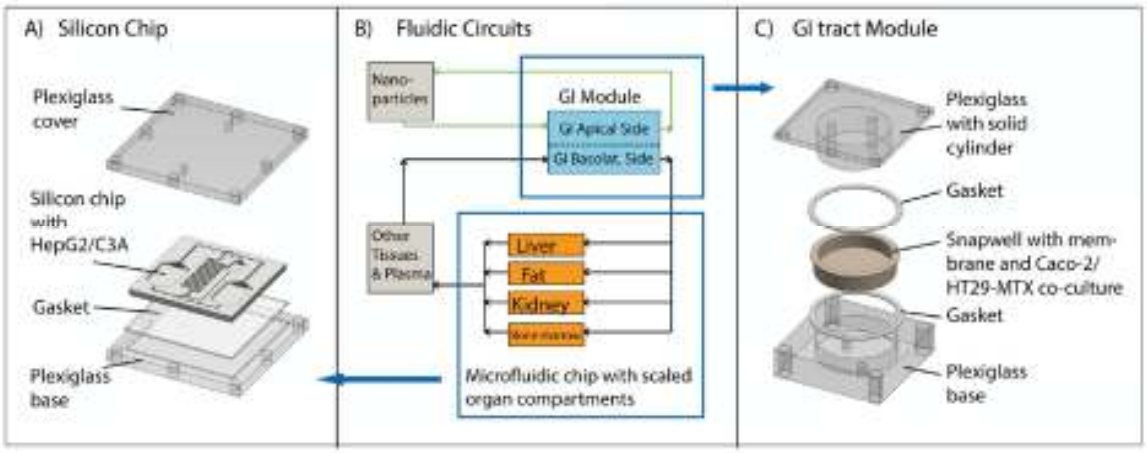

Figure 5.13: Schematic of the body-on-a-chip system made by Esch et al. (Esch et al., 2014).

Chapter 6

Experimental

6.1 Materials and Methods

6.1.1 Microfluidic Device Design And Microfabrication

The geometry of the microfluidic device was designed using a CAD suite (Layout Editor, Juspertor UG, Unterhaching, Germany), slightly modifying the original geometry of Lee et al. (Lee et al., 2007b) and transferred onto a chrome on soda-lime glass mask (JD Photo-Tools, Hitchin, UK), which was used for a 2-layer photolithographic process. First, a 5 μm-thick layer of SU-8 2005 negative resist (MicroChem Corp, Newton, MA) was patterned on a 3 in. silicon wafer to define the microfluidic endothelial-like barrier. Afterwards, SU-8 2015 resist was spin-coated on top of the first layer with a thickness of 30 μm, and the cell culture microchamber together with the transport channels were patterned. The SU-8 on silicon master was then used for the soft-lithographic process. Polydimethylsiloxane (PDMS, Sylgard 184, Dow Corning, Midland, MI) was cast on the master with a 10:1 (v/v) mixture of monomer and curing agent, using the replica molding technique. After degassing for 45 min. in a vacuum chamber, PDMS was cured at 70 °C for 2h, followed by 1h at 100 °C. Inlets and outlets for media and cell loading were manually punched out using a 6 mm biopsy puncher. PDMS devices were bound to microscope glass slides (52 × 76 mm), previously cleaned with piranha

solution (H_2SO_4/H_2O_2 3:1), by means of O_2 plasma bonding (FEMTO plasma cleaner, Diener Electronic, Ebhausen, Germany, 10 W, 1.0 mbar, 36 sec).

6.1.2 Cell Culture And Microfluidic Operation

Cell culture

Human hepatoma HepG2/C3A cells (CRL-10741) were purchased from the American Type Culture Collection (ATCC). Cells were cultured in Dulbecco's Modified Eagle's Medium (DMEM) supplemented with 2 mM L-glutamine, 100 U/mL penicillin, 100 µg/mL streptomycin (Lonza, East Rutherford, NJ, USA), 10% fetal bovine serum (Gibco, Milan, Italy), and incubated in a humidified 37 °C incubator with 5% CO_2.

Microfluidic operation

HepG2 were cultured in 3D under microfluidic perfusion, through a system of parallel microchannels that mimics the endothelial barrier of a liver sinusoid, allowing for continuous diffusion of nutrients and removal of waste products (Lee et al., 2007b). This microarchitecture provides a neglectable shear stress to the cells, as already demonstrated in the literature (Lee et al., 2007b), in which the high fluidic resistance of the microchannel barrier prevents the cell damage due to the shear stress. Prior to cell loading, devices were UV-sterilized, filled with complete culture medium, and left at 37 °C in a cell culture incubator for 30 min. After gently removing the medium, 20 µL of HepG2 suspension at a concentration of 2.0×10^6 cells/mL (corresponding to 4.0×10^4 cells/chip), was pipetted into the cell culture area of the chip *via* the central cells loading channel. The chip was placed on an incline to let the cell culture chamber fill by gravity, and the process was monitored under a Leica DM IL inverted phase-contrast microscope (Leica Microsystems, Wetzlar, Germany) to determine when the microchamber was completely filled. During the cell loading process, a positive flow of the cell suspension was observed, enabling cells to continuously pack into the culture chamber, and no membrane

deformation was visible.

Perfusion was achieved by applying a difference in the level of the medium in each of the two plastic reservoirs glued on top of the medium inlet and outlet, connected with each other through the fluidic channel. Medium was directly filled into the reservoirs, such that a continuous flow from the transport channel (steady flow rate: 18 µL/day) was provided to the cells in agreement with the literature (Lee, Hung et al. 2007, Zhang, Lee et al. 2008), through the endothelial-like barrier of microchannels. The devices were transferred into 150 mm sterile Petri dishes for culturing. In parallel, 2D static cultures of HepG2 cells were plated into 96-well multiwell plates (BD Falcon, BD Biosciences, Italy) at a density of 5.6×10^4 cells/cm^2. Both liver-on-a-chip devices and 2D control cultures were incubated overnight (o.n.) at 37 °C in conventional HepG2 culture medium, before initiating the treatments with FFAs in steatosis medium (see section 2.3) on the following day.

6.1.3 Induction And Evaluation Of Steatosis

For cell treatments, a combination of long-chain free fatty acids (FFAs), namely palmitic acid (PA; lipid number 16:0) and oleic acid (OA; lipid number 18:1 *cis*-9) (Sigma-Aldrich, Milan, Italy) was dissolved in methanol (vehicle) and added to the medium. PA and OA were chosen as they are the most abundant FFAs in western diets and liver triglycerides in both normal subjects and patients with NAFLD (Baylin et al., 2002; Gómez-Lechón et al., 2007). Steatosis was induced by modifying the method previously described (Gori et al., 2014b). Briefly, HepG2 cells were incubated with a mixture of PA (0.33 mM) and OA (0.66 mM) for 24h and 48h. To induce fat-overloading of HepG2 cells, stock solutions of the FFAs were diluted in DMEM supplemented with 1% L-glutamine (Lonza, USA), 1% bovine serum albumin (BSA) Cohn fraction V (Sigma-Aldrich, Italy), 10% charcoal-stripped fetal bovine serum (FBS, Hyclone, GE Healthcare, USA). Internal controls were represented by both liver-on-a-chip

devices and 2D static cultures in medium with vehicle only.

The effects of FFA treatment in terms of intracellular lipid accumulation, cell viability and oxidative stress were evaluated at each timepoint using microscope-based fluorescent functional assays on an epifluorescence inverted microscope (Eclipse Ti-E, Nikon, Tokyo, Japan), equipped with a high sensitivity camera (Neo 5.5, Andor, Ireland) and acquisition/analysis software (NIS Elements AR, Nikon).

6.1.4 Measurement Of Intracellular Lipid Accumulation

Total intracellular triglyceride accumulation was measured by the AdipoRed assay (Lonza, Basel, Switzerland), according to the manufacturer's instructions. After rinsing with PBS, incubation with AdipoRed reagent was performed at room temperature (RT) for 10 min, and mean fluorescence intensity (MFI) of the ROIs occupied by the cells was measured (FITC filter set). In the microfluidic device, the whole cell culture chamber was analyzed, while in the 2D culture plates, fluorescence intensity was evaluated by counting at least 3 randomly selected, non-overlapping microscopic fields per well in four different wells. Values were normalized against their internal controls.

6.1.5 Analysis Of Cell Viability/Cytotoxicity

After incubation with FFAs for 24h and 48h, chips and 2D cultures were rinsed in PBS and incubated with the Live/Dead Viability/Cytotoxicity reagent (ThermoFisher Scientific, Waltham, MA) in PBS at RT for evaluation of cell viability/cytotoxicity according to manufacturer's instructions. Nuclei were counterstained with DAPI (S7113, Merck Millipore, MA; 0.4 μg/mL in PBS for 10 min). Green-fluorescent live cells and red-fluorescent dead cells were separately counted, and results were plotted as a percentage of live cells in FFA-treated

vs. control cultures for both chips and 2D cultures after 24h and 48h.

6.1.6 Analysis Of Oxidative Stress

Oxidative stress was measured by assessing intracellular ROS levels generated after exposure for 24h and 48h with FFAs, through the green-fluorescent ROS detection reagent 6-carboxy-2′,7′-dichlorodihydrofluorescein diacetate, di(acetoxymethyl ester) (carboxy-H_2DCFDA, ThermoFisher Scientific), according to the manufacturer's instructions. Briefly, cells were rinsed in PBS and loaded with 10 μM of the cell-permeant probe carboxy-H_2DCFDA for 30 min at 37 °C in complete FluoroBrite DMEM (Gibco, ThermoFisher Scientific), to exclude hydrogen peroxide generation in phenol red containing medium, before fluorescence analysis. Incubation with 400 μM H_2O_2 (Sigma-Aldrich) was used as a positive control for ROS. The regions of interest (ROIs) occupied by cells were identified from phase contrast micrographs, and used for the fluorescence analysis. Fluorescence intensity (FITC filter set) of positive cells was quantified and expressed in RFUs. All treated cells were normalized to their own internal controls.

6.1.7 Statistical Analysis

Data are presented as means ± standard deviation (SD) of three independent experiments. Data were analyzed using Origin ver. 9 (OriginLab Corp. Northampton, MA) software suite. One-way analysis of variance (ANOVA) was used for multiple means comparisons, followed by post hoc testing (Tukey). Significance was at the 0.05 level.

6.2 Results and Discussion

6.2.1 The 3d Microfluidic Device Enables Long-Term Dynamic Culture Of Hepg2 Cells.

The study of liver physiopathology is essential to understand the initiating events and the progression of NAFLD, to facilitate its diagnosis, and to develop novel therapeutic approaches. Nevertheless, the traditional culture systems present limitations essentially related to the 2D microenvironment of the culture, which is far from the *in vivo* condition, and determines a rapid loss of the tissue-specific cell functions.

Therefore, the geometric configuration of our chip, and the microfluidic mass transport system were designed and fabricated, making some slight changes in size to the model developed by Lee P.J. (Lee et al., 2007b) (see Figure 6.1 a), in order to reproduce the typical human liver micro-unit, the hepatic sinusoid, which consists of a cord of hepatocytes bordered by highly fenestrated and permeable endothelial cells, represented by a grid of closely spaced and parallel microchannels that mimic an endothelial-like barrier and, as such, the tissue microvasculature (Figure 6.1 a, b). Hence, this microarchitecture is similar to a human liver sinusoid, in which each micro-unit consists of approximately 420 tightly packed HepG2 cells surrounded by the transport channel that is filled with culture medium. The channel communicates with the cell microchamber *via* the grid of microchannels that ensure the diffusion of nutrients and the removal of metabolic waste products. Thus, this microfluidic chip design mimics the interface between the endothelium and parenchyma observed in the native liver, similar to the *in vivo*

microvasculature, HepG2 cells confined within the culture microchamber sense a negligible shear stress that may cause damages to the hepatocyte membranes.

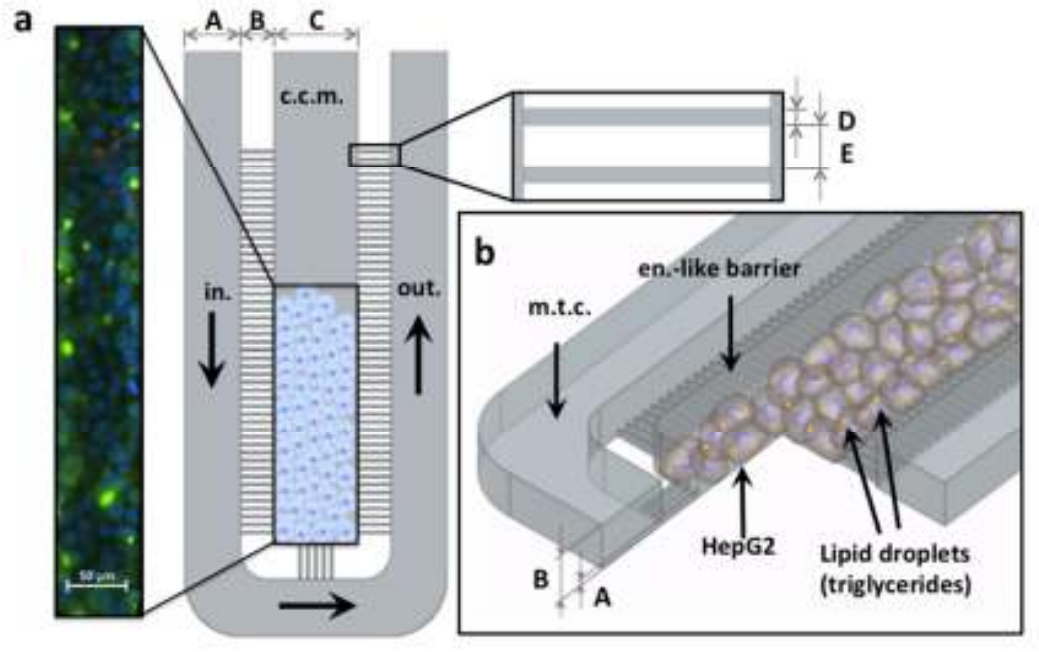

Figure 6.1: Microarchitecture and geometric configuration of the 3D model of NAFLD-on-Chip. (a) Top view of a single microfluidic sinusoid of the liver-on-chip model of NAFLD. Indicated by the black arrows are the two main ports of the mass transport channel (m.t.c.): medium inlet (in.), medium outlet (out.), and the cell culture microchamber (c.c.m.) loaded with HepG2 cells. Left panel shows a representative fluorescence microscopy image (20x) of cultured HepG2, magnified from the selected area within the c.c.m., with live cells (green), dead cells (red), and nuclei stained with DAPI (blue). Itemized are size of the different parts: A) transport channel width = 50 µm, B) microchannels lenght = 30 µm, C) cell culture microchamber width = 75 µm. Magnified in the inset is shown a detail of the endothelial-like barrier (en.-like barrier) of microchannels with respective dimensions: D) microchannel width = 2 µm, E) gap between two consecutive microchannels = 5 µm. 3D model of the microfluidic device (b) showing the high-density culture of hepatic cells overloaded with lipid droplets (in yellow, pointed by the black arrows) of triglycerides, and size of the two layers, respectively: A) first layer height = 5 µm, B) second layer height = 30 µm.

For chip cultures, a total volume of 20 µL with 2.0×10^6 cells/mL was pipetted into the cell loading channel and cells left to enter the culture microchamber by gravity flow. Afterwards, 400 µL of HepG2 medium was added to the medium inlet, whereas 200 µL to both the outlet

and cell loading well to create the medium height difference. Once the cells were loaded, the microfluidic devices were continuously perfused with culture medium in a standard incubator (37°C, 5% CO2). Flow rates were determined by measuring the height difference between inlet and outlet wells every 24h in quadruplicate culture units, and the steady flow rate calculated was 0.76 µL/h. Fresh medium was refilled with a total volume of 800 µL each day in order to preserve constant head pressure throughout the culture period.

Preliminarily, with the aim to analyze the suitability of the microfluidic device to allow HepG2 cell growth and proliferation, and evaluate their morphology, cells were grown under perfusion within the chip for one week and compared to standard 2D monolayer cultures (Figure 6.2 a, b). To this purpose, at day 0, the chip was loaded until approximately half of the microchamber area was filled with cells at high density, namely > $2.0x10^8$ cells/cm^3 (Figure 6.2 a). Cell growth was monitored daily for proliferation ability within the chip. By day 5 the whole chamber was colonized by the proliferating cells that reached the confluence and were distributed in two overlapped layers, showing a densely packed tissue-like morphology with extensive cell-cell contacts. Notably, at day 8, cells were stained with the LIVE/DEAD reagent for cell viability/cytotoxicity, showing extremely high HepG2 viability around 95% (green cells in Figure 6.2 a). Instead, in control 2D cultures (Figure 6.2 b) the percentage of live cells after 8 days was around 79% (green cells in Figure 6.2 b). Unlike the on-chip cultures, cells in the plate acquired a more spread and adherent morphology after a week, showing lower density and the characteristic HepG2 small aggregates that did not covered the whole plate surface. Hence, these results highlight that dynamic cultures of HepG2 with confluent and high-density cell morphology in the microfluidic device enable higher cell viability, after a week, compared to static cultures in standard tissue culture plates.

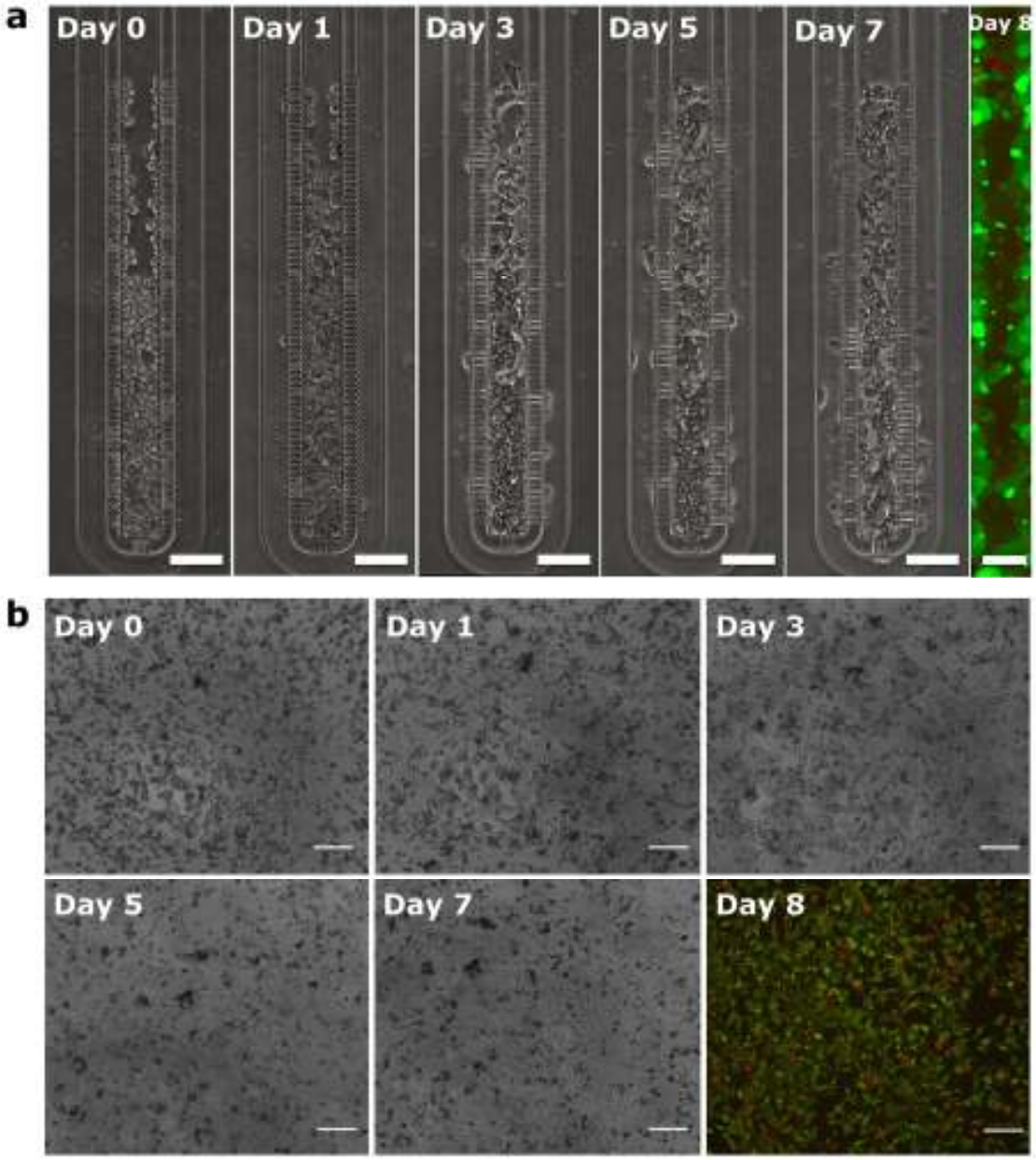

Figure 6.2: Analysis of cell viability/cytotoxicity and cell morphology over a week in culture. Phase contrast micrographs of HepG2 cell growth inside the 3D microfluidic sinusoid (a), and on a standard 96-well tissue culture plate (b) over a week in culture (Day 0, 1, 3, 5 and 7 are shown). Images are at equal magnification (10x) with scale bars representing 100 µm in a (except Day 8 = 50 µm) and 200 µm in b. At day 8, fluorescence microscopy of Live/Dead cells in both culture systems shows higher cell viability in chip (approximately 95%, Figure 6.2a, green cells within the ROI of the cell culture microchamber) compared to standard tissue culture plate (approximately 79%, Figure 6.2b, green cells). Dead cells were stained in red. Notably, a different cell morphology between the two culture systems is evident.

6.2.2 Gradual And Lower Intracellular Lipid Accumulation In 3d Dynamic Cultures Vs. 2d Static Controls

Our 3D model of "NAFLD-on-Chip" (Figure 6.1) was developed by exposing HepG2 cells to a combination of PA and OA at a total concentration of 1mM for 24h and 48h (Figure 6.3), while internal controls were represented by HepG2 cultured in medium with the equivalent concentration of the vehicle. In parallel experiments, 2D cultures of HepG2 cells treated with FFAs and their own internal controls (Figure 6.3) were compared to the corresponding on-chip cultures.

After 24h, intracellular lipid accumulation, in terms of triglyceride content of treated cells vs. internal controls measured by the AdipoRed assay (Figure 6.3 a), was statistically significant only in 2D static cultures but not yet in the chip, as also shown in the representative fluorescent stainings (Figure 6.3 b, c). Interestingly, after 48h, a further increase was measured in 2D cultures as well as in the chip, in which the lipid content became statistically significant compared to its internal control (Figure 6.3 a). Furthermore, the difference between chip and plate was much more higher, as visible in the corresponding fluorescent images (Figure 6.3 b, c).

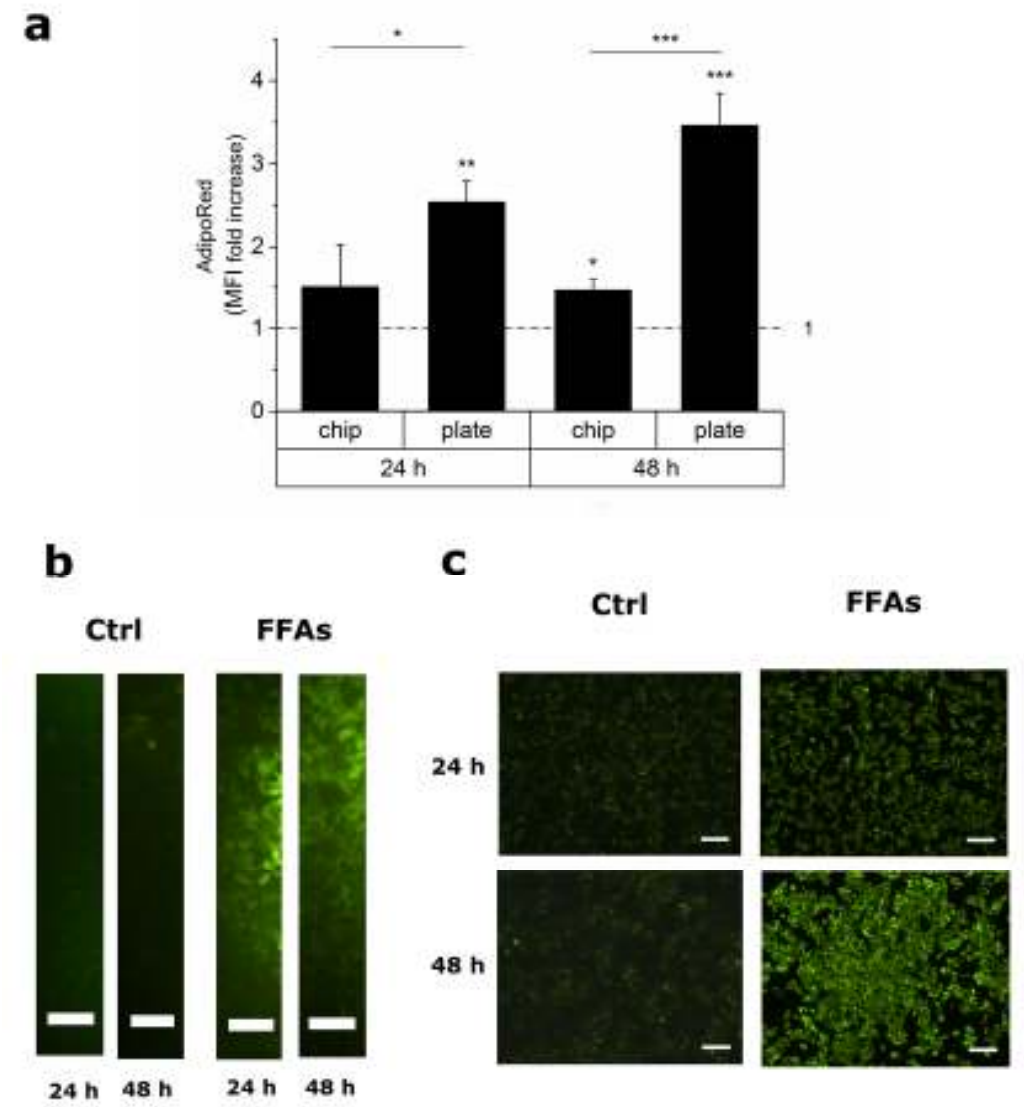

*Figure 6.3: AdipoRed assay for the analysis of intracellular triglyceride accumulation. (a) Histogram showing the mean fluorescence intensity (MFI), expressed as the ratio between FFA-treated cells and controls (plotted as 1.0 on the y axis, dashed line), for both chip and plate cultures after 24h and 48h. * $P < 0.05$, ** $P < 0.01$, *** $P < 0.001$. Representative fluorescent images of the lipid overload (green cells) plotted in (a) in cells cultured within the chip (b) (ROIs of the cell culture microchamber are shown) and the plate (c) after 24h and 48h. Chip images at 20x magnification with scale bars representing 50 µm in (b); plate images at 10x magnification with scale bars representing 200 µm in (c).*

6.2.3 Higher Cell Viability Of Dynamic Hepg2 Cultures Compared To 2d Static Controls Under Conditions Of Hepatic Steatosis

The cytotoxicity of the FFA treatment for both the 3D and 2D cultures was investigated using the differential fluorescent labeling of live and dead cells *via* the Live/Dead assay (Figure 6.4), which allows evaluating the relative percentage of live cells by fluorescence microscopy. As shown in Figure 6.4a and in the representative images in Figure 6.4b, as regards 2D cultures, cell viability of treated cells is decreased, due to the cytotoxic effect of the FFAs, compared to their internal controls, whereas this difference is minimal within 3D cultures in which the FFA overload appears to be much better tolerated by the cells. Importantly, both after 24h and 48h there is a statistically significant difference in the percentage of live cells between the 2D plate and the 3D cultures for the FFA-treated cells and internal controls as well. This outcome is in line with the different intracellular lipid accumulation, previously observed in Figure 6.3, between plate and chip. Moreover, there is a general reduction in cell viability between 24h and 48h, within both the static culture and the dynamic 3D culture, which is however not statistically significant. Overall, under the conditions of steatosis induced in our model the microfluidic system allows higher hepatic cell viability than traditional 2D static cultures.

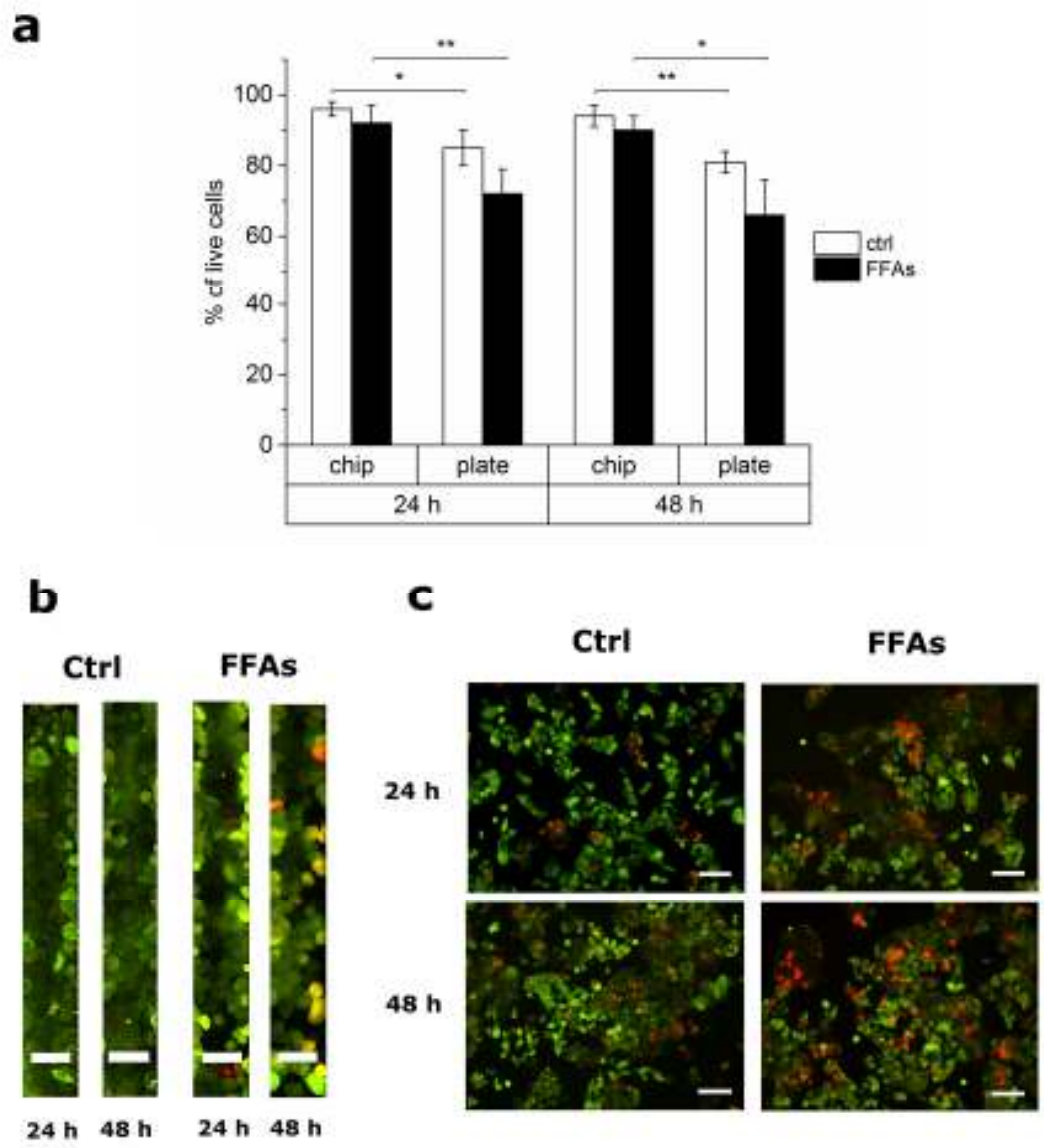

*Figure 6.4: Live/Dead assay for cell viability/cytotoxicity following the treatment with FFAs. (a) Histogram showing the percentage of live control (white bars) and FFA-treated (black bars) cells cultured in both the chip and the plate after 24h and 48h. * $P < 0.05$, ** $P \leq 0.01$. Representative fluorescent images of live cells (green via the calcein AM dye) and dead cells (red via the ethidium homodimer-1 dye) plotted in (a) in cells cultured within the chip (b) (ROIs of the cell culture microchamber are shown) and the plate (c) after 24h and 48h. Images are at equal magnification (20x) with scale bars representing 50 μm in (b) and 100 μm in (c).*

6.2.4 Comparable Levels Of Oxidative Stress Between On-Chip And 2d Cultures In The Setting Of Steatosis

It is known that in response to a metabolic stress, such as the FFA overload induced herein, hepatic cells are able to produce ROS, as intermediates of lipid oxidation reactions, which may have harmful effects provoking cellular damage, oxidative stress and DNA damage, thus leading to apoptosis (Assaily et al., 2011). Thus, with the purpose to investigate the oxidative stress caused by the exogenous lipid accumulation, we evaluated cellular ROS levels in both 3D and 2D cultures after 24h and 48h (Figure 6.5). Cells exposed to 400 μM H_2O_2 (Chavez-Tapia et al., 2012; Sekiya et al., 2008) for 24h and 48h were considered as positive controls (data not shown). ROS levels in cells treated with FFAs, normalized to their internal controls, were very low after both 24h and 48h, and comparable between 3D and 2D cultures (Figure 6.5). The trend of ROS production, passing from 24h to 48h of treatment, was descendant, with a slightly lower level in the chip compared to the 2D culture, though the difference was not statistically significant (Figure 6.5 a). The reported low ROS production is in agreement with previous literature reports (Ricchi, Odoardi et al. 2009, Chavez-Tapia, Rosso et al. 2012).

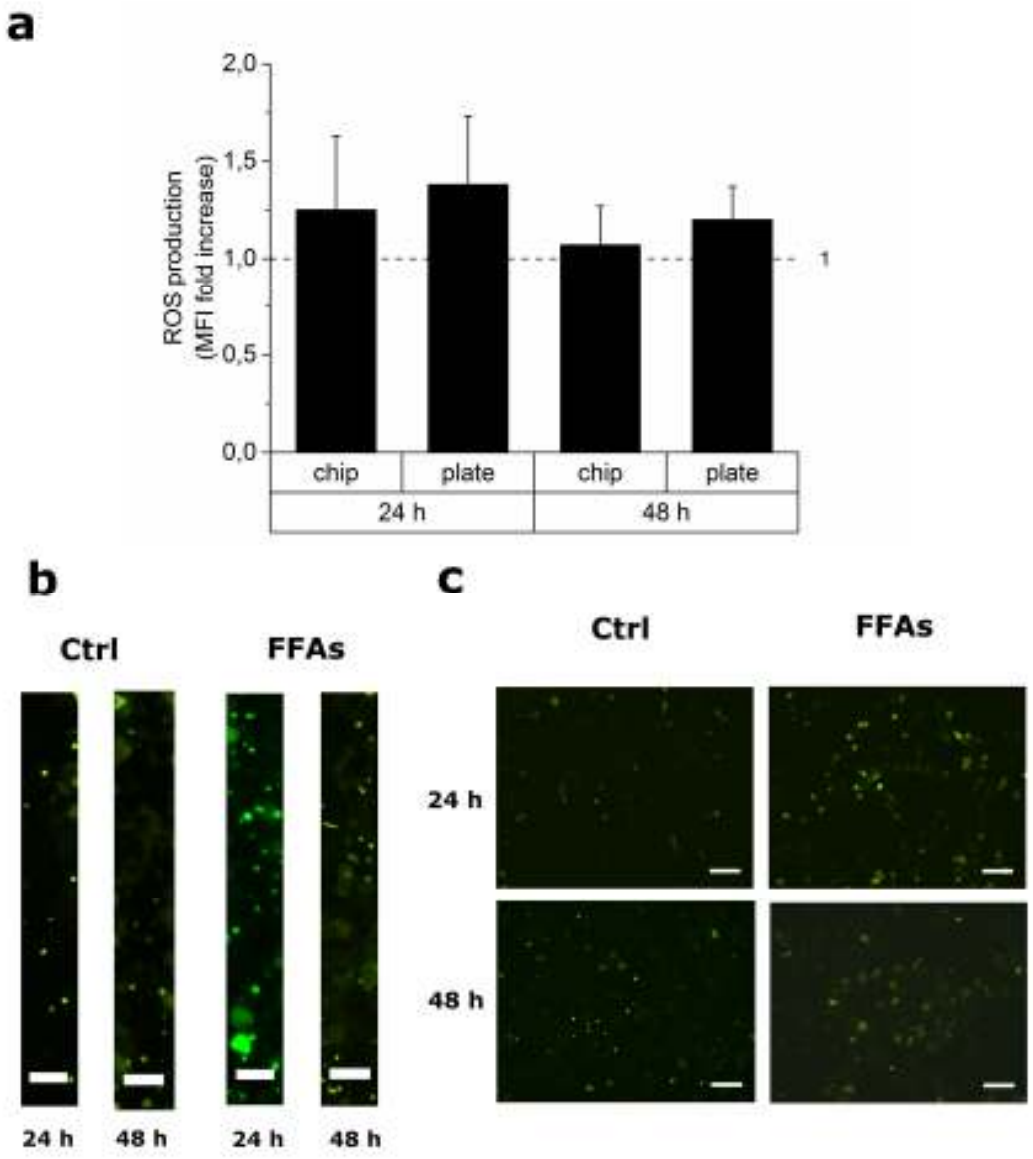

Figure 6.5: ROS detection assay for the analysis of oxidative stress levels, using carboxy-H_2DCFDA, following the treatment with FFAs. (a) Histogram showing the mean fluorescence intensity (MFI), expressed as the ratio between FFA-treated cells and controls (plotted as 1.0 on the y axis, dashed line), for both chip and plate cultures after 24h and 48h. Incubation with 400 μM H_2O_2 (shown in the box) was used as positive control of ROS production. Representative fluorescent images of intracellular ROS (green cells stained via the cell-permeant probe carboxy-H_2DCFDA) plotted in (a) in cells cultured within the chip (b) (ROIs of the cell culture microchamber are shown) and the plate (c) after 24h and 48h. Images are at equal magnification (20x) with scale bars representing 50 μm in (b) and 100 μm in (c).

SECTION II (b): MICROFLUIDIC DEVICE TO STUDY THE INTERPLAY BETWEEN STEM TUMOR COMPARTMENT AND THE IMMUNE SYSTEM

Chapter 7

Introduction and background

In 2012, according to the World Cancer Research Fund International, around 14.1 million cancer cases were diagnosed. Breast cancer is the second most common cancer with nearly 1.7 million cases per year.

Extravasation of cancer cells from the primary tumor and the subsequent metastases in a secondary organ is responsible for more than 90% of cancer related mortality (Jeon et al., 2015) (Wirtz et al., 2011). Therefore, being able to detect and harvest circulating tumor cells (CTCs) to test their chemoresistance would be a crucial step in early stages, before tumor cells intravasation into capillaries and new tissues.

The physical interactions between a cell and its extracellular matrix have a key role in allowing cells to migrate from a tumor to nearby blood vessels (Wirtz et al., 2011).

According to our aim to mimic and study tumor physiological microenvironment, after describing **tumor microenvironment**, and the **role of tumor-associated macrophages (TAMs)**; *in vitro* **extracellular matrices** mimicking will be described in the subsequent paragraph, and **cell migration** analysis techniques in microfluidic devices will be investigated with the same purpose.

7.1 Cancer microenvironment

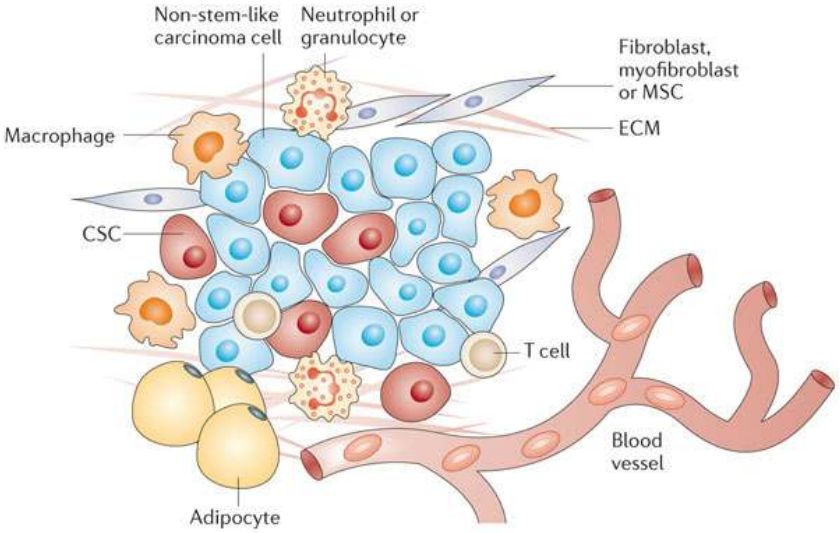

Figure 7.1: Tumor microenvironment heterogeneity (Nature Reviews, Drug Discovery).

The tumor mass is a complex system, where different cell types interact continuously; it includes neoplastic cells, fibroblasts, endothelial cells, and the immune system (Figure 7.1).

The physics of cancer is complex and comprises multistep processes. Epithelial-to-mesenchymal transition (EMT) is the starting point of dissemination of carcinoma leading to the metastatic cascade. In fact, in the oncogenic transformation, epithelial cells undergo a morphological change from a cubical to an elongated shape, often accompanied by loss of expression of the adhesion molecule E-cadherin, showing a high-motility phenotype (Wirtz et al., 2011). Physical interactions are modulated by the interplay of mechanical forces (eg. cell velocity vs. adhesion force) with biochemical changes (they are interconnected and influence each other very strictly). The goal of current therapeutic strategies would be to prevent EMT by identifying targeted drugs capable of interfering with this transition or able to revert the

mesenchymal-like phenotype of cancer cells to an epithelial-like state. To do that it is useful to understand the mechanisms behind the activation of signaling pathways in early metastasis (Aref et al., 2013). About tumor microenvironment, Stephen Paget's "seed and oil" hypothesis is now famous, and it says that the metastasis patterns are the product of favorable interactions between tumor cells ("seed") and their microenvironment ("soil"). In fact, cancer metastasis arises from extravasation of circulating tumor cells (CTCs), which generally have high organ specificity (Jeon et al., 2015). They exit the circulatory system by binding to a blood vessel wall through a ligand-receptor mechanism, and are able to escape immune system by associating with platelets (Wirtz et al., 2011). The interaction between pluripotent stem cells within tumor and the local microenvironment determines the success or suppression of tumorigenesis. For example, Bersini et al. (Bersini et al., 2014a) developed a microfluidic device to analyze the transendothelial migration of human breast cancer cells to a bone-like matrix. As the probable origin of intractable metastatic disease, CTCs represent an alternative to biopsies to detect and characterize tumor cells. Therefore, scientists are continuously developing strategies to identify, isolate and characterize them, in order to find cancer stem biomarkers and expand the understanding of cancer biology (Maheswaran et al., 2008; Nagrath et al., 2007). It has to be taken into account that tissue architecture and intracellular signaling (such as balance of activities of integrins and growth factor receptors) in oncogenic mutations differ from normal organization. Most importantly, the dimensionality of the system used to study cancer invasion can be crucial in determining cell migration behavior (Wirtz et al., 2011), so that the conventional ECM-coated 2D substrate will necessarily need to be substituted by a device allowing a three-dimensional environment. This is the reason why extravasation models evolved in the last years from the traditional transmigration chambers to the more sophisticated microfluidic devices, which enable to study cell-cell and cell-matrix interaction in a highly controlled milieu (Bersini et al., 2014b). Takayama group (Song, 2009) fabricated a

microfluidic device to produce controlled defined flow rates to model the interactions between circulating breast cancer cells with microvascular endothelium as potential sites of metastasis. In general, 3D screening platforms provide a deeper understanding of the complexity and heterogeneity of microenvironments. They also better predict the toxicity and efficacy of drugs in physiologically relevant conditions. Thanks to microscale technology, these cultures can be miniaturized to allow high throughput screenings choosing different parameters (Montanez-Sauri et al., 2015).

Threedimensionality is usually obtained by embedding cell in an adequate scaffold, artificially recreating the extracellular matrix where cells are physiologically submerged (Huang et al., 2009). Sometimes scaffold-free 3D formats are composed by spheroids or cellular aggregates, by cultivating cells in low-adherence and serum-free medium. Nevertheless, as underlined by Yamada (Yamada and Cukierman, 2007), the 3D model chosen influences the experimental outcome.

Spheroids 3D models are the best way to represent tumor cells. In fact, these aggregates, like tumors, usually contain both surface-exposed and deeply buried cells, proliferating and nonproliferating cells, and well-oxygenated and hypoxic cells. Moreover, when grown in a spheroidal configuration, it is higher the Cancer Stem Cells (CSCs) ratio. These cells are the major responsible of chemio- and radioresistance towards conventional drugs, hence the principal reason of disease relapse, thanks to their self-renewal property (O'Brien et al., 2010). Spheroids can be studied in suspension, in bioreactors, or 3D matrices, and can be constituted by mixtures of tumor, stromal, and immune cells (Yamada and Cukierman, 2007). In spheroid culture, cell secrete their own ECM in which they reside (Fennema et al., 2013); moreover, they allow to model critical *in vivo* parameters, such as barriers to mass transport and, more broadly, complex multicellular architectures (Mehta et al., 2012). In Karlsson's study (Karlsson et al., 2012), they evidenced how the development of a hypoxic center in the

spheroids of HCT-116 colon cancer cells line gave an augmented resistance to drugs cytotoxicity, compared to monolayers cell cultures. Kamm group fabricated a microfluidic device (Aref et al., 2013) able to encapsulate 3D A549 lung adenocarcinoma cell spheroids in a gel region to test drug candidates inhibiting receptor activation or signal transduction pathways implicated in EMT.

Transferring traditional methods used in clinical and experimental oncology to microfabricated devices would result in an increased resolution and high throughput analysis, including a dynamic investigation of many variables at the same time, with a costs reduction. Nowadays, the Lab-on-a-Chip (LOC) technology and micro-total analysis systems (μTAS) are promising platforms for massive experimental parallelization and real-time (4D) analysis on a single cell level. Therefore, they can be really helpful in expanding our knowledge of tumor mechanisms and resistance to therapies, hence providing useful tools for the design of new drugs and point-of-care devices (Wlodkowic and Cooper, 2010).

7.2 Role of tumor-associated macrophages

About immune system microenvironment C. J. Love says:

"The immune system is a multicellular network of cells (dendritic cells, macrophages, natural killer (NK) cells, T cells, B cells) that interacts through ligand-receptor complexes mediated by manifold secreted proteins (cytokines, chemokines, antibodies), and glycoproteins expressed on the cells' surfaces. The nature of any response by the immune system, whether to a virus or a tumor, is complex and multifaceted. Analyzing these responses, therefore, requires measuring many aspects, including the types of cells that respond, the magnitude and nature of their response (secretion of cytokines, proliferation, cytolytic activities), and the

dynamics of the response. Presently, evaluating multiple attributes of an immune response related to a particular disease requires a collection of independent assays like flow cytometry and immunoassays as well as other functional assays to characterize proliferation or cytotoxicity. For most clinical research on human diseases, these cells originate from a blood sample. Another disadvantage of sampling blood is that the nature and responsiveness of the cells in circulation may differ significantly from those located in the actual site of infection or inflammation. Current analytical approaches are relatively poor at extracting information from small samples. In the context of analyzing biological samples, the transformation of interest is one that converts living cellular systems into comprehensive knowledge about that system and how it is influenced by external cues, such as drugs or pathogens. Biological systems comprise large and complex networks of variables: intracellular molecules (genes, proteins, metabolites, glycans), extracellular features (surface-expressed proteins that delineate a type of cell or its differentiated state, morphology, size), dynamic functional qualities (secreted proteins, proliferation, cytolytic ability, motility), and the numbers and types of cells, among other traits. Studying how these systems respond to external cues (e.g., drugs, vaccines, pathogens, and reactor conditions) requires gathering information about these variables that uncovers the direct and indirect relationships among them. The integration of those data can then provide new understanding or models for how the biological system operates. Experimental data on one or more variables may provide insights on how cells sense changes in their local environments, and respond by moving, secreting proteins, proliferating, or dying, or how they influence the state and evolution of other cells in a network, such as a tissue or bioreactor, to impact a macroscopic outcome (progression of a disease, titers of manufactured biomolecules). Identifying the structure of the models that best describe these complicated behaviors, therefore, depends on designing a set of appropriate experiments to reveal underlying relationships among the variables. A researcher must currently define a set of self-standing,

independent experiments that probe specific relationships, ignoring others. A logical substrate to consider as an input to a bioanalytical unit operation is the cell. As outlined previously, cells are the focal point of biological systems. The development of new micro- and nanotechnologies for handling and interfacing with many single cells and their molecular components in parallel are well suited for these tasks. Conduct a single operation for testing a specific hypothesis or pursuing discovery-oriented research (J.C. Love, Integrated Process Design for Single-Cell Analytical Technologies, 2010)".

In this paragraph, its behavior and interaction with tumor microenvironment will be highlighted.

Inflammation is a critical component of tumor progression; in fact, many cancers arise at sites of infection, chronic irritation and inflammation. Currently, inflammatory cells, participating in tumor metastasis, largely infiltrate tumor microenvironment, and the major components of the leukocyte infiltrate of tumors are macrophages, which represent up to 50 % of the tumor mass. TAMs can affect different aspects of the neoplastic tissue, and have an important impact on disease progression. In fact, they promote tumor cell proliferation and angiogenesis, matrix turnover, and repression of adaptive immunity[1] (Wang et al., 2010). They originate from blood monocytes, and differentiate into two different phenotypes, which show pro-tumoral (M2) and anti-tumoral (M1) functions respectively (Solinas et al., 2009). The link between high levels of TAMs infiltration and metastasis was previously demonstrated (Condeelis and Pollard, 2006). In fact, in response to cytotoxic therapies, TAMs enhance tumor revascularization, thereby causing cancer relapse (Guo et al., 2013). The presence of pro-tumoral polarized macrophages is justified by cancer ability to mold still immature cells (monocytes) and to reprogram them to suppress anticancer activity; in fact blood monocytes are not fully

[1] ADAPTIVE IMMUNITY: The adaptive immune system, also know as specific immune system, is composed of highly specialized immune system cells, that eliminate or prevent pathogen growth.

differentiated cells and are sensitive to environmental stimuli. Hence, tumor seems to exploit the normal matrix remodeling capacities of macrophages, enabling them to migrate through the surround stroma. Together with tissue remodeling, the presence of several cytokines and chemokines, highlights the presence of inflammation, a part from determining the specific signaling pathways that will be activated (Figure 7.2) (Pollard, 2008; Solinas et al., 2009). M1 macrophages are classically activated by exposure to interferon-γ or lipopolysaccharides (LPS) and elicit tissue destructive activities by secreting high levels of cytokines such as TNF-α, IL-12 and IL-1. M2 macrophages are alternatively activated, and secrete high levels of VEGF, MMPs and IL-10 and have tissue remodeling and immunosuppressive activities (Zervantonakis et al., 2012). Therefore, TAM are M2 polarized because they are derived from circulating monocytes that are recruited to the tumor site by chemotactic factors, such as monocyte colony-stimulating factor (M-CSF) and VEGF, even though the mechanism that programs the M2 macrophage phenotype is still under study. Wang group (Wang et al., 2010) showed interleukin 6 (IL-6) overexpression in macrophages co-cultured with tumor cells and its role in the growth of numerous tumor cell lines and increase of their resistance to apoptosis was also demonstrated.

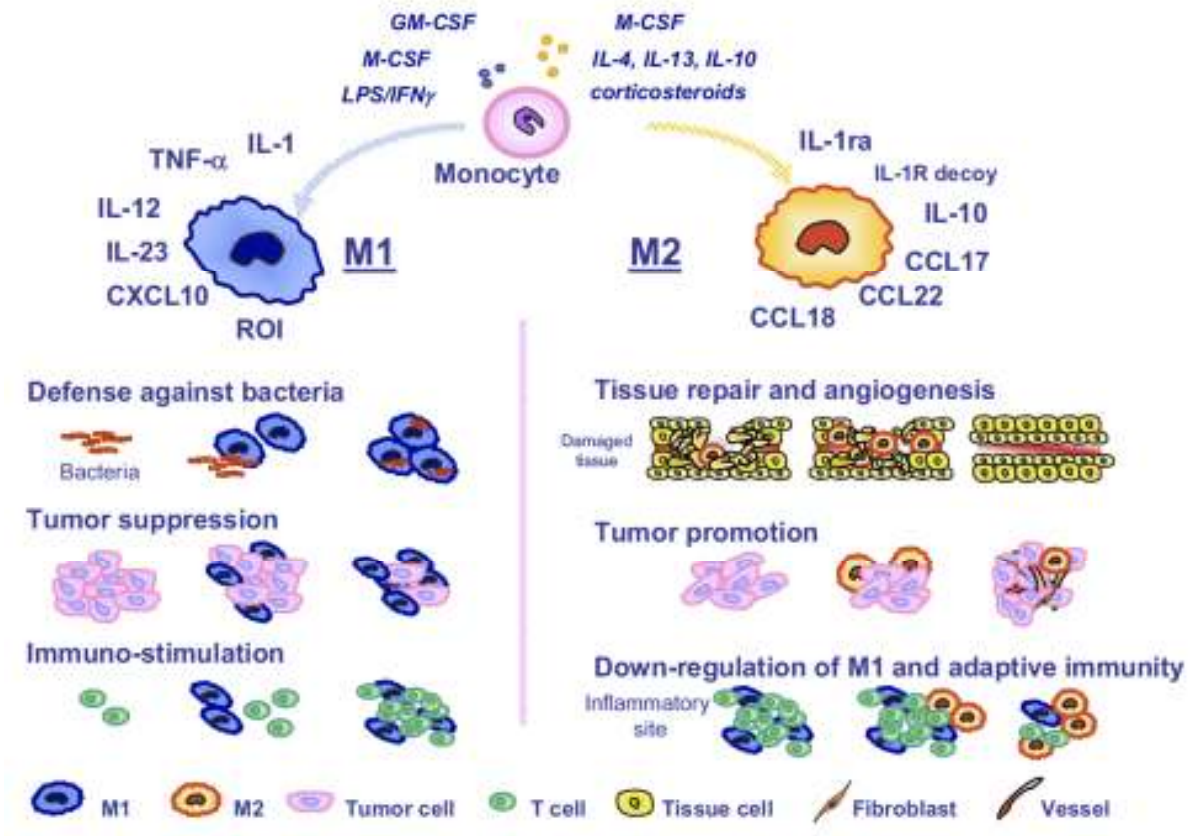

Figure 7.2: Macrophages polarization is influenced by the presence of different cytokines in the surrounding environment, and it will determine the cytokines and interleukines expression with subsequent signaling pathway.

The effect of TAM in modulating endothelial barrier function was also observed by Zervantonakis et al. (Zervantonakis et al., 2012) and they showed the ability to increase endothelial barrier permeability.

Since TAMs seem to favor neoplastic cells invasion and spreading, they are now considered an attractive target for anti-cancer therapies. The best solution is to find a protein expressed or overexpressed only by TAM, in order to focus the therapy and hopefully change macrophages polarization to anticancer phenotype, thus stopping proliferation and avoiding disease relapse. Moreover, studying the signaling pathways that allow macrophages to contribute to tumor progression will lead to new insights into the evolution of the microenvironments supporting

invasion and metastasis. Adams et al. (Adams, 2014) recently observed how some circulating cancer-associated giant macrophages-like cells, not found in healthy individuals and expressing different protein markers, bond to CTCs. This turns them in potential markers of solid tumors. This is just an example of the fact that in the scientific world the power of therapeutic targeting of macrophages in humans already started to be considered as a valuable strategy to complement conventional anticancer strategies.

7.3 Cellular environment and ECM *in vitro* models

Even though 2D culture systems are useful to study cell-cell interactions and cellular responses to biochemical signals, in the last ten years it became more and more clear to scientists that flat layers are not exhaustive tools to study complex cellular and molecular mechanisms (Montanez-Sauri et al., 2015). In fact, in mammalian tissues, cells are connected not only to each other, but also to a support structure called the extracellular matrix (ECM). The ECM is a complex composite material consisting of glycoprotein and polysaccharides hydrogel coupled to an assembly of crosslinked collagen and elastin fibres that are typically 100 nm or less in diameter. The unique three-dimensional architecture provides structural support and also allows sensing and transduction of biochemical and mechanical signals to cells. The properties of the ECM are tissue-dependent; for example, the elasticity of ECM varies from less than 1 kPa in the brain to 100 kPa in skeletal tissues. The interstitial space in the ECM is occupied by fluid that is usually in motion and provides a dynamic environment for cells. The permeability of the ECM is dependent on its composition and structure (Wirtz et al., 2011). On the other hand, cell polarity influences tissue organization and directional secretion of products. Yamada identified stiffness, together with cell/tissue polarity, as the principal parameters to

classify the extracellular matrix to be provided by the 3D model used (Yamada and Cukierman, 2007). ECM is a key regulator of normal homeostasis and tissue phenotype (Lee et al., 2007a). Certainly, cellular behavior is strongly influenced by the microenvironment, and the first aspect to be recreated is threedimensionality. 3D culture conditions can better simulate *in vivo* metabolic activity or drug efficacy (Breslin and O'Driscoll, 2013; Kenny, 2007; Rimann and Graf-Hausner, 2012). Nevertheless, although the importance of a three-dimensional space to recreate physiological conditions has been widely demonstrated (Asthana and Kisaalita, 2013), the composition of the microenvironment strongly depends on the application; an adequate material need to be chosen depending on the tissue to be reproduced/simulated. First of all, the rigidity of the matrix, along with the number of receptor-mediated adhesions formed by the cells with the surrounding environment, influence the ratio of stress exerted by the cells on the matrix, together with the ability of the latter to be contracted by the cells themselves. The intracellular tension leads to the formation of stress fibers, hence resulting in differential cell functions. Therefore, the chemical composition of the ECM and the resulting mechanical properties are both important aspects, in fact the transduction of both physical and chemical signals affects cell shape, polarization, migration and differentiation (Verhulsel et al., 2014) (Figure 7.3).

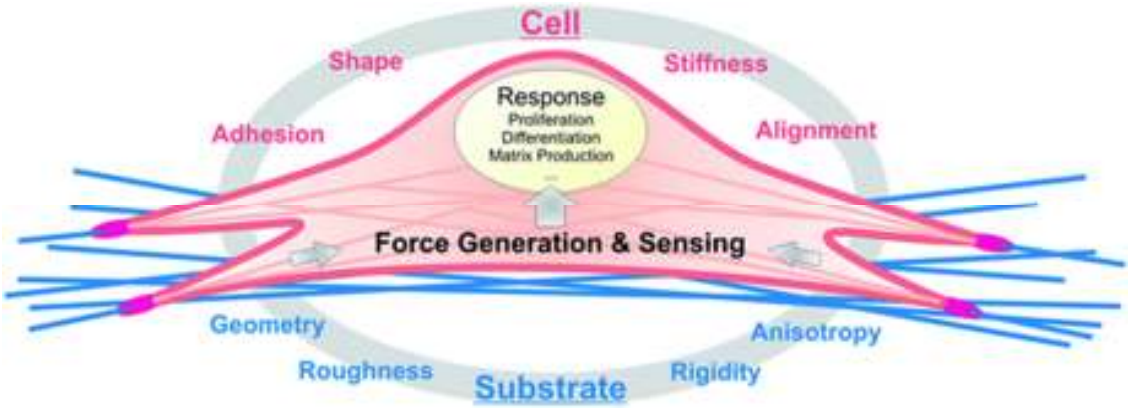

Figure 7.3: Cell-ECM interaction.

Mostly, 3D scaffold can be classified in hydrogel-forming, which provide a "soft" environment, and synthetic microporous constructs, made of stiffer materials having high modulus of elasticity such as polystyrene, Poly-L-lactide acid (PLLA), Polylactic-co-glycolic acid (PLGA) and plycaprolactone (PCL). Hydrogel properties can be modulated by changing the concentration of the polymer, the extent of crosslinking, or the proportion of the ECM proteins (Asthana and Kisaalita, 2013). Cells embedded in natural matrices (Collagen I, Matrigel, etc.,) have shown different morphologies and behaviors depending on the composition and mechanical properties of matrices (Montanez-Sauri et al., 2015). Most importantly, soft hydrogel are better in providing good physiological cues, while stiffer scaffolds are better in imposing physical constrains and a controlled porosity, by providing adhesion sites for cells to attach and adapt in response to topography. These kinds of scaffolds are the most used in regenerative medicine to replace damaged tissues, being the hydrogels more suitable for *in vitro* microfluidic models (Yamada and Cukierman, 2007).

Hydrogels can be classified into natural and synthetic; the first one includes collagen, fibrin, hyaluronic acid, Matrigel, and derivatives of natural materials such as chitosan, alginate and silk fibers. In general, natural matrices better recreate the natural environment, by providing the chemical cues found *in vivo*, but the batch-to-batch variations and their limited modification of mechanical and chemical properties, is the major limitation for obtaining reproducible outcomes, while synthetic polymers offer more defined properties. In contrast, common synthetic matrices used for 3D cell culture are polyethylene glycol (PEG), polylactic acid (PLA), polyclycolic acid (PGA), polyacrylamide (PAM), polyvinyl alcohol (PVA), and the synthetic matrix peptide PuraMatrix (Verhulsel et al., 2014). Moreover, 3D scaffolds are also suitable for selective incorporation of signaling factors, adhesion factors, and proteins (Rimann and Graf-Hausner, 2012). To enrich "bioactive" potential of synthetic materials, they are

generally functionalized on their surface with adhesion molecules by covalent grafting, adsorption, or electrostatic interaction. In case of photoactivable materials such as polyethylene glycol diacrilate (PEGDA), they can be chemically modified to covalently attach to the hydrogel backbone (Montanez-Sauri et al., 2015; Verhulsel et al., 2014). In some cases can be useful to create interpenetrating polymer networks of different hydrogels in order to combine their properties (Donati et al., 2005; Lee and Kurisawa, 2013). Additive manufacturing together with current fabrication and deposition technologies allow building structures with increasingly complex architectures (Malda et al., 2013). By choosing different fabrication processes, appropriately porous scaffolds can be manufactured (Breslin and O'Driscoll, 2013). Hydrogel porosity must be sufficient to ensure a homogeneous supply of oxygen and nutrients through it without damaging the gel structure and its mechanical properties. Solvent casting, freeze drying, and gas foaming are the common techniques that can be used to obtain an adequate porosity. On the other side, to replicate collagen fibrillar structure, several techniques have been proposed ranging from self-organization of peptides, to electrospinning, or microfluidic co-flow of a polymer and a gelation solution, or finally spontaneous organization of collagen fibrils by raising the pH of the solution to 7.4. Furthermore, micropatterning methods such as soft lithography and microcontact printing can be exploited to replicate cells topography (Verhulsel et al., 2014).

To make some example of different kind of hydrogel used, collagen gels can mimic loose or dense connective tissue depending on the concentration of collagen; such gels have been widely used in studies of fibroblast and tumor cell migration and signaling (Grinnell, 2003). For growth and differentiation of epithelial cells, however, reconstituted gels of an extract containing basement membrane components and growth factors, such as Matrigel are much more effective (Kleinman and Martin, 2005). Each type of matrix can also have experimental drawbacks. For example, collagen gels lack other components of connective tissue, and they

differ in the extent of covalent crosslinking. Matrigel consists of basement membrane components, but it is a 3D cell culture material rather than a mimetic of the flat basement membranes underneath cells. Finally, cell-derived matrices can have lower amounts of collagen, larger internal spaces, and less depth than mature tissue matrices.

Thus, it is important to appropriately select the matrix for the study to be done. Chau et al. (Chau et al., 2013) used an agarose-fibronectin gel on a spun PES/viscose rayon microfiber material to construct an immunocompetent 3D human skin model comprising dendritic cells co-culture with keratinocytes and fibroblasts. Tumor spheroids were formed from breast tumor cells within alginate gel (Chen et al., 2010). Alginate was also previously used by Maguire et al. to create a controlled environment for hepatocyte differentiation (Maguire et al., 2006). Allen et al. (Allen et al., 2011) tested type I collagen, fibrin and PuraMatrix matrices to form neovascular networks. Bersini et al. (Bersini et al., 2014a) used instead a 6.0 mg/mL collagen type I gel, conditioned to recreate the bone-like matrix, and study breast cancer cell metastasis through bone with a 3D microfluidic device.

Microfluidics allows confining cells to a restricted area and accurately controlling their environment spatially and temporally. Moreover, the indispensable high throughput screening (HTS) analysis is possible. The ability of microscale 3D culture systems to decrease the volume of reagents and the number of cells needed, while reducing costs as well, is particularly useful for analysis of rare cells (Montanez-Sauri et al., 2015).

A great advantage of microfluidics in cell biology is the ability to provide physiological microenvironments under constant perfusion systems. As said before, the most common way to create these 3D tissue-like structures is by embedding cells in 3D natural or synthetic hydrogels (Matrigel, collagen, alginate, fibrin, chitosan, agarose). Very challenging is to overcome related mass transport problems. In fact, cellular metabolic activity and viability could be compromised by threedimensionality due to the inadequate medium supply. One way

to improve nutrients recruitment by cells and tissues is using dynamic 3D cultures through continuous perfusion. Dealing with hydrogels, it must be also taken into account they swell and deswell in buffered pH solutions (De et al., 2002), since it is important when confining them within microfluidic channels.

A wide number of platforms were designed in the last years to allow patterning of gels and cells in a 3D microenvironment, and capable of generating gradients in stationary conditions (flow-free). Most of them exploit linear arrays of regularly spaced posts between juxtaposed channels (Farahat et al., 2012; Huang et al., 2009). Their scope is to separate gel and medium compartments, preventing leakage into neighboring channels, thus allowing diffusion and movement of molecules and cells. The interface area, which could be varied according to the need, is determined by **surface tension, hydrophobic interactions and spatial geometry**. Empirically we might say that the creation of this interface depend on the spacing between posts, the surface properties of the device, and the viscosity of the hydrogel precursors solutions. The physical explanation is given by Huang et al. (Huang et al., 2009) in their article. Microfluidic is also useful for mimicking organs physiology, hence they are characterized by sub units organized in 3D at the cellular level; besides channel compartmentalization, which is good to reproduce interfaces in organs (Verhulsel et al., 2014).

The development of *in vitro* models of ECM that can mimic tissue-specific physicochemical properties, molecular composition, elasticity, pore size and local fibers orientation will be crucial to further advance our understanding of cancer cell motility in three dimensions and how this relates to migration *in vivo*. Nevertheless, current 3D platforms drawbacks must be taken into account. First of all, to allow high fluid control, additional compartments, pumps, and connectors, which increase the total volume and makes their incorporation more difficult. Secondly, collection of data is more challenging, due to the multiple focal planes and the need to transfer cells to a different plate for subsequent analysis. However, last generation of

microfluidic devices already solved most of these problems with an adequate design. Third, conventional biochemical assays still need to accompany the immunocytochemistry (ICC) assay performed on chip, and all the 3D quantitative analysis still have to be validated by 2D conventional methods (Montanez-Sauri et al., 2015).

7.4 Cell migration analysis in microfluidic devices

Cell migration is a characteristic involved in both physiology and pathology of human body; several models have been developed in order to study this complex process. Cell migration in a matrix involves dynamic cell-shape changes through actomyosin assembly and contractility, and adhesion to the extracellular matrix. Motile cells exhibit matrix metalloproteinases (MMPs) on their surface, which promote the digestion of the laminin and collagen IV rich basement membrane. The physics of tumor cells motility is widely reviewed elsewhere (Wirtz et al., 2011), but the goal of this paragraph is to focus and describe different migration techniques present in literature. Nowadays principal challenge of these techniques is to provide a substrate properly mimicking the properties of the extracellular matrix (ECM) in order to finely control experimental parameters. Moreover, more and more imaging devices are developed to efficiently monitor cell dynamics (Rolli, 2011)

Conventional migration assays *in vitro* include the wound assay, the Teflon fence, and the Boyden chamber with its subsequent variations, such as the gel invasion assay. The first two have provided useful insight in 2D cellular and molecular migration mechanism. The latters instead are commonly used in 3D, even though they don't allow a real-time quantification of migration. The wound-healing assay (Todaro et al., 1965) is performed by physically scratching a portion of confluent cells on normal culture surfaces and comparing the time cells

need to close the scrape, like platelets do *in vivo* in case of injury. This method requires an increased number of reagents and cells and is not suitable for high-throughput screening. The Boyden chamber (BOYDEN, 1962) consist of a cylindrical cell culture insert included inside a microwell, which contains a polycarbonate membrane at the bottom with a defined pore size. Cells are inserted on top of the insert, while chemoattractans are placed in the well below to make migratory cells move through the membrane. Its principal drawbacks are the lack of information about cells speed and morphology during migration. Three-dimensional techniques rely on cell count at defined time points, therefore the proliferation that occurs during the assay need to be subtracted from the counting of migrating cells. Moreover, to better reproduce physiological conditions, challenging tools need to be added to the technology used. Microfabrication and microfluidics allow controlling multiple environmental factors, such as fluid shear stress and fluid-matrix interfaces, in order to differentiate chemokinetic and chemotactic effects with real-time high-resolution imaging (Chung et al., 2009). For example, microfabricated patterns were used to demonstrate cell preferential migration on stiff substrates (Csaderova et al., 2005). Furthermore, biochemical gradients can be created inside microchannels or gel scaffold with the same investigation purpose. Okano group (Nie et al., 2007) transferred wound-healing assay to microfluidics by injecting a laminar flow of trypsin solution in microfluidic channels to achieve a controlled cell detachment in a portion of confluent monolayer. They could observe the distance reached by the cells after 24h culture in different medium conditions, like the presence or absence of serum or soluble factors, such as epidermal growth factor on one side, and inhibitors, such as phalloidin and cytochalasin D., on the other. Hence, in a subsequent work Chung *et al.* (Chung et al., 2009) developed a collagen scaffold into a PDMS device to perform a migration assay in response to multiple biophysical, biochemical or co-culture conditions, such as scaffold stiffness, cell types and growth factor gradients. The device consists of three channels; the central one was used as the cell culture

channel and migration within hydrogel through the side channels was analyzed, being the first one filled with soluble factors of interest, and the latter used as the control channel. In a different study, Irimia *et al.* (Irimia and Toner, 2009) analyzed the effect of mechanical confinement on cancer cell migration. Time-lapse imaging was performed for 24-48 h, followed by image analysis using the manual tracking function of the Image J software. They found out that cells show a continuous and persistent motility in one direction when constrained inside channels of size comparable with their dimensions, also in the absence of an external gradient. They quantified the velocity of cells from several human cancer cell lines. Furthermore, after exposing them to concentrations of drugs able to stop proliferation, they noticed that some of them still retained the ability to migrate, thus showing the inefficiency of some regimes of chemotherapy. The physical reason is possibly in the reorganization of the cytoskeleton along the axis of the channel, which drives the internal cell polarization.

In a previous work Doyle et al. (Doyle et al., 2009) brilliantly demonstrated that 1D migratory mechanism is well suited to recreate 3D cell migration properties, witch are lost in 2D matrices. This reason justifies our choice to use microchannels to perform the migration analysis. In fact, cells seem to exhibit highly persistent and uniaxial migration phenotype both in 1D and 3D migration respect to 2D systems (Figure 7.4). Therefore, quasi-1D fibrillar migration provides a suitable model to mimic 3D dynamics of cell adhesions, cytoskeleton and signaling expressed during cell migration. In fact, topography seems to highly influence cell migratory behavior; for example, leukocyte show an adhesion dependent mechanism when seeded on a flat surface (Lämmermann et al., 2008).

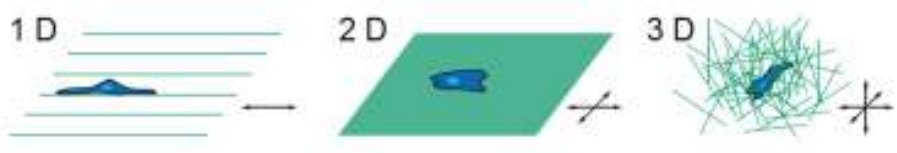

Figure 7.4: Cell migration in different dimensions.

Huang *et al.* (Huang et al., 2011) used microchannels to characterize the migratory capacity of brain tumor stem cells (BTSC), which are believed to be the main responsible for cancer therapeutic resistance and recurrence. Basing on morphological changes, they identified six cell stages during migration. After approaching the entrance of the microchannel, the cell with the highest migratory capacity start to explore the path thanks to membrane protrusions; it cross the channel with a constant velocity by maintaining a large protrusion heading forward. Once reached the opposite culture channel, it start to explore the new place, and finally turn into star-shaped with the same motility property, but with no determined direction (Figure 7.5).

Figure 7.5: adapted from Huang (Huang et al., 2011) BTSC migration through a microchannel.

Quake's group instead (Vedel et al., 2013) put his attention in collective cell migration behavior. They observed how properties such as directionality and speed are modulated by local cell density.

Biomolecular pathways can also be included in 3D micropatterned scaffolds to guide cell migration. Lee *et al.* (Lee et al., 2008) used two-photon laser scanning (TPLS) photolithography to dictate the precise location of cell adhesive ligands (RGDS) within regions of a poly(ethylene glycol-co-peptide) diacrylate hydrogel. Cells proteolytically degrade the synthetic hydrogel locally and replace it with extracellular matrix proteins, moving through previously patterned trajectories. A different technique exploits photo-switchable surfaces, able to dynamically adjust conditions during the experiment, spatially and temporally defining their properties (Rolli, 2011).

Migration analysis is a useful assay to characterize both the immune system response during an inflammation process, and primary tumor cells invasion capability to predict their metastatic power. Furthermore, in our experiment we focused on the interplay between the two cell types and how they mutually influence, changing their migration properties.

7.4.1 CHARACTERIZATION OF CELL MIGRATION

Mechanical structure and stability of a cell are provided by cytoskeleton, which is composed of actin, intermediate filaments and microtubuli. Actin filaments, together with myosin proteins, are responsible of cell contraction. Intermediate filaments instead, are involved in mechanical stiffness and elasticity properties, while microtubuli are designated to determine cell polarization, a part from being platforms for intracellular transport. Since cell moves within their environment, it is extremely important to know how they are mechanically linked to the ECM, and this role is carried out by ligand-integrin binding and other cell membrane receptors. Depending on the mechanism cells use to move, migration can be classified in amoeboid or mesenchymal (Callan-Jones and Voituriez, 2016). The first one, characterized by weak interactions with the substrate, is mostly proper to fast moving cells, able to quickly move through many organs. The latter, on the contrary, include a sequence of independent steps, which involve cell-ECM interactions.

Different parameters can be used to describe single cell migration, whereof the most important are velocity and directionality.

- **Velocity** (v) It is obtained from the accumulated distance, which represents the whole length of a cell track, related to the duration of the cell track.

$$v = \frac{d_{accum}}{\Delta t} = \frac{\sum_{k=1}^{i} r_{k+1} - r_k}{t_{k+i} - t_k}$$

However, it is not sufficient for describing cell delocalization, and Euclidian distance, which is the shortest distance between beginning and end of a cell track, needs also to be taken into account (Figure 7.6)

Figure 7.6: Cell track A) accumulated distance, B) Euclidian distance.

- **Directionality** (D) It is a measure of directness of a cell trajectory, and is calculated by comparing Euclidian distance with the accumulated distance.

$$D = \frac{d_{euclid}}{d_{accum}} = \frac{r_{k+1} - r_k}{\sum_{k=1}^{i} r_{k+1} - r_k}$$

To give more information about cell migration behavior, parameters as directional persistence time and root-mean speed can be exploited. This is particularly true when cell movement persist in the same direction over short times, but is random if observed over longer times (Dickinson and Tranquillo, 1993).

Traction force measurements can monitor forces exerted by the cells on a flat surface coated with a layer of soft gel with a stiffness similar to the ECM with fluorescently labeled micro beads embedded (Doyle and Lee, 2002).

Chapter 8

Experimental

8.1 Materials and methods

8.1.1 Tumor Cells Culture

Triple negative breast cancer cell line MDA-MB-231 (American Type Culture Collection, ATCC, Manassas, VA, USA) was cultured in DMEM low glucose medium supplemented by 10% of fetal bovine serum (FBS), 100 units/ml penicillin, 100 mg/ml streptomycin, and 2 mM L-glutamine and grown in 5% CO_2 atmosphere at 37 °C. Cells were detached and subcultured every 3-4 days.

In order to obtain Cancer Stem Cells (CSC) enriched population we expanded MDA-MB-231 cells as mammospheres. Cells were seeded on ultra low adherent plate at low density (5000 cells/cm^2) and cultured with MammoCult medium (#05620 Stemcell). After one week, spheres exceeding 60 μm of diameter were collected by gentle centrifugation and considered as first generation mammospheres. These cell clusters were dissociated to single cell suspensions and reseeded in an ultra low adherent plate. After three weeks, third generation mammospheres were used in each experiment.

8.1.2 Macrophages Cell Culture

Macrophage differentiation and polarization were performed according to Mantovani et al. (Mantovani et al., 1992) Human peripheral blood mononuclear cells (PBMCs) were isolated from buffy-coat of female healthy donors by Lympholyte®-H density gradient (Cedarlane Laboratories) and monocytes were sorted using beads conjugated anti-human CD14 (Miltenyi Biotech) and cultured for 6 days in RPMI culture medium (Euroclone) supplemented with 10% fetal bovine serum (Hyclone, Thermo Scientific), 5% of Human Serum, 100 units/ml penicillin, 100 mg/ml streptomycin (Euroclone), 2 mM L-glutamine (Euroclone) and 25 ng/mL macrophage-colony stimulating factor (M-CSF) (R&D Systems) to differentiate them into macrophages. M1 polarization was achieved culturing macrophages with interferon-γ (IFN- γ) (10ng/mL) and lipopolysaccharide (LPS) (100 ng/mL) for 48 hours, whereas M2 polarization was obtained culturing macrophages with interleukin-4 (IL-4) (20ng/mL) for 48 hours. After polarization, M1/M2 macrophages were analyzed and used in co-culture experiments.

8.1.3 Stemness Assay

Aldefluor kit (Stem Cell Technologies) was performed, according to the manufacturer's protocol, to determine aldehyde dehydrogenase 1 (ALDH1) activity in MDA-MB-231 cells and in CSCs. Briefly, for each sample 1×10^5 viable cells were incubated for 30 min at 37°C in ALDEFLUOR® assay buffer with the fluorescent substrate BODIPY aminoacetaldehyde at final concentration 1 µM alone or plus the aldehyde dehydrogenase inhibitor diethylaminobenzaldehyde (DEAB; final concentration 50 mM) as negative control. Samples were analyzed with flow cytometry (FACScanto, BD Biosciences).

8.1.4 Gene Expression Analysis

Total RNA was extracted from both MDA-MB-231 cell line cultured in adherent condition and dissociated third generation mammospheres and from M1/M2 macrophages using the Trizol reagent (Invitrogen) according to the manufacturer's instructions. RNA was treated with DNase buffer and DNase (DNAse Turbo, Applied Biosystems) to avoid genomic DNA contamination. cDNA was produced using the High Capacity cDNA Reverse Transcription kit (Applied Biosystems) according to the manufacturer's instructions. mRNA levels were measured by quantitative real-time polymerase chain reaction (qRT-PCR) using TaqMan Gene Expression Assays in 7900HT Real-Time PCR System (Applied Biosystems). *OCT4*, *SOX-2*, and *NANOG* (stemness genes) and *IL-10, IL-12, TNF* and *MR* (macrophages polarization marker genes) expression levels were normalized to the endogenous housekeeping gene glucuronidase beta (GUSb) (Hs99999908_m1) for mammospheres and PPIA for macrophages (choose for their respective low level of variability across the experiments), using the ΔCT calculation. Subsequently relative expression levels of each gene in mammospheres or M2 macrophages were normalized to the mRNA levels detected in MDA-MB-231 cell line or M1 macrophages, respectively, using the ΔΔCT calculation.

8.1.5 Tumor Cells Transfection

Red Fluorescent Protein positive (RFP+) MDA-MB-231 cell were obtained transfecting MDA-MB-231 cells with MISSION® pLKO.1-puro-CMV-TurboRFP™ Positive Control Transduction Particles. Puromycin resistance were used as selection of transfected cells.

8.1.6 2d In Vitro Co-Culture

All *in vitro* co-culture experiments were assessed by seeding RFP+ CSCs into a 24 well multiplate and M1/M2 macrophages into a 24 well transwell. Three days before of each co-culture experiment, puromycin selection of RFP+ MDA-MB-231 was interrupted not to affect macrophage viability.

8.1.7 2d Cell Proliferation Assay

$1x10^4$ RFP+ CSCs were seeded into each well of a 24 well plate and co-cultured with M1/M2 macrophages for 96 hours using transwell system. Tumor cell proliferation was monitored reading the increase of fluorescence (excitation = 532 nm; emission = 588 nm) from day 0 to day 4 every 24 hours using the Tecan M200 microplate reader. Population Doubling Time (PDT) was calculated in each sample using the following formula:

$$PDT = 1/[3.32(\log N_H - \log N_1)/(t_2 - t_1)],$$

where N_H is the number of harvested cells at the end of the growth period, N_1 is the number of seeded cells, t_1 is the time at seeding, and t_2 is the time elapsed between t_1 and cell harvesting.

8.1.8 2d Migration Assay

RFP+ CSCs were seeded into a 24 well plate at 90% of confluence. Cell monolayer was scratched using a p200 pipet tip and cells were co-cultured with M1/M2 macrophage using transwell system. Migration rate was analysed under time-lapse microscopy and uncovered area was calculated every 10 hours.

8.1.9 Microfluidic Device Design And Microfabrication

The co-culture model used consists of a microfluidic platform with three main channels connected by micron-sized channels used for the migration analysis. The device was fabricated by replica molding in polydimethylsiloxane (PDMS, Sylgard 184, Dow Corning) as described by Businaro et al. (Businaro et al., 2013). MDA-MB-231 cells were seeded in the left channel while the immune cells in the central one. The aim of this study was to observe and analyze macrophages migration toward the antagonist tumor cells (Figure 8.1 right) and toward a control medium channel (Figure 8.1 left) relatively in both tumor-supportive (M1) and inhibitory (M2) polarization *status*. The migration and proliferation of MDA-MB-231 cells in both cases was also analyzed.

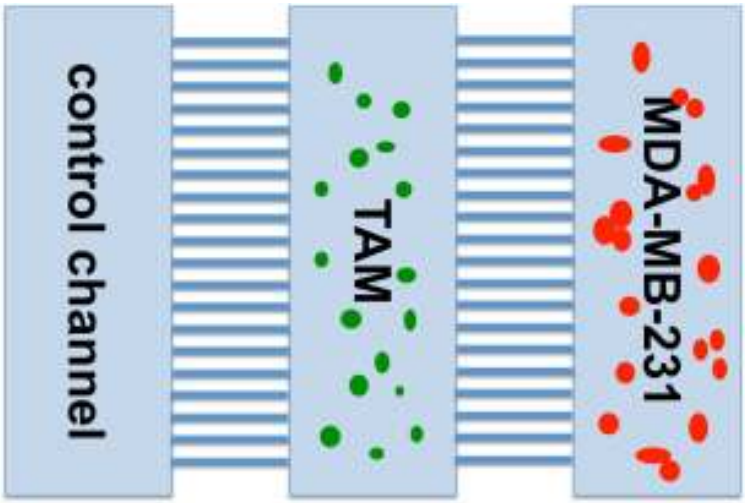

Figure 8.1: microfluidic device scheme.

8.1.10 Cell Loading And Time-Lapse Recording

The devices were sterilized under UV light for 15 minutes, filled with RPMI medium supplemented with 10% fetal bovine serum (FBS), 1% L-glutamine and antibiotics and

stabilized at 37 °C. After 1 hour the medium was gently aspirated and red fluorescent protein (RFP)-expressing MDA-MB-231 breast cancer line cells were introduced in the left channel by injecting 20 µl of $5x10^6$ cells/ml cell suspension. The devices were then left in the incubator for 1,5 h in order to let tumor cells adhere to the bottom of the platform.

After that, green-labeled (Cell-tracker CMFDA) peripheral-blood derived macrophages (M1/M2 polarized) were injected in the central channel in 10 µl volume of $5x10^7$ cells/ml cell suspension and left adhering for 45 minutes. Finally each reservoir was loaded with 200 µl medium and the devices were placed under the fluorescence inverted microscope (Nikon Eclipse Ti) at 37 °C and 5% CO_2 (OkoLab Incubator System, Warner Instruments) for time-lapse recording.

A long-term 48 h experiment was performed taking phase-contrast and fluorescence microphotographs of defined regions with a 10 minutes interval.

8.1.11 Macrophages Tracking Analysis On Chip

The interaction between MDA-MB-231 and M1/M2 polarized macrophages was investigated analyzing the migration of the latters within the micro-sized channels. Object tracking of macrophages was performed acquiring the trajectories of distinct cells throughout the time-lapse experiment. Tracking analysis was performed using the manual tracking plug-in of the Fiji (ImageJ) open source software. Cell velocity was quantified in response to the presence or absence of the tumor in both tumor-supportive (M1) and inhibitory (M2) polarized macrophages.

8.1.12 Tumor Migration And Proliferation Analysis On Chip

MDA-MB-231 migration was also analyzed comparing the number of tumor cells within the microchannels and in the culture channel nearby, occupied by the immune system cells M1 and M2 polarized respectively. Cell count analysis package from NIS-Elements imaging software (Nikon) was used for the objects count. Breast cancer cell proliferation was observed at the same time in order to distinguish whether the increase in the cell number in the opposite channel was due to a major doubling time of one of the two polarized *status* or to the migration directionality itself. The proliferation assay was performed as a function of density calculated in a defined region of the tumor cells (Shih et al., 2013). Binary area fraction occupied by the cells was obtained and normalized to confluence at a distance of 250 μm from the microchannels. NIS-Elements software was used for the analysis of the fluorescence images acquired throughout the experiment.

8.2 Results and discussion

Culture of MDA-MB-231 cell line in ultra-low adherent condition, using MammoCult medium, led to an enrichment of cell population stemness. In particular, ALDH-1 positivity increase from 1.3 in 2D cultures to 30.6% in third generation mammosphere cultures (Figure 8.2). Moreover, the expression of the main stemness marker genes, that is OCT4, SOX-2 and NANOG, increased in third generation mammospheres compared to 2D culture.

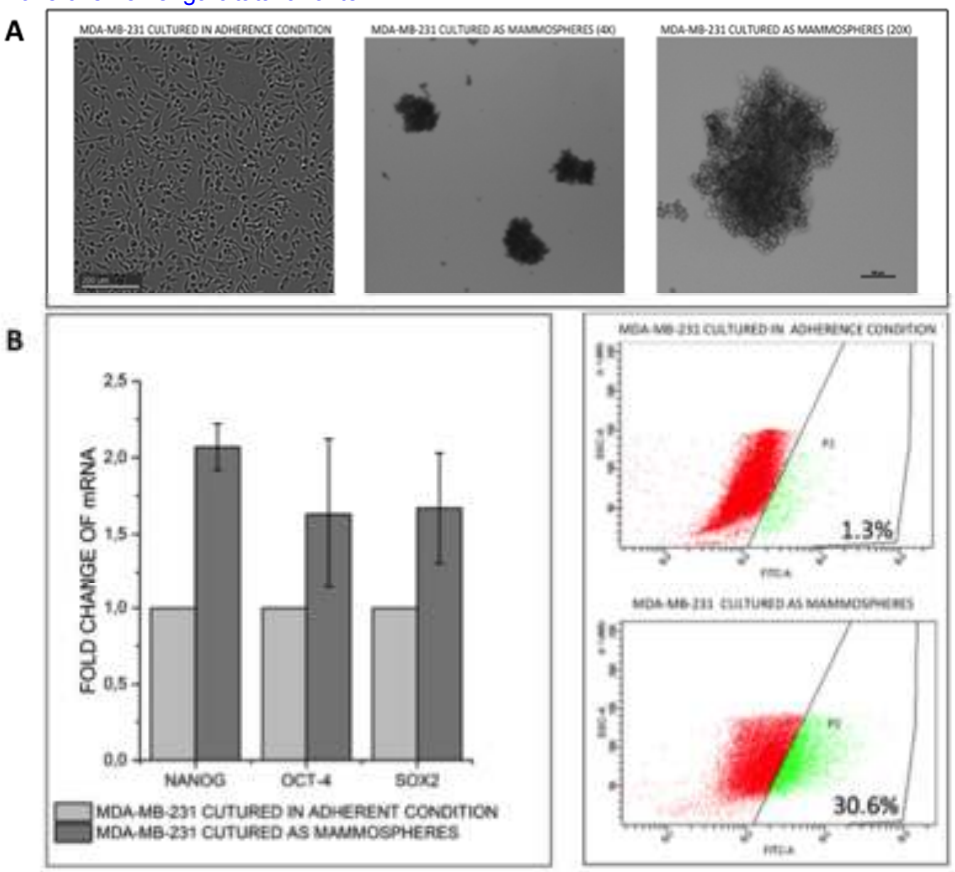

Figure 8.2: A) MDA-MB-231 cells cultured in adherence conditions (left) and in ultra-low adherence condition as mammospheres (centre and right). B) ALDH-1 stemness assay through genes expression (left) and cytofluorimetry (right).

In order to perform microscope analysis of co-culture between CSCs and macrophages, we induced stable expression of RFP in MDA-MB-231. Figure 8.3 shows that RFP+ MDA-MB-231 cells maintain the same ability to form mammospheres. Furthermore, RFP+ mammospheres showed the same percentage of ALDH-1 positive cells compared to RFP- mammospheres.

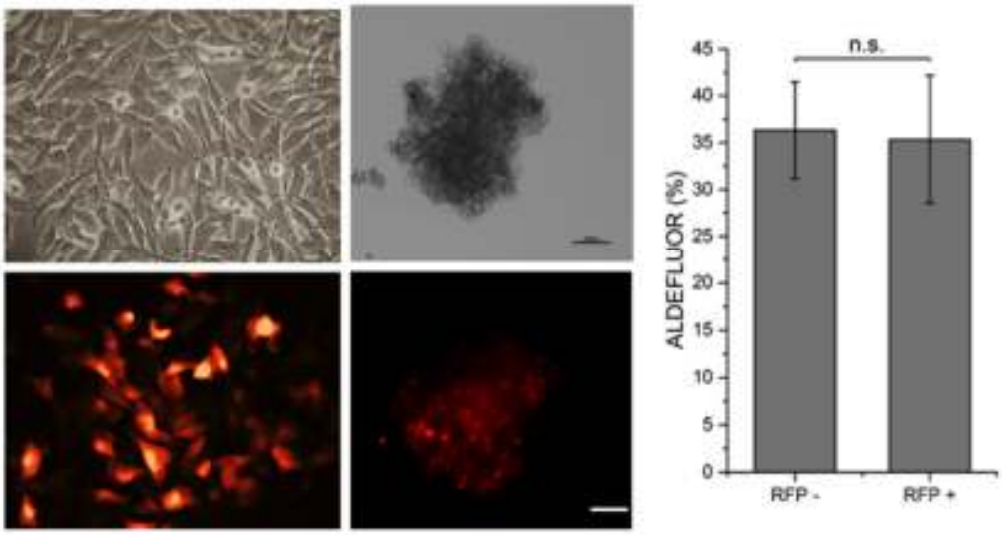

Figure 8.3: RFP- and RFP+ MDA-MB-231 cells cultured in adherence and low-adherence conditions (left) and ALDH-1 assay comparison on RFP- and RFP+ (right).

Cell growth curves of RFP+ CSCs show that M2 macrophages significantly increased the proliferation rate of tumour cells compared to M1 macrophages at 72 hours and 96 hours of co-culture ($p = 0.024$ and $p = 0.047$, respectively; t-student test) (Figure 8.4 a). Intriguingly, RFP+ CSCs cultured alone proliferate with the same rate of cells co-cultured with M1 macrophages (Figure 8.4 a). PDT analysis performed at 96h of co-culture showed a significant decrease of PDT in RFP+ CSCs co-cultured with M2 macrophages compared to cells co-cultured with M1-macrophages ($p = 0{,}030$; t-student test) (Figure 8.4 a).

Wound healing assay (Figure 8.4 b) was performed in order to evaluate the migration rate of tumour cells co-cultured with immune cells. This analysis didn't show significant differences between RFP+ CSCs co-cultured with M2 macrophages and the same cells co-cultured with M1 macrophages; in particular, after 20 hours, RFP+ CSCs co-cultured with M2 macrophages cover 100% of wounded area, whereas cancer cells co-cultured with M1 macrophages cover 93% circa, but this difference didn't reach the statistical significance.

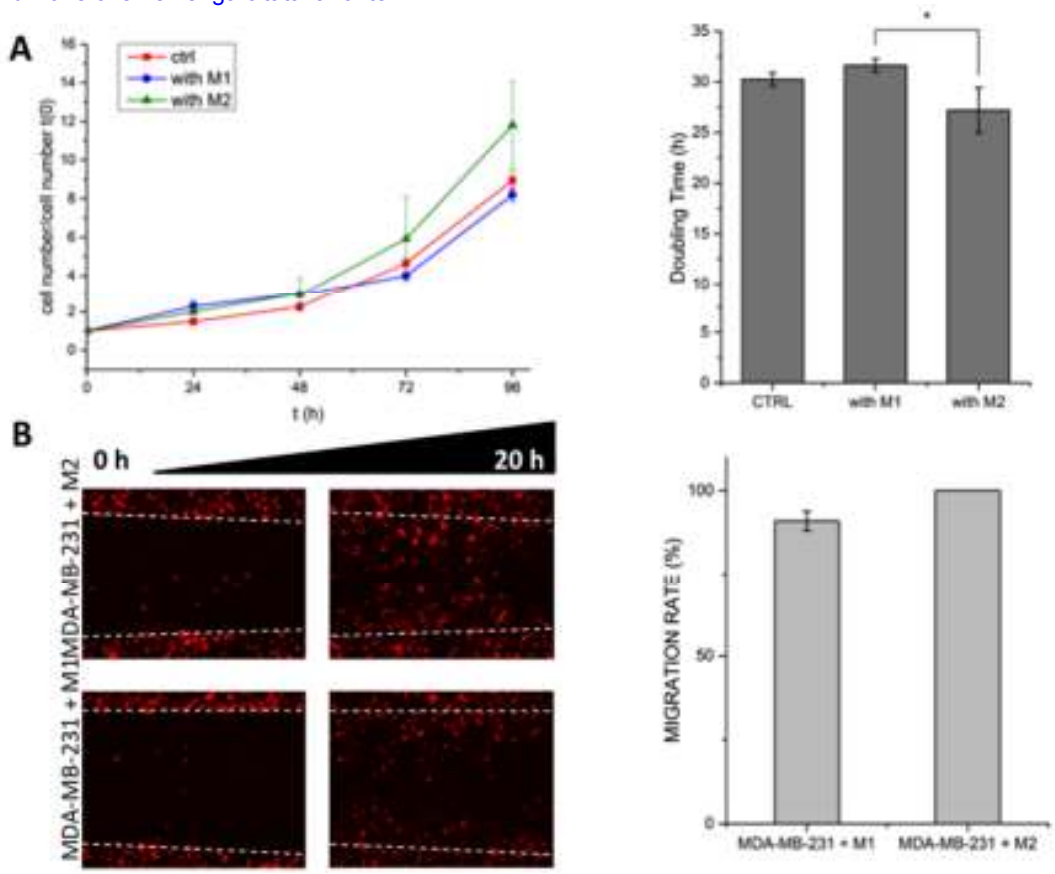

Figure 8.4: A) 2D tumor cells proliferation assay comparison. B) 2D tumor cells co-cultured with M1/M2 macrophages migration assay comparison. (=P<0.05)*

Real time PCR analysis of M1/M2 macrophages demonstrates that these two types of cells exhibit different gene expression profile. In particular, M2 macrophages show IL-10/IL-12 ratio significantly higher than M1 (371,0426 versus 2,317116; p = 0,0004; t-student test). Moreover, M1 macrophages exhibit high levels of TNF and low levels of MR, whereas M2 macrophages express high MR and low TNF.

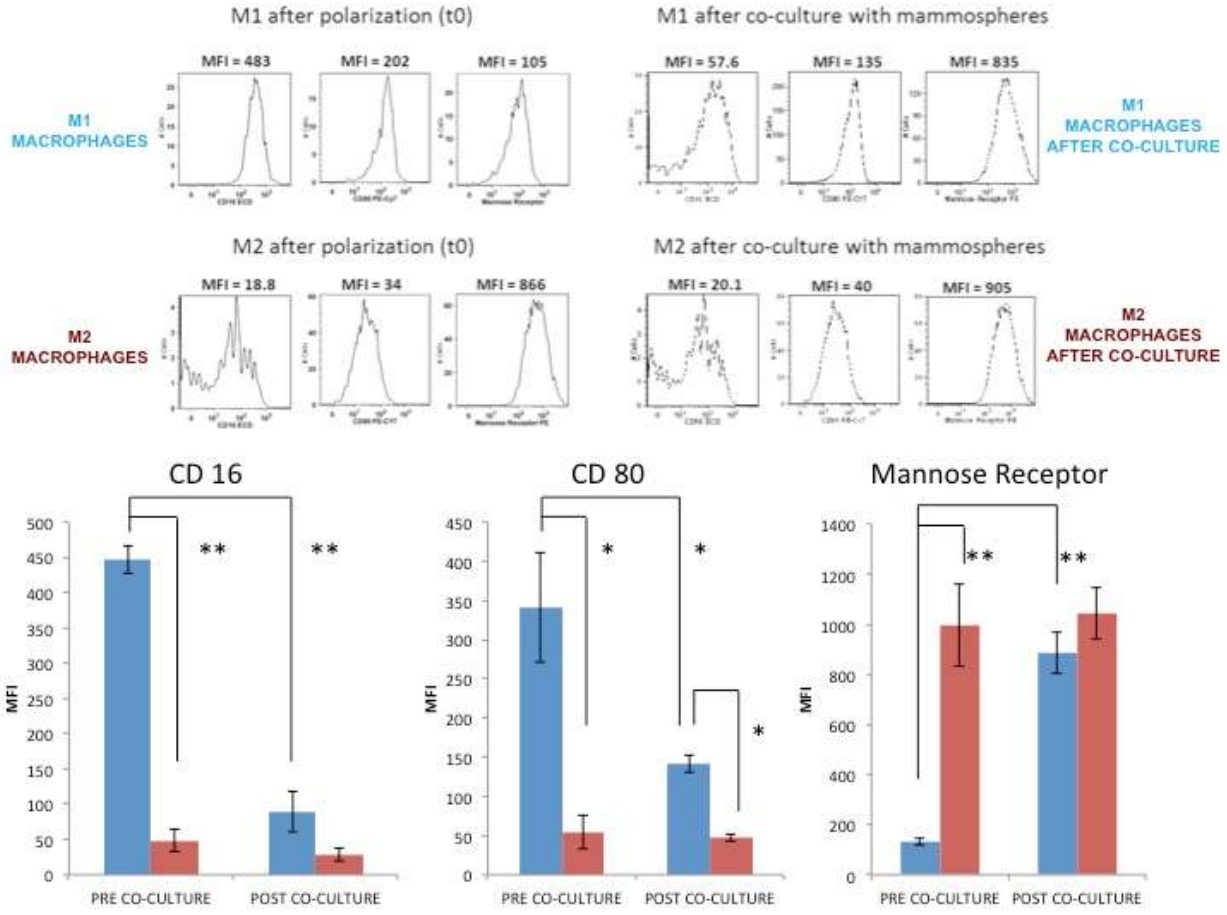

Figure 8.5: Flow cytometry analysis of M1 (blue) and M2 (red) macrophages polarization through CD16, CD80 and Mannose Receptor markers gene expression. (=p<0.05, **=p<0.01)*

The aim of the present work was to create co-culture platform that enable to observe real-time interactions between different cell types. The custom made geometry was designed in order to perform a high-throughput and quantitative kinetic analysis of differently polarized macrophages in a tumor microenvironment. On this purpose, we seeded each cell type in its own culture channel, which was connected to the other by micron-sized channels (500 x 12 x 10 µm). Cells are able to migrate into them as a consequence of chemoattractive factors released from distinct ones, to physically get in contact and interact, recreating their microenvironment and making possible to observe them in long-time experiments. Most importantly, qualitative and quantitative analysis can be made from the images acquired

constantly. In fact, we were able to follow the trajectories of around 50 immune system cells throughout the second day of the time-lapse experiment (Figure 8.6 b). A statistically significant ($p<0.05$) difference can be evidenced between M1 and M2 macrophages, in terms of migration, in response to MDA-MB-231 tumor cells. Moreover, M1 macrophages showed an enhanced velocity towards the antagonist cells compared to the control medium channel (Figure 8.6 a)

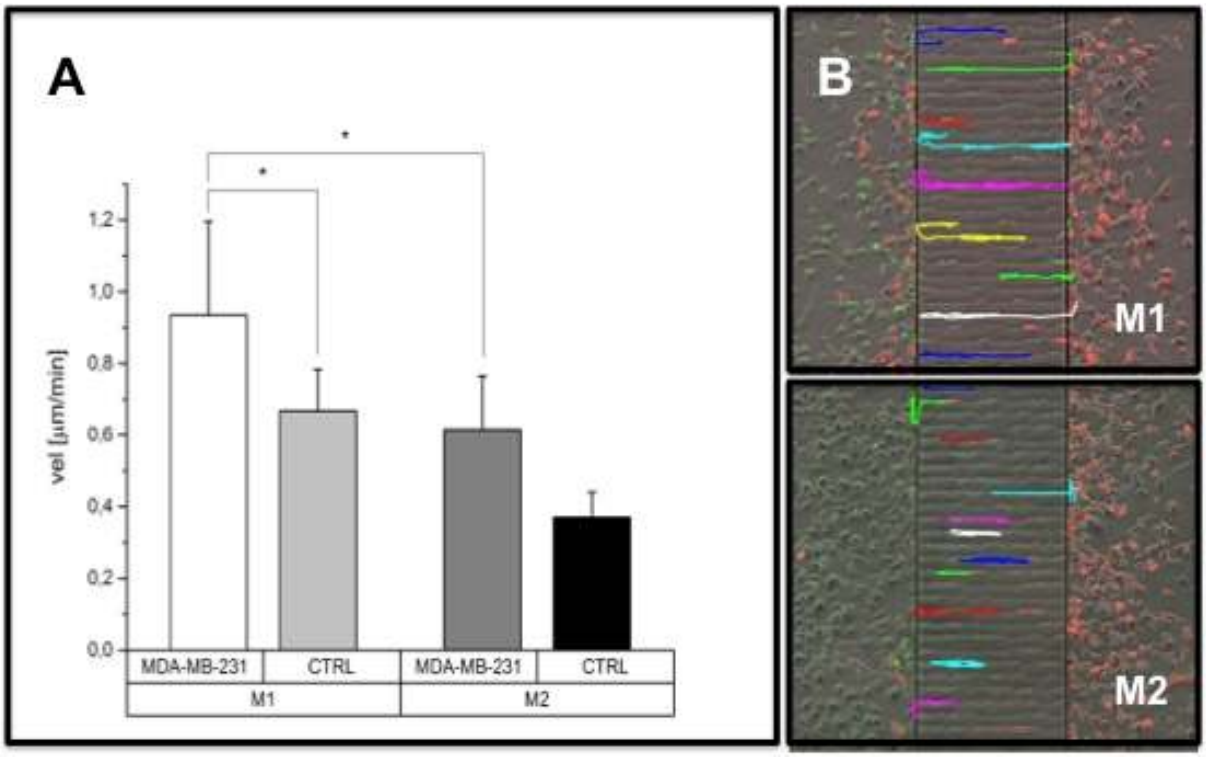

Figure 8.6: A) Results of image analysis performed on object tracking data. B) Fluorescence micrograph of the on-chip co-culture of MDA-MB-231 cells (in red) and peripheral-blood-derived macrophages (in green) overloaded with the object tracking of macrophages migration in response to tumor cells for M1 (top) and M2 (bottom) macrophages. Each picture represents the trajectories of distinct cells acquired throughout a time-lapse experiment. (=P<0.05)*

Tumor migration behavior was also observed counting the number of cells in the microchannel area and in the opposite channel, co-cultured with M1 and M2 macrophages respectively. After 15 hours there are approximately 2 tumor cells in every channel both in the presence of M1 or M2 macrophages but in the presence of the antagonist (M1) the tumor migration is higher. In

fact an increased number of MDA-MB-231 can be evidenced starting from the second day of co-culture (Figure 8.7).

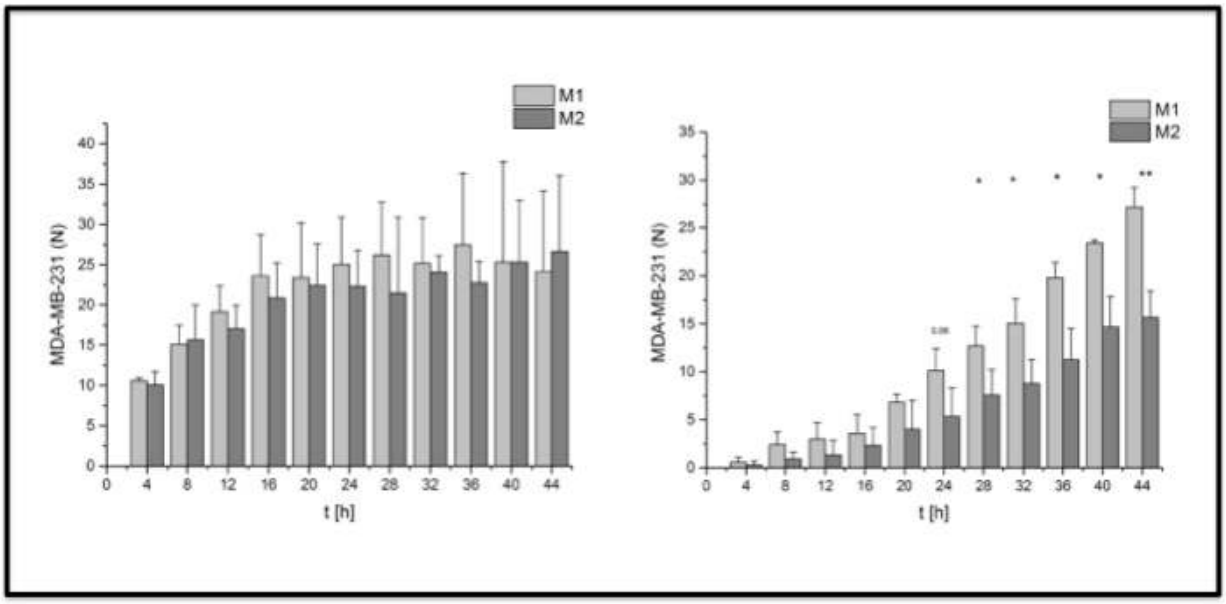

Figure 8.7: Number of MDA-MB-231 in the microchannel area (15 microchannels - ROI: 500x650 µm) (left) and number of MDA-MB-231 in the opposite channel (length: 650 µm) (right). (=P<0.05, **=P<0.01)*

Furthermore, tumor proliferation was evaluated in terms of density increase, but no significant differences were found out in the two co-cultures with M1 and M2 polarized macrophages (Figure 8.8).

These results (i.e. the significant major number of cells migrated in the opposite channel) weren't due to an enhanced tumor cell proliferation at least in the first 48 h, but were directly affected by the directionality of MDA-MB-231 towards the immune system's culture channel.

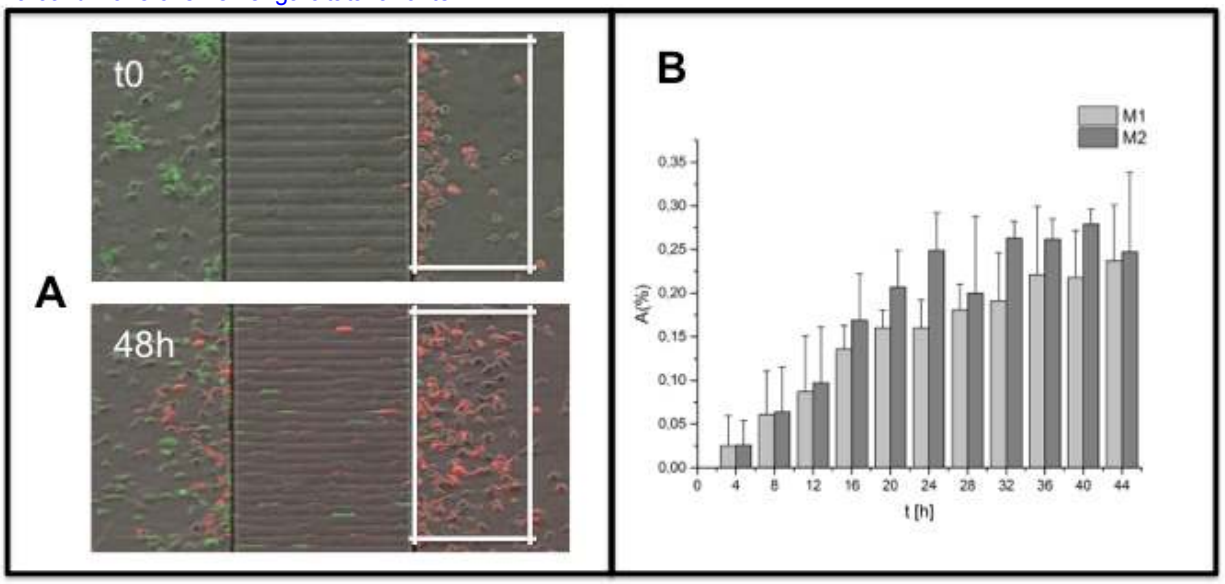

Figure 8.8: A) Tumor proliferation assay as cell density variation and B) binary area fraction (length=250 µm) during the first 48 h calculated and normalized as %A= [A(X)-A(0)]/[1-A(0)].

Our microfluidic platform was fabricated to allow the observation and quantification of cell behavior with a high precision degree. Our goal, in detail, was to investigate cell migration and interactions among breast cancer cells and tumor-associated macrophages.

In cell culture channels we aimed to recreate physiological cell behavior, therefore we chose to use a microfluidic device. In order to analyze cell migration we preferred a relatively simple but representative system to quantify and characterize the subtle differences in differently polarized (M1/M2) macrophages. Further work, which will be the objective of the next paragraph, was done to optimize the artificial ECM to better mimic cancer microenvironment.

8.3 Custom-made device to increase threedimensionality

With the aim to include tumorsphere model inside our experiment, we designed a new custom-made device (Figure 8.9 a) with a gel region for the culture of MDA-MB-231 cells in a mammosphere configuration.

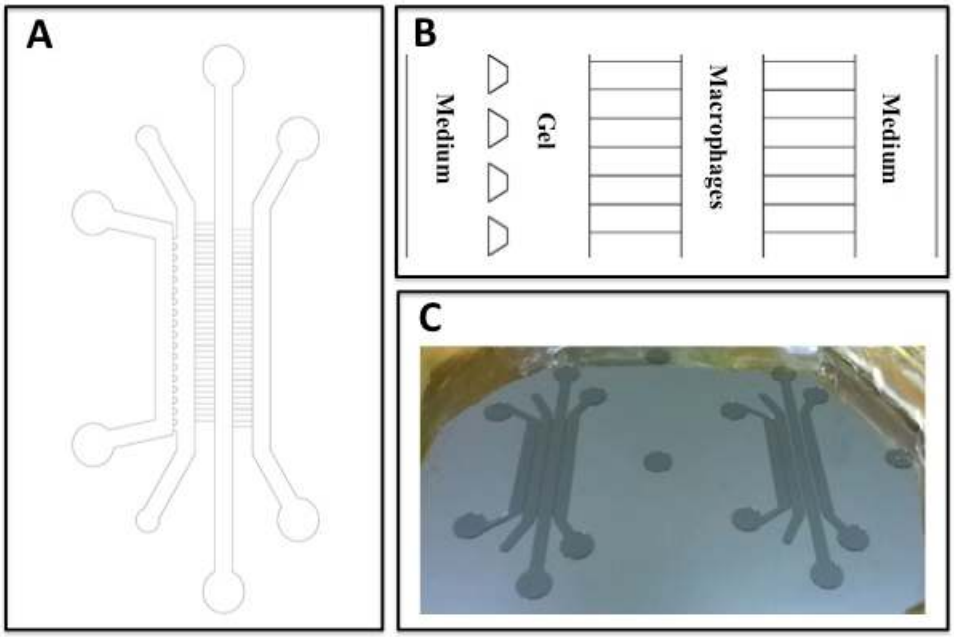

Figure 8.9: A) Structure of the custom-made platform with detail of the microchannels (B); C) master of the device fabricated by photolithographic technique.

It was fabricated in PDMS as previously described (Figure 8.9 c). The hydrogel was inserted in a defined region delimitated by trapezoidal posts and confined there by surface tension. The linear gradient concentration with the hydrogel was tested by inserting a FITC solution within the platform (Figure 8.10). The left medium channel (Figure 8.9 b) allows the nutrients supply to the gel region; while the medium channel on the right (Figure 8.9 b) work as the control channel for microphages migration analysis.

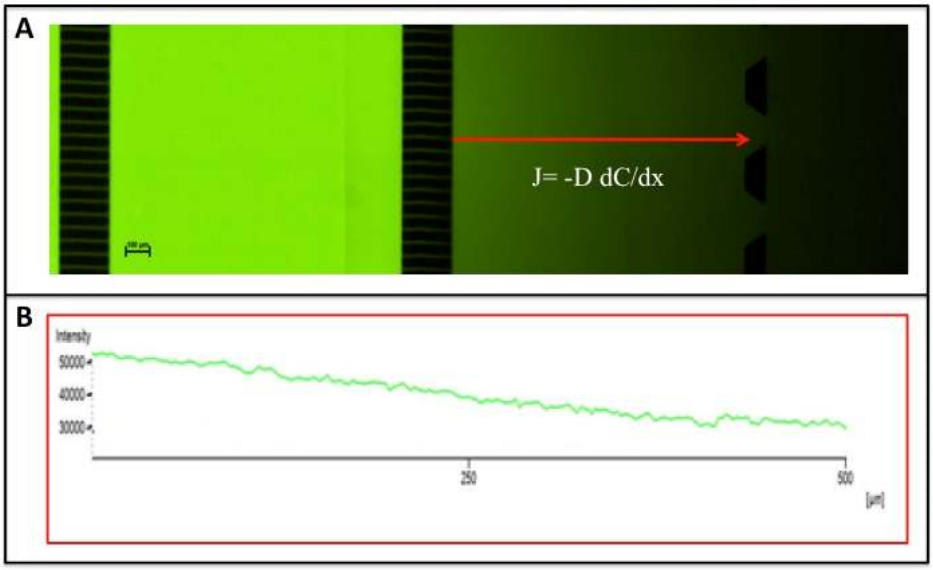

Figure 8.10: A) Insertion of a FITC solution in the left channel of the device and a control solution in the right one, to observe the gradient concentration within the hydrogel channel (red arrow) in stationary conditions and B) graph of the linear gradient concentration in the latter.

Different hydrogels were tested to check the better one suitable for tumorspheres formation and maintenance of stemness properties (Figure 8.11).

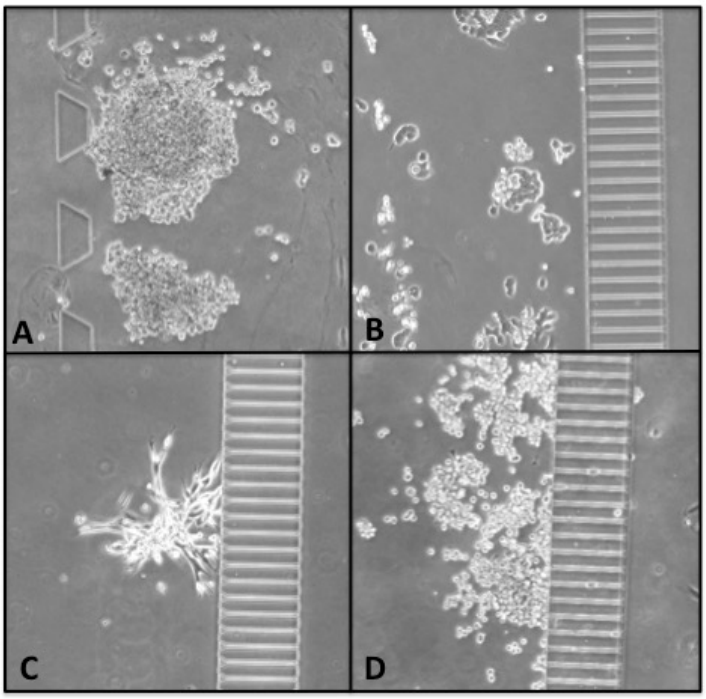

Figure 8.11: Tumorspheres cultured within different hydrogels: A) PuraMatrix, B) alginate, C) Matrigel, D) fibrin gel, inside the device.

After inserting MDA-MB-231 cells in the gel area, green-labeled macrophages were seeded in the side channel for the co-culture (Figure 8.12).

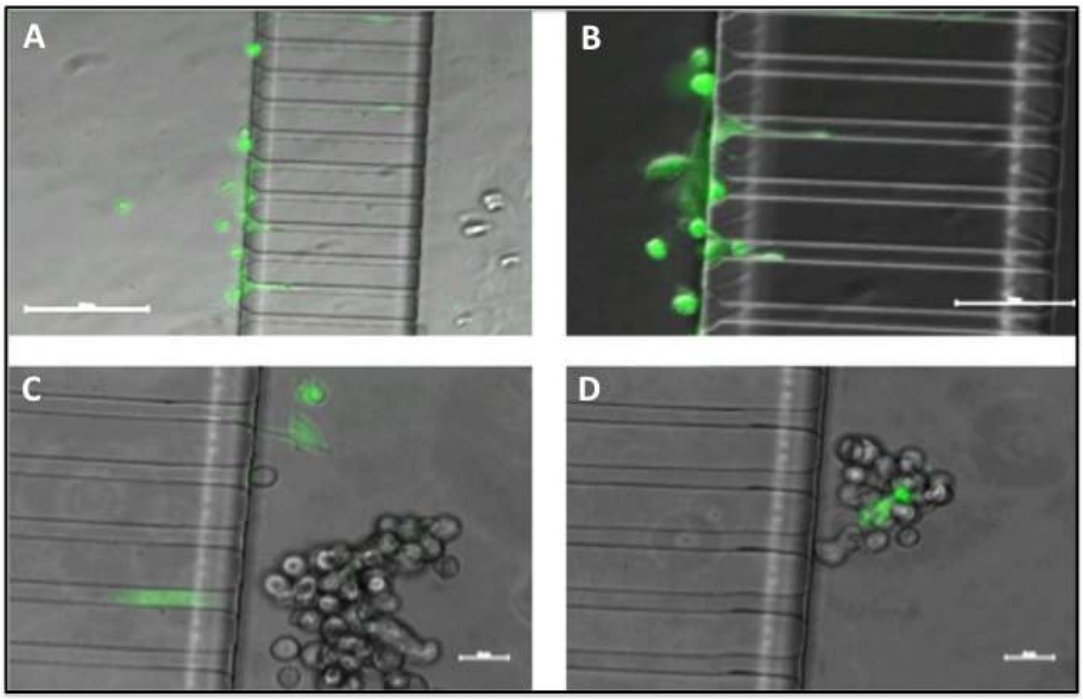

Figure 8.12: A, B, C and D) Microspheres of MDA-MB-231 tumorspheres and cell-tracker CMFDA green-labeled macrophages co-culture.

To test the device analysis ability different assays were performed within it (Figures 8.13 and 8.14).

The platform showed its suitability for an advanced analysis in a more physiological microenvironment, resulting in a high-throughput tool to create reliable *in vitro* models.

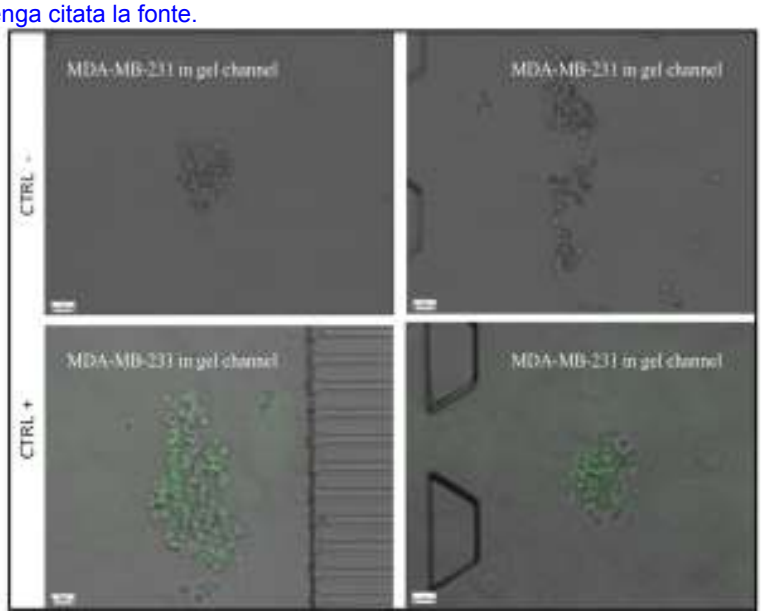

Figure 8.13: A*aldehyde-dehydrogenase 1 (ALDH1) tumorspheres stemness assay on-chip. Negative (up) and positive (down) controls (in green) are evidenced.*

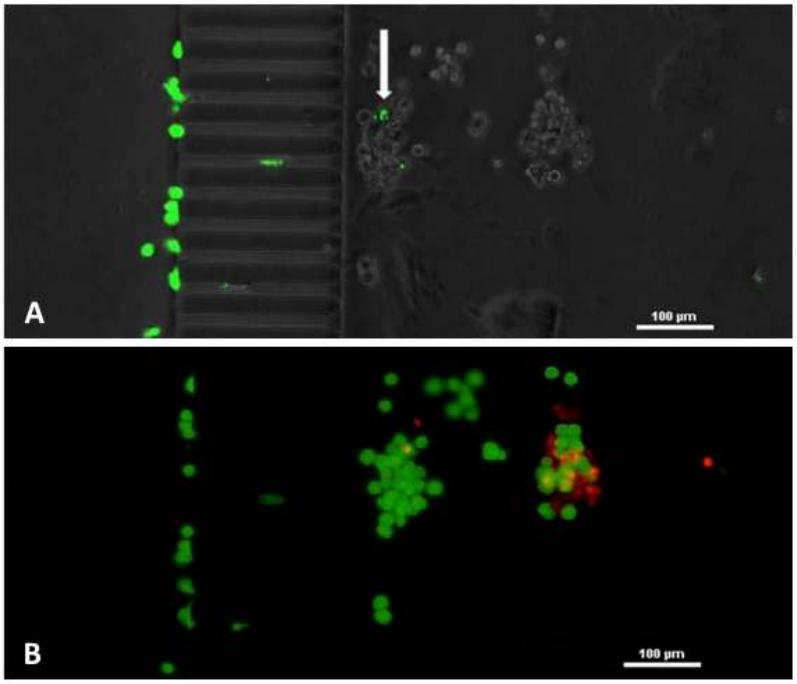

Figure 8.14: Micrograph of the device with cell tracker CMFDA green-labeled macrophages (A); and LIVE/DEAD Viability/Cytotoxicity assay were live cells are evidenced in green and the dead ones in red.

Chapter 9

Conclusions and outlook

In conclusion two complex models were developed by exploiting microfabrication techniques to produce optically transparent platforms, enabling quantitative and qualitative information about cells morphology and behavior.

The "NAFLD-on-a-chip" system presented in this work is a *in vitro* model of human NAFLD developed within a microfluidic device in a sinusoid-like fashion, representing a more permissive tissue-like microenvironment for long-term culture of hepatic cells than conventional 2D static cultures. The developed model enables gradual and milder intracellular triglyceride accumulation, a higher hepatic cell viability, and minimal oxidative stress levels in prolonged dynamic cultures compared to 2D static cultures, thereby mimicking more tightly the chronic condition of steatosis observed *in vivo*.

Extensive cell-cell contacts are known to be essential in *in vitro* hepatic cultures to preserve high cell viability and retain liver-specific metabolic activity, also after several weeks in culture, as demonstrated in previous works (Hamilton et al., 2001; Landry et al., 1985). Likewise, the better performance provided by the on-chip system, compared to traditional 2D static cultures, is most likely due to the high cell-density culture and cell contacts combined with the microfluidic mass transport, closer to the native liver tissue in comparison to monolayers of static cultures.

The "CSCs-immunity" microfluidic device, instead, exploits ad advanced co-culture system for real-time imaging and interaction analysis. First of all, based on a tumor spheroid model, stemness ratio can be increased in order to study the most aggressive and resistive case. Secondly, the microchannel-based system definitely better reproduces 3D migration properties, compared to 2D cultures as previously demonstrated by Doyle et al. work (Doyle et al., 2009). A detailed tracking analysis was performed to show cells behavior.

The observed and quantified subtle differences between the two macrophages polarization states may help the challenging research of specific markers, with the final purpose to act on them to convert M2 polarized cells towards the antitumoral condition.

Finally, results confirmed the capability of producing a high-throughput augmented analysis respect to conventional 2D systems, thus being just two more examples in new diagnostic devices generation. In a long-term perspective, the implementation of the on-chip technology may boost the evaluation of therapeutic effects, selection of tailored treatments and targets of drug discovery in a wide range of diseases. The present approach aims at filling the gap between conventional *in vitro* models, often scarcely predictive of an *in vivo* condition, and animal models that are potentially biased by their xenogeneic nature. That may represent another step forward to progressively build custom made devices to fasten and optimize clinical analysis and disease cure.

References

Abdul Keyon, A. S., R. M. Guijt, C. J. Bolch, and M. C. Breadmore, 2014, Droplet microfluidics for postcolumn reactions in capillary electrophoresis: Anal Chem, v. 86, p. 11811-8.

Abhyankar, V. V., M. A. Lokuta, A. Huttenlocher, and D. J. Beebe, 2006, Characterization of a membrane-based gradient generator for use in cell-signaling studies: Lab Chip, v. 6, p. 389-93.

Accoto, D., 2010, Lessons of Biomicrosystems.

Adams, L. A., O. R. Waters, M. W. Knuiman, R. R. Elliott, and J. K. Olynyk, 2009, NAFLD as a risk factor for the development of diabetes and the metabolic syndrome: an eleven-year follow-up study: Am J Gastroenterol, v. 104, p. 861-7.

Allen, P., J. Melero-Martin, and J. Bischoff, 2011, Type I collagen, fibrin and PuraMatrix matrices provide permissive environments for human endothelial and mesenchymal progenitor cells to form neovascular networks: J Tissue Eng Regen Med, v. 5, p. e74-86.

Ananthanarayanan, A., B. C. Narmada, X. Mo, M. McMillian, and H. Yu, 2011, Purpose-driven biomaterials research in liver-tissue engineering: Trends Biotechnol, v. 29, p. 110-8.

Angulo, P., 2002, Nonalcoholic fatty liver disease: N Engl J Med, v. 346, p. 1221-31.

Aref, A. R., R. Y. Huang, W. Yu, K. N. Chua, W. Sun, T. Y. Tu, J. Bai, W. J. Sim, I. K. Zervantonakis, J. P. Thiery, and R. D. Kamm, 2013, Screening therapeutic EMT blocking agents in a three-dimensional microenvironment: Integr Biol (Camb), v. 5, p. 381-9.

Assaily, W., D. A. Rubinger, K. Wheaton, Y. Lin, W. Ma, W. Xuan, L. Brown-Endres, K. Tsuchihara, T. W. Mak, and S. Benchimol, 2011, ROS-mediated p53 induction of Lpin1 regulates fatty acid oxidation in response to nutritional stress: Mol Cell, v. 44, p. 491-501.

Asthana, A., and W. S. Kisaalita, 2013, Biophysical microenvironment and 3D culture physiological relevance: Drug Discov Today, v. 18, p. 533-40.

Aufderhorst-Roberts, A., W. J. Frith, and A. M. Donald, 2014, A microrheological study of hydrogel kinetics and micro-heterogeneity: Eur Phys J E Soft Matter, v. 37, p. 44.

Bai, J., T. Y. Tu, C. Kim, J. P. Thiery, and R. D. Kamm, 2015, Identification of drugs as single agents or in combination to prevent carcinoma dissemination in a microfluidic 3D environment: Oncotarget.

Balaban, N. Q., U. S. Schwarz, D. Riveline, P. Goichberg, G. Tzur, I. Sabanay, D. Mahalu, S. Safran, A. Bershadsky, L. Addadi, and B. Geiger, 2001, Force and focal adhesion assembly: a close relationship studied using elastic micropatterned substrates: Nat Cell Biol, v. 3, p. 466-72.

Barata, D., C. van Blitterswijk, and P. Habibovic, 2015, High-throughput screening approaches and combinatorial development of biomaterials using microfluidics: Acta Biomater.

Barkefors, I., S. Le Jan, L. Jakobsson, E. Hejll, G. Carlson, H. Johansson, J. Jarvius, J. W. Park, N. Li Jeon, and J. Kreuger, 2008, Endothelial cell migration in stable gradients of vascular endothelial growth factor A and fibroblast growth factor 2: effects on chemotaxis and chemokinesis: J Biol Chem, v. 283, p. 13905-12.

Baroud, C. N., F. Gallaire, and R. Dangla, 2010, Dynamics of microfluidic droplets: Lab Chip, v. 10, p. 2032-45.

Bashford, G., D. Lamb, D. Grone, B. Eckles, K. Kornelsen, L. Middendorf, and J. Williams, 2008, Automated bead-trapping apparatus and control system for single-molecule DNA sequencing: Opt Express, v. 16, p. 3445-55.

Bates, S. P., 2000, Silicon Wafer Processing, Applied Materials.

Baudoin, R., G. Alberto, A. Legendre, P. Paullier, M. Naudot, M. J. Fleury, S. Jacques, L. Griscom, and E. Leclerc, 2014a, Investigation of expression and activity levels of primary rat hepatocyte detoxication genes under various flow rates and cell densities in microfluidic biochips: Biotechnol Prog, v. 30, p. 401-10.

Baudoin, R., A. Corlu, L. Griscom, C. Legallais, and E. Leclerc, 2007, Trends in the development of microfluidic cell biochips for in vitro hepatotoxicity: Toxicol In Vitro, v. 21, p. 535-44.

Baudoin, R., L. Griscom, J. M. Prot, C. Legallais, and E. Leclerc, 2011, Behavior of HepG2/C3A cell cultures in a microfluidic bioreactor: Biochemicla Engineering Journal, v. 53, p. 172-181.

Baudoin, R., A. Legendre, S. Jacques, J. Cotton, F. Bois, and E. Leclerc, 2014b, Evaluation of a liver microfluidic biochip to predict in vivo clearances of seven drugs in rats: J Pharm Sci, v. 103, p. 706-18.

Baylin, A., E. K. Kabagambe, X. Siles, and H. Campos, 2002, Adipose tissue biomarkers of fatty acid intake: Am J Clin Nutr, v. 76, p. 750-7.

Beebe, D. J., D. E. Ingber, and J. den Toonder, 2013, Organs on Chips 2013: Lab Chip, v. 13, p. 3447-8.

Beebe, D. J., J. S. Moore, J. M. Bauer, Q. Yu, R. H. Liu, C. Devadoss, and B. H. Jo, 2000, Functional hydrogel structures for autonomous flow control inside microfluidic channels: Nature, v. 404, p. 588-90.

Benam, K. H., S. Dauth, B. Hassell, A. Herland, A. Jain, K. J. Jang, K. Karalis, H. J. Kim, L. MacQueen, R. Mahmoodian, S. Musah, Y. S. Torisawa, A. D. van der Meer, R. Villenave, M. Yadid, K. K. Parker, and D. E. Ingber, 2015, Engineered in vitro disease models: Annu Rev Pathol, v. 10, p. 195-262.

Bersini, S., J. S. Jeon, G. Dubini, C. Arrigoni, S. Chung, J. L. Charest, M. Moretti, and R. D. Kamm, 2014a, A microfluidic 3D in vitro model for specificity of breast cancer metastasis to bone: Biomaterials, v. 35, p. 2454-61.

Bersini, S., J. S. Jeon, M. Moretti, and R. D. Kamm, 2014b, In vitro models of the metastatic cascade: from local invasion to extravasation: Drug Discov Today, v. 19, p. 735-42.

Berthier, J., and P. Silberzan, 2010, Microfluidics for biotechnology.

Bhatia, S. N., and D. E. Ingber, 2014, Microfluidic organs-on-chips: Nat Biotechnol, v. 32, p. 760-72.

Bhatia, S. N., G. H. Underhill, K. S. Zaret, and I. J. Fox, 2014, Cell and tissue engineering for liver disease: Sci Transl Med, v. 6, p. 245sr2.

Bhise, N. S., J. Ribas, V. Manoharan, Y. S. Zhang, A. Polini, S. Massa, M. R. Dokmeci, and A. Khademhosseini, 2014, Organ-on-a-chip platforms for studying drug delivery systems: J Control Release, v. 190, p. 82-93.

Bontoux, N., L. Dauphinot, T. Vitalis, V. Studer, Y. Chen, J. Rossier, and M. C. Potier, 2008, Integrating whole transcriptome assays on a lab-on-a-chip for single cell gene profiling: Lab Chip, v. 8, p. 443-50.

Borenstein, J. T., and G. Vunjak-Novakovic, 2011, Engineering tissue with BioMEMS: IEEE Pulse, v. 2, p. 28-34.

Borish, L. C., and J. W. Steinke, 2003, 2. Cytokines and chemokines: J Allergy Clin Immunol, v. 111, p. S460-75.

BOYDEN, S., 1962, The chemotactic effect of mixtures of antibody and antigen on polymorphonuclear leucocytes: J Exp Med, v. 115, p. 453-66.

Brennan, M. D., M. L. Rexius-Hall, L. J. Elgass, and D. T. Eddington, 2014, Oxygen control with microfluidics: Lab Chip, v. 14, p. 4305-18.

Breslauer, D. N., P. J. Lee, and L. P. Lee, 2006, Microfluidics-based systems biology: Mol Biosyst, v. 2, p. 97-112.

Breslin, S., and L. O'Driscoll, 2013, Three-dimensional cell culture: the missing link in drug discovery: Drug Discov Today, v. 18, p. 240-9.

Bricks, T., P. Paullier, A. Legendre, M. J. Fleury, P. Zeller, F. Merlier, P. M. Anton, and E. Leclerc, 2014, Development of a new microfluidic platform integrating co-cultures of intestinal and liver cell lines: Toxicol In Vitro, v. 28, p. 885-95.

Burger, R., D. Kirby, M. Glynn, C. Nwankire, M. O'Sullivan, J. Siegrist, D. Kinahan, G. Aguirre, G. Kijanka, R. A. Gorkin, and J. Ducrée, 2012, Centrifugal microfluidics for cell analysis: Curr Opin Chem Biol, v. 16, p. 409-14.

Burger, R., P. Reith, P. Abgrall, and J. Ducrée, 2011, INTEGRATION OF HIGH-EFFICIENCY CAPTURE AND MAGNETO-HYDRODYNAMIC RETRIEVAL OF PARTICLES ON A CENTRIFUGAL MICROFLUIDIC PLATFORM MEMS, IEEE.

Businaro, L., A. De Ninno, G. Schiavoni, V. Lucarini, G. Ciasca, A. Gerardino, F. Belardelli, L. Gabriele, and F. Mattei, 2013, Cross talk between cancer and immune cells: exploring complex dynamics in a microfluidic environment: Lab Chip, v. 13, p. 229-39.

Callan-Jones, A. C., and R. Voituriez, 2016, Actin flows in cell migration: from locomotion and polarity to trajectories: Curr Opin Cell Biol, v. 38, p. 12-17.

Caspi, O., A. Lesman, Y. Basevitch, A. Gepstein, G. Arbel, I. H. Habib, L. Gepstein, and S. Levenberg, 2007, Tissue engineering of vascularized cardiac muscle from human embryonic stem cells: Circ Res, v. 100, p. 263-72.

Chabert, M., and J. L. Viovy, 2008, Microfluidic high-throughput encapsulation and hydrodynamic self-sorting of single cells: Proc Natl Acad Sci U S A, v. 105, p. 3191-6.

Chan, C., F. Berthiaume, B. D. Nath, A. W. Tilles, M. Toner, and M. L. Yarmush, 2004, Hepatic tissue engineering for adjunct and temporary liver support: critical technologies: Liver Transpl, v. 10, p. 1331-42.

Chang, R., K. Emami, H. Wu, and W. Sun, 2010, Biofabrication of a three-dimensional liver micro-organ as an in vitro drug metabolism model: Biofabrication, v. 2, p. 045004.

Charvin, G., F. R. Cross, and E. D. Siggia, 2008, A microfluidic device for temporally controlled gene expression and long-term fluorescent imaging in unperturbed dividing yeast cells: PLoS One, v. 3, p. e1468.

Chatterjee, D., B. Hetayothin, A. R. Wheeler, D. J. King, and R. L. Garrell, 2006, Droplet-based microfluidics with nonaqueous solvents and solutions: Lab Chip, v. 6, p. 199-206.

Chau, D. Y., C. Johnson, S. MacNeil, J. W. Haycock, and A. M. Ghaemmaghami, 2013, The development of a 3D immunocompetent model of human skin: Biofabrication, v. 5, p. 035011.

Chavez-Tapia, N. C., N. Rosso, and C. Tiribelli, 2012, Effect of intracellular lipid accumulation in a new model of non-alcoholic fatty liver disease: BMC Gastroenterol, v. 12, p. 20.

Chen, M. C., M. Gupta, and K. C. Cheung, 2010, Alginate-based microfluidic system for tumor spheroid formation and anticancer agent screening: Biomed Microdevices, v. 12, p. 647-54.

Chen, Y. C., S. G. Allen, P. N. Ingram, R. Buckanovich, S. D. Merajver, and E. Yoon, 2015, Single-cell Migration Chip for Chemotaxis-based Microfluidic Selection of Heterogeneous Cell Populations: Sci Rep, v. 5, p. 9980.

Cheng, W., N. Klauke, G. Smith, and J. M. Cooper, 2010, Microfluidic cell arrays for metabolic monitoring of stimulated cardiomyocytes: Electrophoresis, v. 31, p. 1405-13.

Chiu, D. T., 2001, A microfluidics platform for cell fusion: Curr Opin Chem Biol, v. 5, p. 609-12.

Choucha Snouber, L., A. Bunescu, M. Naudot, C. Legallais, C. Brochot, M. E. Dumas, B. Elena-Herrmann, and E. Leclerc, 2013, Metabolomics-on-a-chip of hepatotoxicity induced by anticancer drug flutamide and Its active metabolite hydroxyflutamide using HepG2/C3a microfluidic biochips: Toxicol Sci, v. 132, p. 8-20.

Chung, S., R. Sudo, P. J. Mack, C. R. Wan, V. Vickerman, and R. D. Kamm, 2009, Cell migration into scaffolds under co-culture conditions in a microfluidic platform: Lab Chip, v. 9, p. 269-75.

Chung, S., R. Sudo, V. Vickerman, I. K. Zervantonakis, and R. D. Kamm, 2010, Microfluidic platforms for studies of angiogenesis, cell migration, and cell-cell interactions. Sixth International Bio-Fluid Mechanics Symposium and Workshop March 28-30, 2008 Pasadena, California: Ann Biomed Eng, v. 38, p. 1164-77.

Condeelis, J., and J. W. Pollard, 2006, Macrophages: obligate partners for tumor cell migration, invasion, and metastasis: Cell, v. 124, p. 263-6.

Csaderova, L., M. Riehle, A. McIntosh, and M. Robertson, 2005, Cell Response to Microfabricated Surface Rigidity Patterns: European Cells and Materials, v. 10.

de la Rica, R., and H. Matsui, 2010, Applications of peptide and protein-based materials in bionanotechnology: Chem Soc Rev, v. 39, p. 3499-509.

de la Rica, R., C. Pejoux, and H. Matsui, 2011, Assemblies of Functional Peptides and Their Applications in Building Blocks for Biosensors: Adv Funct Mater, v. 21, p. 1018-1026.

De, S. K., N. R. Aluru, B. Johnson, W. C. Crone, D. J. Beebe, and J. Moore, 2002, Equilibrium Swelling and Kinetics of pH-Responsive Hydrogels: Models, Experiments, and Simulations Journal of microelectromechanical systems, v. 11.

Derda, R., S. K. Tang, A. Laromaine, B. Mosadegh, E. Hong, M. Mwangi, A. Mammoto, D. E. Ingber, and G. M. Whitesides, 2011, Multizone paper platform for 3D cell cultures: PLoS One, v. 6, p. e18940.

Dertinger, S. K., X. Jiang, Z. Li, V. N. Murthy, and G. M. Whitesides, 2002, Gradients of substrate-bound laminin orient axonal specification of neurons: Proc Natl Acad Sci U S A, v. 99, p. 12542-7.

Di Carlo, D., L. Y. Wu, and L. P. Lee, 2006, Dynamic single cell culture array: Lab Chip, v. 6, p. 1445-9.

Dickinson, R. B., and R. T. Tranquillo, 1993, Optimal estimation of cell movement indices from the statistical analysis of cell tracking data: AIChE Journal.

Domansky, K., W. Inman, J. Serdy, and L. Griffith, 2005, Perfused microreactors for liver tissue engineering: Conf Proc IEEE Eng Med Biol Soc, v. 7, p. 7490-2.

Donati, I., S. Stredanska, G. Silvestrini, A. Vetere, P. Marcon, E. Marsich, P. Mozetic, A. Gamini, S. Paoletti, and F. Vittur, 2005, The aggregation of pig articular

chondrocyte and synthesis of extracellular matrix by a lactose-modified chitosan: Biomaterials, v. 26, p. 987-98.

Doré, E., and C. Legallais, 1999, A new concept of bioartificial liver based on a fluidized bed bioreactor: Ther Apher, v. 3, p. 264-7.

Doyle, A. D., and J. Lee, 2002, Simultaneous, real-time imaging of intracellular calcium and cellular traction force production: Biotechniques, v. 33, p. 358-64.

Doyle, A. D., F. W. Wang, K. Matsumoto, and K. M. Yamada, 2009, One-dimensional topography underlies three-dimensional fibrillar cell migration: J Cell Biol, v. 184, p. 481-90.

Dutta, R. C., and A. K. Dutta, 2009, Cell-interactive 3D-scaffold; advances and applications: Biotechnol Adv, v. 27, p. 334-9.

El-Ali, J., P. K. Sorger, and K. F. Jensen, 2006, Cells on chips, Nature Publishing Group, p. 403-411.

Elliott, N. T., and F. Yuan, 2011, A review of three-dimensional in vitro tissue models for drug discovery and transport studies: J Pharm Sci, v. 100, p. 59-74.

Esch, M. B., T. L. King, and M. L. Shuler, 2011, The role of body-on-a-chip devices in drug and toxicity studies: Annu Rev Biomed Eng, v. 13, p. 55-72.

Esch, M. B., G. J. Mahler, T. Stokol, and M. L. Shuler, 2014, Body-on-a-chip simulation with gastrointestinal tract and liver tissues suggests that ingested nanoparticles have the potential to cause liver injury: Lab Chip, v. 14, p. 3081-92.

Esch, M. B., J. M. Prot, Y. I. Wang, P. Miller, J. R. Llamas-Vidales, B. A. Naughton, D. R. Applegate, and M. L. Shuler, 2015, Multi-cellular 3D human primary liver cell culture elevates metabolic activity under fluidic flow: Lab Chip, v. 15, p. 2269-77.

Farahat, W. A., L. B. Wood, I. K. Zervantonakis, A. Schor, S. Ong, D. Neal, R. D. Kamm, and H. H. Asada, 2012, Ensemble analysis of angiogenic growth in three-dimensional microfluidic cell cultures: PLoS One, v. 7, p. e37333.

Feldstein, A. E., A. Canbay, M. E. Guicciardi, H. Higuchi, S. F. Bronk, and G. J. Gores, 2003, Diet associated hepatic steatosis sensitizes to Fas mediated liver injury in mice: J Hepatol, v. 39, p. 978-83.

Fennema, E., N. Rivron, J. Rouwkema, C. van Blitterswijk, and J. de Boer, 2013, Spheroid culture as a tool for creating 3D complex tissues: Trends Biotechnol, v. 31, p. 108-15.

Frey, O., F. Rudolf, G. W. Schmidt, and A. Hierlemann, 2015, Versatile, simple-to-use microfluidic cell-culturing chip for long-term, high-resolution, time-lapse imaging: Anal Chem, v. 87, p. 4144-51.

Funatsu, K., H. Ijima, K. Nakazawa, Y. Yamashita, M. Shimada, and K. Sugimachi, 2001, Hybrid artificial liver using hepatocyte organoid culture: Artif Organs, v. 25, p. 194-200.

García-Cañaveras, J. C., N. Jiménez, M. J. Gómez-Lechón, J. V. Castell, M. T. Donato, and A. Lahoz, 2015, LC-MS untargeted metabolomic analysis of drug-induced hepatotoxicity in HepG2 cells: Electrophoresis.

Gemoets, H. P., Y. Su, M. Shang, V. Hessel, R. Luque, and T. Noël, 2015, Liquid phase oxidation chemistry in continuous-flow microreactors: Chem Soc Rev.

Gerontas, S., M. S. Shapiro, and D. G. Bracewell, 2013, Chromatography modelling to describe protein adsorption at bead level: J Chromatogr A, v. 1284, p. 44-52.

Ghaemmaghami, A. M., M. J. Hancock, H. Harrington, H. Kaji, and A. Khademhosseini, 2012, Biomimetic tissues on a chip for drug discovery: Drug Discov Today, v. 17, p. 173-81.

Ghosh, A., 2011, Scaling Laws, Mechanics Over Micro and Nano Scales, Springer Science+Business Media.

Gilbert, P. M., K. L. Havenstrite, K. E. Magnusson, A. Sacco, N. A. Leonardi, P. Kraft, N. K. Nguyen, S. Thrun, M. P. Lutolf, and H. M. Blau, 2010, Substrate elasticity regulates skeletal muscle stem cell self-renewal in culture: Science, v. 329, p. 1078-81.

Gori, M., M. Arciello, and C. Balsano, 2014a, MicroRNAs in nonalcoholic fatty liver disease: novel biomarkers and prognostic tools during the transition from steatosis to hepatocarcinoma: Biomed Res Int, v. 2014, p. 741465.

Gori, M., B. Barbaro, M. Arciello, R. Maggio, C. Viscomi, A. Longo, and C. Balsano, 2014b, Protective effect of the Y220C mutant p53 against steatosis: good news?: J Cell Physiol, v. 229, p. 1182-92.

Grinnell, F., 2003, Fibroblast biology in three-dimensional collagen matrices: Trends Cell Biol, v. 13, p. 264-9.

Guo, C., A. Buranych, D. Sarkar, P. B. Fisher, and X. Y. Wang, 2013, The role of tumor-associated macrophages in tumor vascularization: Vasc Cell, v. 5, p. 20.

Guzzardi, M. A., F. Vozzi, and A. D. Ahluwalia, 2009, Study of the crosstalk between hepatocytes and endothelial cells using a novel multicompartmental bioreactor: a comparison between connected cultures and cocultures: Tissue Eng Part A, v. 15, p. 3635-44.

Gómez-Lechón, M. J., M. T. Donato, A. Martínez-Romero, N. Jiménez, J. V. Castell, and J. E. O'Connor, 2007, A human hepatocellular in vitro model to investigate steatosis: Chem Biol Interact, v. 165, p. 106-16.

Haeberle, S., and R. Zengerle, 2007, Microfluidic platforms for lab-on-a-chip applications: Lab Chip, v. 7, p. 1094-110.

Hamilton, G. A., C. Westmorel, and A. E. George, 2001, Effects of medium composition on the morphology and function of rat hepatocytes cultured as spheroids and monolayers: In Vitro Cell Dev Biol Anim, v. 37, p. 656-67.

Ho, C. T., R. Z. Lin, R. J. Chen, C. K. Chin, S. E. Gong, H. Y. Chang, H. L. Peng, L. Hsu, T. R. Yew, S. F. Chang, and C. H. Liu, 2013, Liver-cell patterning lab chip: mimicking the morphology of liver lobule tissue: Lab Chip, v. 13, p. 3578-87.

Huang, C. P., J. Lu, H. Seon, A. P. Lee, L. A. Flanagan, H. Y. Kim, A. J. Putnam, and N. L. Jeon, 2009, Engineering microscale cellular niches for three-dimensional multicellular co-cultures: Lab Chip, v. 9, p. 1740-8.

Huang, W. H., F. Ai, Z. L. Wang, and J. K. Cheng, 2008, Recent advances in single-cell analysis using capillary electrophoresis and microfluidic devices: J Chromatogr B Analyt Technol Biomed Life Sci, v. 866, p. 104-22.

Huang, Y., B. Agrawal, P. A. Clark, J. C. Williams, and J. S. Kuo, 2011, Evaluation of cancer stem cell migration using compartmentalizing microfluidic devices and live cell imaging: J Vis Exp, p. e3297.

Huh, D., G. A. Hamilton, and D. E. Ingber, 2011, From 3D cell culture to organs-on-chips: Trends Cell Biol, v. 21, p. 745-54.

Huh, D., H. J. Kim, J. P. Fraser, D. E. Shea, M. Khan, A. Bahinski, G. A. Hamilton, and D. E. Ingber, 2013, Microfabrication of human organs-on-chips: Nat Protoc, v. 8, p. 2135-57.

Huh, D., B. D. Matthews, A. Mammoto, M. Montoya-Zavala, H. Y. Hsin, and D. E. Ingber, 2010, Reconstituting organ-level lung functions on a chip: Science, v. 328, p. 1662-8.

Huh, D., Y. S. Torisawa, G. A. Hamilton, H. J. Kim, and D. E. Ingber, 2012, Microengineered physiological biomimicry: organs-on-chips: Lab Chip, v. 12, p. 2156-64.

Hulme, S. E., S. S. Shevkoplyas, and G. M. Whitesides, 2009, Incorporation of prefabricated screw, pneumatic, and solenoid valves into microfluidic devices: Lab Chip, v. 9, p. 79-86.

Hutmacher, D. W., B. M. Holzapfel, E. M. De-Juan-Pardo, B. A. Pereira, S. J. Ellem, D. Loessner, and G. P. Risbridger, 2015, Convergence of regenerative medicine and synthetic biology to develop standardized and validated models of human diseases with clinical relevance: Curr Opin Biotechnol, v. 35, p. 127-32.

Hwa, A. J., R. C. Fry, A. Sivaraman, P. T. So, L. D. Samson, D. B. Stolz, and L. G. Griffith, 2007, Rat liver sinusoidal endothelial cells survive without exogenous VEGF in 3D perfused co-cultures with hepatocytes: FASEB J, v. 21, p. 2564-79.

Hwang, N. S., M. S. Kim, S. Sampattavanich, J. H. Baek, Z. Zhang, and J. Elisseeff, 2006, Effects of three-dimensional culture and growth factors on the chondrogenic differentiation of murine embryonic stem cells: Stem Cells, v. 24, p. 284-91.

Illa, X., S. Vila, J. Yeste, C. Peralta, J. Gracia-Sancho, and R. Villa, 2014, A novel modular bioreactor to in vitro study the hepatic sinusoid: PLoS One, v. 9, p. e111864.

Imura, Y., E. Yoshimura, and K. Sato, 2012, Micro total bioassay system for oral drugs: evaluation of gastrointestinal degradation, intestinal absorption, hepatic metabolism, and bioactivity: Anal Sci, v. 28, p. 197-9.

Ingber, D. E., 2006, Cellular mechanotransduction: putting all the pieces together again: FASEB J, v. 20, p. 811-27.

Ingber, D. E., 2008, Tensegrity and mechanotransduction: J Bodyw Mov Ther, v. 12, p. 198-200.

Ionescu-Zanetti, C., R. M. Shaw, J. Seo, Y. N. Jan, L. Y. Jan, and L. P. Lee, 2005, Mammalian electrophysiology on a microfluidic platform: Proc Natl Acad Sci U S A, v. 102, p. 9112-7.

Irimia, D., D. A. Geba, and M. Toner, 2006, Universal microfluidic gradient generator: Anal Chem, v. 78, p. 3472-7.

Irimia, D., and M. Toner, 2009, Spontaneous migration of cancer cells under conditions of mechanical confinement: Integr Biol (Camb), v. 1, p. 506-12.

Jang, K. J., A. P. Mehr, G. A. Hamilton, L. A. McPartlin, S. Chung, K. Y. Suh, and D. E. Ingber, 2013, Human kidney proximal tubule-on-a-chip for drug transport and nephrotoxicity assessment: Integr Biol (Camb), v. 5, p. 1119-29.

Jang, K. J., and K. Y. Suh, 2010, A multi-layer microfluidic device for efficient culture and analysis of renal tubular cells: Lab Chip, v. 10, p. 36-42.

Javitt, N. B., 1990, Hep G2 cells as a resource for metabolic studies: lipoprotein, cholesterol, and bile acids: FASEB J, v. 4, p. 161-8.

Jeon, J. S., S. Bersini, M. Gilardi, G. Dubini, J. L. Charest, M. Moretti, and R. D. Kamm, 2015, Human 3D vascularized organotypic microfluidic assays to study breast cancer cell extravasation: Proc Natl Acad Sci U S A, v. 112, p. 214-9.

Jeon, J. S., S. Bersini, J. A. Whisler, M. B. Chen, G. Dubini, J. L. Charest, M. Moretti, and R. D. Kamm, 2014, Generation of 3D functional microvascular networks with human mesenchymal stem cells in microfluidic systems: Integr Biol (Camb), v. 6, p. 555-63.

Jeon, N. L., S. K. W. Dertinger, D. T. Chiu, I. S. Choi, A. D. Stroock, and G. M. Whitesides, 2000, Generation of solution and surface gradients using microfluidic systems.: Langmuir, v. 16, p. 8311-8316.

Jubery, T. Z., S. K. Srivastava, and P. Dutta, 2014, Dielectrophoretic separation of bioparticles in microdevices: a review: Electrophoresis, v. 35, p. 691-713.

Juncker, D., H. Schmid, and E. Delamarche, 2005, Multipurpose microfluidic probe: Nat Mater, v. 4, p. 622-8.

Kamholz, A. E., and P. Yager, 2001, Theoretical analysis of molecular diffusion in pressure-driven laminar flow in microfluidic channels: Biophys J, v. 80, p. 155-60.

Karlsson, H., M. Fryknäs, R. Larsson, and P. Nygren, 2012, Loss of cancer drug activity in colon cancer HCT-116 cells during spheroid formation in a new 3-D spheroid cell culture system: Exp Cell Res, v. 318, p. 1577-85.

Karp, J. M., J. Yeh, G. Eng, J. Fukuda, J. Blumling, K. Y. Suh, J. Cheng, A. Mahdavi, J. Borenstein, R. Langer, and A. Khademhosseini, 2007, Controlling size, shape and homogeneity of embryoid bodies using poly(ethylene glycol) microwells: Lab Chip, v. 7, p. 786-94.

Kasuya, J., and K. Tanishita, 2012, Microporous membrane-based liver tissue engineering for the reconstruction of three-dimensional functional liver tissues in vitro: Biomatter, v. 2, p. 290-5.

Kenny, P. A., 2007, Three-dimensional extracellular matrix culture models of EGFR signalling and drug response: Biochem Soc Trans, v. 35, p. 665-8.

Khademhosseini, A., L. Ferreira, J. Blumling, J. Yeh, J. M. Karp, J. Fukuda, and R. Langer, 2006, Co-culture of human embryonic stem cells with murine embryonic fibroblasts on microwell-patterned substrates: Biomaterials, v. 27, p. 5968-77.

Kim, H. J., D. Huh, G. Hamilton, and D. E. Ingber, 2012, Human gut-on-a-chip inhabited by microbial flora that experiences intestinal peristalsis-like motions and flow: Lab Chip, v. 12, p. 2165-74.

Kim, S., H. J. Kim, and N. L. Jeon, 2010, Biological applications of microfluidic gradient devices: Integr Biol (Camb), v. 2, p. 584-603.

Kleinman, H. K., and G. R. Martin, 2005, Matrigel: basement membrane matrix with biological activity: Semin Cancer Biol, v. 15, p. 378-86.

Kobel, S., A. Valero, J. Latt, P. Renaud, and M. Lutolf, 2010, Optimization of microfluidic single cell trapping for long-term on-chip culture: Lab Chip, v. 10, p. 857-63.

Kogot, J. M., Y. Zhang, S. J. Moore, P. Pagano, D. N. Stratis-Cullum, D. Chang-Yen, M. Turewicz, P. M. Pellegrino, A. de Fusco, H. T. Soh, and N. E. Stagliano, 2011, Screening of peptide libraries against protective antigen of Bacillus anthracis in a disposable microfluidic cartridge: PLoS One, v. 6, p. e26925.

Köster, S., F. E. Angilè, H. Duan, J. J. Agresti, A. Wintner, C. Schmitz, A. C. Rowat, C. A. Merten, D. Pisignano, A. D. Griffiths, and D. A. Weitz, 2008, Drop-based microfluidic devices for encapsulation of single cells: Lab Chip, v. 8, p. 1110-5.

Landry, J., D. Bernier, C. Ouellet, R. Goyette, and N. Marceau, 1985, Spheroidal aggregate culture of rat liver cells: histotypic reorganization, biomatrix deposition, and maintenance of functional activities: J Cell Biol, v. 101, p. 914-23.

Larrea, A., V. Sebastian, A. Ibarra, M. Arruebo, and J. Santamaria, 2015, Gas Slug Microfluidics: A Unique Tool for Ultrafast, Highly Controlled Growth of Iron Oxide Nanostructures: Chem Mater, v. 27, p. 4254-4260.

Lautt, W., 2009, Hepatic circulation: physiology and pathophysiology.

Lazo, M., and J. M. Clark, 2008, The epidemiology of nonalcoholic fatty liver disease: a global perspective: Semin Liver Dis, v. 28, p. 339-50.

Leclerc, E., J. Hamon, I. Claude, R. Jellali, M. Naudot, and F. Bois, 2015, Investigation of acetaminophen toxicity in HepG2/C3a microscale cultures using a system biology model of glutathione depletion: Cell Biol Toxicol, v. 31, p. 173-85.

Leclerc, E., Y. Sakai, and T. Fujii, 2004, Perfusion culture of fetal human hepatocytes in microfluidic environments Biochemical Engineering Journal, v. 20, p. 143-148.

Lee, D. W., I. Doh, Y. Kim, and Y. H. Cho, 2013a, Advanced combinational microfluidic multiplexer using multiple levels of control pressures: Lab Chip, v. 13, p. 3658-62.

Lee, F., and M. Kurisawa, 2013, Formation and stability of interpenetrating polymer network hydrogels consisting of fibrin and hyaluronic acid for tissue engineering: Acta Biomater, v. 9, p. 5143-52.

Lee, G. Y., P. A. Kenny, E. H. Lee, and M. J. Bissell, 2007a, Three-dimensional culture models of normal and malignant breast epithelial cells: Nat Methods, v. 4, p. 359-65.

Lee, J., S. H. Kim, Y. C. Kim, I. Choi, and J. H. Sung, 2013b, Fabrication and characterization of microfluidic liver-on-a-chip using microsomal enzymes: Enzyme Microb Technol, v. 53, p. 159-64.

Lee, P., T. Gaige, and P. Hung, 2011, Microfluidic systems for live cell imaging: Methods Cell Biol, v. 102, p. 77-103.

Lee, P., R. Lin, J. Moon, and L. P. Lee, 2006, Microfluidic alignment of collagen fibers for in vitro cell culture: Biomed Microdevices, v. 8, p. 35-41.

Lee, P. J., P. J. Hung, and L. P. Lee, 2007b, An artificial liver sinusoid with a microfluidic endothelial-like barrier for primary hepatocyte culture: Biotechnol Bioeng, v. 97, p. 1340-6.

Lee, P. J., P. J. Hung, R. Shaw, L. Jan, and L. P. Lee, 2005, Microfluidic application integrated device for monitoring direct cell-cell communication via gap junctions between individual cell pairs: Applied Physics Letters, v. 86.

Lee, S. H., J. J. Moon, and J. L. West, 2008, Three-dimensional micropatterning of bioactive hydrogels via two-photon laser scanning photolithography for guided 3D cell migration: Biomaterials, v. 29, p. 2962-8.

Legallais, C., B. David, and E. Doré, 2001, Bioartificial livers (BAL): current technological aspects and future developments Journal of Membrane Science, v. 181, p. 81-95.

Legendre, A., R. Baudoin, G. Alberto, P. Paullier, M. Naudot, T. Bricks, J. Brocheton, S. Jacques, J. Cotton, and E. Leclerc, 2013, Metabolic characterization of primary rat hepatocytes cultivated in parallel microfluidic biochips: J Pharm Sci, v. 102, p. 3264-76.

Legendre, A., S. Jacques, F. Dumont, J. Cotton, P. Paullier, M. J. Fleury, and E. Leclerc, 2014, Investigation of the hepatotoxicity of flutamide: pro-survival/apoptotic and necrotic switch in primary rat hepatocytes characterized by metabolic and transcriptomic profiles in microfluidic liver biochips: Toxicol In Vitro, v. 28, p. 1075-87.

Lei, K. F., 2012, Microfluidic systems for diagnostic applications: a review: J Lab Autom, v. 17, p. 330-47.

Li, C. Y., K. R. Stevens, R. E. Schwartz, B. S. Alejandro, J. H. Huang, and S. N. Bhatia, 2014, Micropatterned cell-cell interactions enable functional encapsulation of primary hepatocytes in hydrogel microtissues: Tissue Eng Part A, v. 20, p. 2200-12.

Lin, W. Y., Y. Wang, S. Wang, and H. R. Tseng, 2009, Integrated Microfluidic Reactors: Nano Today, v. 4, p. 470-481.

Lindström, S., M. Eriksson, T. Vazin, J. Sandberg, J. Lundeberg, J. Frisén, and H. Andersson-Svahn, 2009a, High-density microwell chip for culture and analysis of stem cells: PLoS One, v. 4, p. e6997.

Lindström, S., K. Mori, T. Ohashi, and H. Andersson-Svahn, 2009b, A microwell array device with integrated microfluidic components for enhanced single-cell analysis: Electrophoresis, v. 30, p. 4166-71.

Liu, C., Y. Qu, Y. Luo, and N. Fang, 2011, Recent advances in single-molecule detection on micro- and nano-fluidic devices: Electrophoresis, v. 32, p. 3308-18.

Liu, P., and R. A. Mathies, 2009, Integrated microfluidic systems for high-performance genetic analysis: Trends Biotechnol, v. 27, p. 572-81.

Luni, C., E. Serena, and N. Elvassore, 2014, Human-on-chip for therapy development and fundamental science: Curr Opin Biotechnol, v. 25, p. 45-50.

Lutolf, M. P., and H. M. Blau, 2009, Artificial stem cell niches: Adv Mater, v. 21, p. 3255-68.

Lämmermann, T., B. L. Bader, S. J. Monkley, T. Worbs, R. Wedlich-Söldner, K. Hirsch, M. Keller, R. Förster, D. R. Critchley, R. Fässler, and M. Sixt, 2008, Rapid leukocyte migration by integrin-independent flowing and squeezing: Nature, v. 453, p. 51-5.

Madou, M., BIOMEMS, http://mmadou.eng.uci.edu/: Irvine UC.

Madou, M. J., 2011a, From MEMS to Bio-MEMS and Bio-NEMS Manufacturing Techniques and Applications, *in* C. Press, ed., Fundamentals of microfabrication and nanotechnology, v. III.

Madou, M. J., 2011b, Manufacturing techniques for Microfabrication and Nanotechnology, *in* C. Press, ed., Fundamentals of microfabrication and nanotechnology, v. II.

Maercker, C., 2005, Protein arrays in functional genome research: Biosci Rep, v. 25, p. 57-70.

Maguire, T., E. Novik, R. Schloss, and M. Yarmush, 2006, Alginate-PLL microencapsulation: effect on the differentiation of embryonic stem cells into hepatocytes: Biotechnol Bioeng, v. 93, p. 581-91.

Maheswaran, S., L. V. Sequist, S. Nagrath, L. Ulkus, B. Brannigan, C. V. Collura, E. Inserra, S. Diederichs, A. J. Iafrate, D. W. Bell, S. Digumarthy, A. Muzikansky, D. Irimia, J. Settleman, R. G. Tompkins, T. J. Lynch, M. Toner, and D. A. Haber, 2008, Detection of mutations in EGFR in circulating lung-cancer cells: N Engl J Med, v. 359, p. 366-77.

Malda, J., J. Visser, F. P. Melchels, T. Jungst, W. E. Hennik, W. J. A. Dhert, J. Groll, and D. W. Hutmacher, 2013, 25th Anniversary Article: Engineering Hydrogels for Biofabrication: Advanced Materials, v. 25, p. 5011-5028.

Mammoto, T., and D. E. Ingber, 2010, Mechanical control of tissue and organ development: Development, v. 137, p. 1407-20.

Mantovani, A., B. Bottazzi, F. Colotta, S. Sozzani, and L. Ruco, 1992, The origin and function of tumor-associated macrophages: Immunol Today, v. 13, p. 265-70.

Mao, H., P. S. Cremer, and M. D. Manson, 2003, A sensitive, versatile microfluidic assay for bacterial chemotaxis: Proc Natl Acad Sci U S A, v. 100, p. 5449-54.

Mao, H., T. Yang, and P. S. Cremer, 2002, A microfluidic device with a linear temperature gradient for parallel and combinatorial measurements: J Am Chem Soc, v. 124, p. 4432-5.

Mao, Z., F. Guo, Y. Xie, Y. Zhao, M. I. Lapsley, L. Wang, J. D. Mai, F. Costanzo, and T. J. Huang, 2015, Label-free measurements of reaction kinetics using a droplet-based optofluidic device: J Lab Autom, v. 20, p. 17-24.

Marchesini, G., E. Bugianesi, G. Forlani, F. Cerrelli, M. Lenzi, R. Manini, S. Natale, E. Vanni, N. Villanova, N. Melchionda, and M. Rizzetto, 2003, Nonalcoholic fatty liver, steatohepatitis, and the metabolic syndrome: Hepatology, v. 37, p. 917-23.

Marcus, J. S., W. F. Anderson, and S. R. Quake, 2006, Microfluidic single-cell mRNA isolation and analysis: Anal Chem, v. 78, p. 3084-9.

Marra, F., A. Gastaldelli, G. Svegliati Baroni, G. Tell, and C. Tiribelli, 2008, Molecular basis and mechanisms of progression of non-alcoholic steatohepatitis: Trends Mol Med, v. 14, p. 72-81.

Matharu, Z., D. Patel, Y. Gao, A. Haque, Q. Zhou, and A. Revzin, 2014, Detecting transforming growth factor-β release from liver cells using an aptasensor integrated with microfluidics: Anal Chem, v. 86, p. 8865-72.

McDonald, J. C., D. C. Duffy, J. R. Anderson, D. T. Chiu, H. Wu, O. J. Schueller, and G. M. Whitesides, 2000, Fabrication of microfluidic systems in poly(dimethylsiloxane): Electrophoresis, v. 21, p. 27-40.

McFadden, R., A basic introduction to clean rooms, *in* C. Laboratories, ed.

Mehta, G., A. Y. Hsiao, M. Ingram, G. D. Luker, and S. Takayama, 2012, Opportunities and challenges for use of tumor spheroids as models to test drug delivery and efficacy: J Control Release, v. 164, p. 192-204.

Minteer, S. D., and C. M. Moore, 2005, Overview of Advances in Microfluidics and Microfabrication: Methods in Molecular Biology, v. 321, Humana Press, 2 p.

Mohanty, S. K., J. Warrick, J. Gorski, and D. J. Beebe, 2009, An accessible micro-capillary electrophoresis device using surface-tension-driven flow: Electrophoresis, v. 30, p. 1470-81.

Montanez-Sauri, S. I., D. J. Beebe, and K. E. Sung, 2015, Microscale screening systems for 3D cellular microenvironments: platforms, advances, and challenges: Cell Mol Life Sci, v. 72, p. 237-49.

Moussavi-Harami, S. F., H. M. Pezzi, A. Huttenlocher, and D. J. Beebe, 2015, Simple microfluidic device for studying chemotaxis in response to dual gradients: Biomed Microdevices, v. 17, p. 9955.

Mulvana, H., S. Cochran, and M. Hill, 2013, Ultrasound assisted particle and cell manipulation on-chip: Adv Drug Deliv Rev, v. 65, p. 1600-10.

Murzabaev, M., T. Kojima, T. Mizoguchi, I. Kobayashi, B. J. DeKosky, G. Georgiou, and H. Nakano, 2015, Handmade microfluidic device for biochemical applications in emulsion: J Biosci Bioeng.

Müller, T., A. Pfennig, P. Klein, G. Gradl, M. Jäger, and T. Schnelle, 2003, The potential of dielectrophoresis for single-cell experiments: IEEE Eng Med Biol Mag, v. 22, p. 51-61.

Nagrath, S., L. V. Sequist, S. Maheswaran, D. W. Bell, D. Irimia, L. Ulkus, M. R. Smith, E. L. Kwak, S. Digumarthy, A. Muzikansky, P. Ryan, U. J. Balis, R. G. Tompkins, D. A. Haber, and M. Toner, 2007, Isolation of rare circulating tumour cells in cancer patients by microchip technology: Nature, v. 450, p. 1235-9.

Ng, J. M., I. Gitlin, A. D. Stroock, and G. M. Whitesides, 2002, Components for integrated poly(dimethylsiloxane) microfluidic systems: Electrophoresis, v. 23, p. 3461-73.

Nie, F. Q., M. Yamada, J. Kobayashi, M. Yamato, A. Kikuchi, and T. Okano, 2007, On-chip cell migration assay using microfluidic channels: Biomaterials, v. 28, p. 4017-22.

Nikolov, A., and H. Zhang, 2015, The dynamics of capillary-driven two-phase flow: the role of nanofluid structural forces: J Colloid Interface Sci, v. 449, p. 92-101.

Niu, X., and A. J. deMello, 2012, Building droplet-based microfluidic systems for biological analysis: Biochem Soc Trans, v. 40, p. 615-23.

Noguchi, M. A., TakahiroSumitomo, Keiko, and Y. S. Yamaguchi, Shuichi, 2009, LARGE SCALE MICROFLUIDIC SYSTEMS FOR SEQUENTIAL TRAPPING, LABELING AND CONTENT EXTRACTION OF SINGLE CELLS Transducers, IEEE.

O'Brien, C. A., A. Kreso, and C. H. Jamieson, 2010, Cancer stem cells and self-renewal: Clinical Cancer Research.

O-Charoen, S., O. Srivannavit, and E. Gulari, 2007, Simulation and visualization of flow pattern in microarrays for liquid phase oligonucleotide and peptide synthesis: Biotechnol Prog, v. 23, p. 755-61.

Paguirigan, A. L., and D. J. Beebe, 2009, From the cellular perspective: exploring differences in the cellular baseline in macroscale and microfluidic cultures: Integr Biol (Camb), v. 1, p. 182-95.

Pan, T., and W. Wang, 2011, From cleanroom to desktop: emerging micro-nanofabrication technology for biomedical applications: Ann Biomed Eng, v. 39, p. 600-20.

Pavšič, J., J. Žel, and M. Milavec, 2015, Assessment of the real-time PCR and different digital PCR platforms for DNA quantification: Anal Bioanal Chem.

Perestrelo, A. R., A. C. Águas, A. Rainer, and G. Forte, 2015, Microfluidic Organ/Body-on-a-Chip Devices at the Convergence of Biology and Microengineering: Sensors (Basel), v. 15, p. 31142-70.

Plecis, A., and T. Houssin, 2015, Flow control in microfluidic devices, http://www.elveflow.com.

Pollard, J. W., 2008, Macrophages define the invasive microenvironment in breast cancer: J Leukoc Biol, v. 84, p. 623-30.

Prager-Khoutorsky, M., A. Lichtenstein, R. Krishnan, K. Rajendran, A. Mayo, Z. Kam, B. Geiger, and A. D. Bershadsky, 2011, Fibroblast polarization is a matrix-rigidity-dependent process controlled by focal adhesion mechanosensing: Nat Cell Biol, v. 13, p. 1457-65.

Puleo, C. M., H. C. Yeh, and T. H. Wang, 2007, Applications of MEMS technologies in tissue engineering: Tissue Eng, v. 13, p. 2839-54.

Qin, D., Y. Xia, J. A. Rogers, R. J. Jackman, X.-M. Zhao, and G. M. Whitesides, 1998, Microfabrication, Microstructures and Microsystems, Berlin Heidelberg, Springer-Verlag p. 1-20.

Ranga, A., S. Gobaa, Y. Okawa, K. Mosiewicz, A. Negro, and M. P. Lutolf, 2014, 3D niche microarrays for systems-level analyses of cell fate: Nat Commun, v. 5, p. 4324.

Rettig, J. R., and A. Folch, 2005, Large-scale single-cell trapping and imaging using microwell arrays: Anal Chem, v. 77, p. 5628-34.

Ricchi, M., M. R. Odoardi, L. Carulli, C. Anzivino, S. Ballestri, A. Pinetti, L. I. Fantoni, F. Marra, M. Bertolotti, S. Banni, A. Lonardo, N. Carulli, and P. Loria, 2009, Differential effect of oleic and palmitic acid on lipid accumulation and apoptosis in cultured hepatocytes: J Gastroenterol Hepatol, v. 24, p. 830-40.

Rimann, M., and U. Graf-Hausner, 2012, Synthetic 3D multicellular systems for drug development: Curr Opin Biotechnol, v. 23, p. 803-9.

Rolli, C. G., 2011, Development of in vitro model systems to study single and collective cell migration Ruperto-Carola University of Heidelberg, Germany.

Sant, S., M. J. Hancock, J. P. Donnelly, D. Iyer, and A. Khademhosseini, 2010, BIOMIMETIC GRADIENT HYDROGELS FOR TISSUE ENGINEERING: Can J Chem Eng, v. 88, p. 899-911.

Saucedo-Espinosa, M. A., A. LaLonde, A. Gencoglu, M. F. Romero-Creel, J. Dolas, and B. H. Lapizco-Encinas, 2015, Dielectrophoretic manipulation of particle mixtures employing asymmetric insulating posts: Electrophoresis.

Schmitz, C. H., A. C. Rowat, S. Köster, and D. A. Weitz, 2009, Dropspots: a picoliter array in a microfluidic device: Lab Chip, v. 9, p. 44-9.

Scholten, K., X. Fan, and E. T. Zellers, 2014, A microfabricated optofluidic ring resonator for sensitive, high-speed detection of volatile organic compounds: Lab Chip, v. 14, p. 3873-80.

Schütte, J., B. Hagmeyer, F. Holzner, M. Kubon, S. Werner, C. Freudigmann, K. Benz, J. Böttger, R. Gebhardt, H. Becker, and M. Stelzle, 2011, "Artificial micro organs"--a

microfluidic device for dielectrophoretic assembly of liver sinusoids: Biomed Microdevices, v. 13, p. 493-501.

Seemann, R., M. Brinkmann, T. Pfohl, and S. Herminghaus, 2012, Droplet based microfluidics: Rep Prog Phys, v. 75, p. 016601.

Sekiya, M., A. Hiraishi, M. Touyama, and K. Sakamoto, 2008, Oxidative stress induced lipid accumulation via SREBP1c activation in HepG2 cells: Biochem Biophys Res Commun, v. 375, p. 602-7.

Serrao, G. W., I. C. Turnbull, D. Ancukiewicz, d. E. Kim, E. Kao, T. J. Cashman, L. Hadri, R. J. Hajjar, and K. D. Costa, 2012, Myocyte-depleted engineered cardiac tissues support therapeutic potential of mesenchymal stem cells: Tissue Eng Part A, v. 18, p. 1322-33.

Shapiro, M. S., S. J. Haswell, G. J. Lye, and D. G. Bracewell, 2009, Design and characterization of a microfluidic packed bed system for protein breakthrough and dynamic binding capacity determination: Biotechnol Prog, v. 25, p. 277-85.

Sharma, N. S., M. G. Ierapetritou, and M. L. Yarmush, 2005, Novel quantitative tools for engineering analysis of hepatocyte cultures in bioartificial liver systems: Biotechnol Bioeng, v. 92, p. 321-35.

Shih, S. C., I. Barbulovic-Nad, X. Yang, R. Fobel, and A. R. Wheeler, 2013, Digital microfluidics with impedance sensing for integrated cell culture and analysis: Biosens Bioelectron, v. 42, p. 314-20.

Shintu, L., R. Baudoin, V. Navratil, J. M. Prot, C. Pontoizeau, M. Defernez, B. J. Blaise, C. Domange, A. R. Péry, P. Toulhoat, C. Legallais, C. Brochot, E. Leclerc, and M. E. Dumas, 2012, Metabolomics-on-a-chip and predictive systems toxicology in microfluidic bioartificial organs: Anal Chem, v. 84, p. 1840-8.

Sims, C. E., and N. L. Allbritton, 2007, Analysis of single mammalian cells on-chip: Lab Chip, v. 7, p. 423-40.

Situma, C., M. Hashimoto, and S. A. Soper, 2006, Merging microfluidics with microarray-based bioassays: Biomol Eng, v. 23, p. 213-31.

Skafte-Pedersen, P., M. Hemmingsen, D. Sabourin, F. S. Blaga, H. Bruus, and M. Dufva, 2012, A self-contained, programmable microfluidic cell culture system with real-time microscopy access: Biomed Microdevices, v. 14, p. 385-99.

Solinas, G., G. Germano, A. Mantovani, and P. Allavena, 2009, Tumor-associated macrophages (TAM) as major players of the cancer-related inflammation: J Leukoc Biol, v. 86, p. 1065-73.

Song, H., D. L. Chen, and R. F. Ismagilov, 2006, Reactions in droplets in microfluidic channels: Angew Chem Int Ed Engl, v. 45, p. 7336-56.

Songok, J., M. Tuominen, H. Teisala, J. Haapanen, J. Mäkelä, J. Kuusipalo, and M. Toivakka, 2014, Paper-based microfluidics: fabrication technique and dynamics of capillary-driven surface flow: ACS Appl Mater Interfaces, v. 6, p. 20060-6.

Soto-Gutierrez, A., N. Navarro-Alvarez, H. Yagi, Y. Nahmias, M. L. Yarmush, and N. Kobayashi, 2010, Engineering of an hepatic organoid to develop liver assist devices: Cell Transplant, v. 19, p. 815-22.

Squires, T. M., and S. R. Quake, 2005, Microfluidics: Fluid Physics at the Nanoliter Scale

Starley, B. Q., C. J. Calcagno, and S. A. Harrison, 2010, Nonalcoholic fatty liver disease and hepatocellular carcinoma: a weighty connection: Hepatology, v. 51, p. 1820-32.

Streetman, B. G., 1990, Solid State Electronics, *in* P. Hall, ed.

Strohmeier, O., M. Keller, F. Schwemmer, S. Zehnle, D. Mark, F. von Stetten, R. Zengerle, and N. Paust, 2015, Centrifugal microfluidic platforms: advanced unit operations and applications: Chem Soc Rev, v. 44, p. 6187-229.

Tabeling, P., 2006, Introduction to microfluidics, Oxford University Press.
Tan, Y. C., J. S. Fisher, A. I. Lee, V. Cristini, and A. P. Lee, 2004, Design of microfluidic channel geometries for the control of droplet volume, chemical concentration, and sorting: Lab Chip, v. 4, p. 292-8.
Teh, S. Y., R. Lin, L. H. Hung, and A. P. Lee, 2008, Droplet microfluidics: Lab Chip, v. 8, p. 198-220.
Tian, T., X. Wei, S. Jia, R. Zhang, J. Li, Z. Zhu, H. Zhang, Y. Ma, Z. Lin, and C. J. Yang, 2015, Integration of target responsive hydrogel with cascaded enzymatic reactions and microfluidic paper-based analytic devices (μPADs) for point-of-care testing (POCT): Biosens Bioelectron, v. 77, p. 537-542.
Tibbitt, M. W., and K. S. Anseth, 2009, Hydrogels as extracellular matrix mimics for 3D cell culture: Biotechnol Bioeng, v. 103, p. 655-63.
Todaro, G. J., G. K. Lazar, and H. Green, 1965, The initiation of cell division in a contact-inhibited mammalian cell line: J Cell Physiol, v. 66, p. 325-33.
Toner, M., and D. Irimia, 2005, Blood-on-a-chip: Annu Rev Biomed Eng, v. 7, p. 77-103.
Tourlomousis, F., and R. C. Chang, 2015, Numerical investigation of dynamic microorgan devices as drug screening platforms: Part I: Macroscale modeling approach & validation: Biotechnol Bioeng.
Tourovskaia, A., X. Figueroa-Masot, and A. Folch, 2005, Differentiation-on-a-chip: a microfluidic platform for long-term cell culture studies: Lab Chip, v. 5, p. 14-9.
Truskett, V. N., and M. P. Watts, 2006, Trends in imprint lithography for biological applications: Trends Biotechnol, v. 24, p. 312-7.
Tsutsui, H., and C. M. Ho, 2009, Cell Separation by Non-Inertial Force Fields in Microfluidic Systems: Mech Res Commun, v. 36, p. 92-103.
Tung, Y. C., N. T. Huang, B. R. Oh, B. Patra, C. C. Pan, T. Qiu, P. K. Chu, W. Zhang, and K. Kurabayashi, 2012, Optofluidic detection for cellular phenotyping: Lab Chip, v. 12, p. 3552-65.
Tzanakakis, E. S., D. J. Hess, T. D. Sielaff, and W. S. Hu, 2000, Extracorporeal tissue engineered liver-assist devices: Annu Rev Biomed Eng, v. 2, p. 607-32.
van der Meer, A. D., and A. van den Berg, 2012, Organs-on-chips: breaking the in vitro impasse: Integr Biol (Camb), v. 4, p. 461-70.
van Midwoud, P. M., E. Verpoorte, and G. M. Groothuis, 2011, Microfluidic devices for in vitro studies on liver drug metabolism and toxicity: Integr Biol (Camb), v. 3, p. 509-21.
Vedel, S., S. Tay, D. M. Johnston, H. Bruus, and S. R. Quake, 2013, Migration of cells in a social context: Proc Natl Acad Sci U S A, v. 110, p. 129-34.
Velve-Casquillas, G., M. Le Berre, M. Piel, and P. T. Tran, 2010, Microfluidic tools for cell biological research: Nano Today, v. 5, p. 28-47.
Velve-Casquillas, G., M. Le Berre, M. Piel, and P. T. Tran, 2015, Microfluidic for cell biology: concept and methodologies, Elveflow.
Verhulsel, M., M. Vignes, S. Descroix, L. Malaquin, D. M. Vignjevic, and J. L. Viovy, 2014, A review of microfabrication and hydrogel engineering for micro-organs on chips: Biomaterials, v. 35, p. 1816-32.
Veteläinen, R., A. van Vliet, D. J. Gouma, and T. M. van Gulik, 2007, Steatosis as a risk factor in liver surgery: Ann Surg, v. 245, p. 20-30.
Wagner, I., E. M. Materne, S. Brincker, U. Süssbier, C. Frädrich, M. Busek, F. Sonntag, D. A. Sakharov, E. V. Trushkin, A. G. Tonevitsky, R. Lauster, and U. Marx, 2013, A dynamic multi-organ-chip for long-term cultivation and substance testing proven by 3D human liver and skin tissue co-culture: Lab Chip, v. 13, p. 3538-47.

Walker, G. M., and D. J. Beebe, 2002, An evaporation-based microfluidic sample concentration method: Lab Chip, v. 2, p. 57-61.

Wang, Q., H. Ni, L. Lan, X. Wei, R. Xiang, and Y. Wang, 2010, Fra-1 protooncogene regulates IL-6 expression in macrophages and promotes the generation of M2d macrophages: Cell Res, v. 20, p. 701-12.

Wang, X., C. Cheng, S. Wang, and S. Liu, 2009, Electroosmotic pumps and their applications in microfluidic systems: Microfluid Nanofluidics, v. 6, p. 145.

Weibel, D. B., M. Kruithof, S. Potenta, S. K. Sia, A. Lee, and G. M. Whitesides, 2005, Torque-actuated valves for microfluidics: Anal Chem, v. 77, p. 4726-33.

White, A. K., M. VanInsberghe, O. I. Petriv, M. Hamidi, D. Sikorski, M. A. Marra, J. Piret, S. Aparicio, and C. L. Hansen, 2011, High-throughput microfluidic single-cell RT-qPCR: Proc Natl Acad Sci U S A, v. 108, p. 13999-4004.

Whitesides, G. M., 2006, The origins and the future of microfluidics: Nature, v. 442, p. 368-73.

Whitesides, G. M., E. Ostuni, S. Takayama, X. Jiang, and D. E. Ingber, 2001, Soft lithography in biology and biochemistry: Annu Rev Biomed Eng, v. 3, p. 335-73.

Wikswo, J. P., F. E. Block, D. E. Cliffel, C. R. Goodwin, C. C. Marasco, D. A. Markov, D. L. McLean, J. A. McLean, J. R. McKenzie, R. S. Reiserer, P. C. Samson, D. K. Schaffer, K. T. Seale, and S. D. Sherrod, 2013, Engineering challenges for instrumenting and controlling integrated organ-on-chip systems: IEEE Trans Biomed Eng, v. 60, p. 682-90.

Wirtz, D., K. Konstantopoulos, and P. C. Searson, 2011, The physics of cancer: the role of physical interactions and mechanical forces in metastasis: Nat Rev Cancer, v. 11, p. 512-22.

Wlodkowic, D., and J. M. Cooper, 2010, Tumors on chips: oncology meets microfluidics: Curr Opin Chem Biol, v. 14, p. 556-67.

Xu, C. X., and X. F. Yin, 2011, Continuous cell introduction and rapid dynamic lysis for high-throughput single-cell analysis on microfludic chips with hydrodynamic focusing: J Chromatogr A, v. 1218, p. 726-32.

Yamada, K. M., and E. Cukierman, 2007, Modeling tissue morphogenesis and cancer in 3D: Cell, v. 130, p. 601-10.

Yan, E., F. Durazo, M. Tong, and K. Hong, 2007, Nonalcoholic fatty liver disease: pathogenesis, identification, progression, and management: Nutr Rev, v. 65, p. 376-84.

Yang, L., Y. Shi, M. Abolhasani, and K. F. Jensen, 2015, Characterization and modeling of multiphase flow in structured microreactors: a post microreactor case study: Lab Chip, v. 15, p. 3232-41.

Yip, D., and C. H. Cho, 2013, A multicellular 3D heterospheroid model of liver tumor and stromal cells in collagen gel for anti-cancer drug testing: Biochem Biophys Res Commun, v. 433, p. 327-32.

Zaouk, R., B. Y. Park, and M. J. Madou, 2006, Introduction to microfabrication techniques: Methods Mol Biol, v. 321, p. 5-15.

Zeng, J., and T. Korsmeyer, 2004, Principles of droplet electrohydrodynamics for lab-on-a-chip: Lab Chip, v. 4, p. 265-77.

Zervantonakis, I. K., S. K. Hughes-Alford, J. L. Charest, J. S. Condeelis, F. B. Gertler, and R. D. Kamm, 2012, Three-dimensional microfluidic model for tumor cell intravasation and endothelial barrier function: Proc Natl Acad Sci U S A, v. 109, p. 13515-20.

Zhang, B., M. C. Kim, T. Thorsen, and Z. Wang, 2009a, A self-contained microfluidic cell culture system: Biomed Microdevices, v. 11, p. 1233-7.

Zhang, C., Z. Zhao, N. A. Abdul Rahim, D. van Noort, and H. Yu, 2009b, Towards a human-on-chip: culturing multiple cell types on a chip with compartmentalized microenvironments: Lab Chip, v. 9, p. 3185-92.

Zhang, M. Y., P. J. Lee, P. J. Hung, T. Johnson, L. P. Lee, and M. R. Mofrad, 2008, Microfluidic environment for high density hepatocyte culture: Biomed Microdevices, v. 10, p. 117-21.

Zhong, Q., S. Bhattacharya, S. Kotsopoulos, J. Olson, V. Taly, A. D. Griffiths, D. R. Link, and J. W. Larson, 2011, Multiplex digital PCR: breaking the one target per color barrier of quantitative PCR: Lab Chip, v. 11, p. 2167-74.